ERBIUM AND YTTERBIUM DOPED PHOSPHOTELLURITE GLASSES FOR LASERS AND OPTICAL AMPLIFIERS

A thesis submitted by

Purnananda Nandi

to

Indian Institute of Technology Guwahati

in partial fulfilment of the requirements

for the degree of

Doctor of Philosophy in Physics

Department of Physics

Indian Institute of Technology Guwahati

Guwahati-781039, India.

January 2007

STATEMENT

The work contained in the thesis entitled "ERBIUM AND YTTERBIUM DOPED PHOSPHOTELLURITE GLASSES FOR LASERS AND OPTICAL AMPLIFIERS" has been carried out by me under the supervision of Dr. Gin Jose, Assistant Professor, Department of Physics, Indian Institute of Technology Guwahati. This work has not been submitted elsewhere for the award of any degree.

Date: 1st January 2007

Purnananda Nandi

Research Scholar
Department of Physics
Indian Institute of Technology Guwahati
Assam - 781039
India.

CERTIFICATE

It is certified that the work contained in the thesis entitled "ERBIUM AND YTTERBIUM DOPED PHOSPHOTELLURITE GLASSES FOR LASERS AND OPTICAL AMPLIFIERS" by Purnananda Nandi, a student in the Department of Physics, Indian Institute of Technology Guwahati, for the award of the degree of Doctor of Philosophy has been carried out under my supervision. This work has not been submitted elsewhere for a degree.

Date: 1st January 2007

Dr. Gin Jose

Assistant Professor

Department of Physics

Indian Institute of Technology Guwahati

Guwahati - 781039

India.

Dedicated

to

my parents

ACKNOWLEDGEMENTS

I would like to express my deepest gratitude to my supervisor Dr. Gin Jose, for his confidence, kindness, and patience with me for all these years. We have had a number of conversations about research, science, politics, and many other topics that I value a lot. I consider myself lucky and most honored to be his first research student.

I would like to thank Prof. A. Srinivasan, Chairman of my doctoral committee and other members of the committee, Dr. P. K. Giri, Dr. R. Swaminathan for reviewing my research work regularly and for all valuable suggestions for my doctoral research.

I specially acknowledge Prof. A. Srinivasan, Prof. A. Khare, Dr. S. Ravi, Dr. S. V. Rao, Dr. S. K. Khijwania and Dr. P. S. Robi for extending their experimental facilities to me. I am grateful to Prof. Deepak Mathur, TIFR, Mumbai, and Dr. Reji Philip, RRI Banaglore, for their kind collaboration for femtosecond laser experiments. I am thankful to SAMEER, Mumbai, India, for the waveguides characterizations.

I am very fortunate to have Indrada, Monoda as my senior. Their expertise has been a great help to me. Without Kamlesh my thesis would have not be completed by this time. It is my pleasure to say my gratitude to Sidada, Lokeshda, Atulda, Pankaj, Bimal, Basab and Madan for helping me during my PhD tenure. My sincere thanks are due to members in the Mechanical department workshop and SOs of CIF, IITG.

I am deeply indebted to dadu thakuma, bapi, ma, bubu, and all family members for their moral support.

My special thanks are due towards Sabitha, Sunish and Veena for friendly atmosphere in the Fibre and Integrated Optics Laboratory.

Finally, I express my sincere thanks to all who helped me in whatever form during my stay at IIT Guwahati, particularly Patrada, Kamlesh, Sankar, Promod, Santanu, Amal, Krishno, Manas, Rajenda, Rajen, Kaushik, Munimadi, Purabi, Poulumi for all the (good and bad) moments we shared. I would like to thank my friends from Chemistry department Ballav, Anirban, Abhijit, for their help. Thanks to all research scholars, senior juniors, present past, for being there. Thanking you,

Purnananda Nandi.

PREFACE

The luminescence from rare earth ions offer ample prospect for fabrication of laser and amplifier. Erbium (Er) doped tellurite glasses provide broad C+L band (1535-1610nm) amplification suitable for wavelength division multiplexed (WDM) optical communication networks. Tellurite glasses are important because of their high emission cross-section, higher gain bandwidth, wide range of transparency and higher nonlinear refractive index comparing to many other glasses. However, tellurite based glasses have some drawbacks such as low glass transition temperature (T_g) and low phonon energy. The multiphonon relaxation rate of the Er^{3+} ions from $^4I_{11/2}$ (pump level) to $^4I_{13/2}$ level (lasing level) is less due to low phonon energy of the tellurite glass, thus making the 980nm pumping of Er^{3+} ions from $^4I_{15/2}$ (ground state) to $^4I_{11/2}$ transition less efficient. To increase the phonon energy of the tellurite based glasses, approaches like addition of tungsten oxide and borate are reported. In the present thesis work, phosphate has been used as an additive in the tellurite host in order to address the issue of low phonon energy as well as low glass transition temperature. Phosphotellurite (PT) glasses have attracted the attention of many researchers in the past due to the interesting structural properties that results from mixed network formers viz., tellurite and phosphate. Neodymium doped PT glasses have been studied for laser applications and PT glasses containing heavy metal oxides have been reported for ultra broadband fibre Raman amplifiers.

In this thesis work, the thermal and optical properties of glasses with phosphate and tellurite as main components, doped with erbium and ytterbium, have been investigated. The increase in the phonon energy as well as T_g with the addition of phosphate in tellurite glass would facilitate the fabrication of waveguide laser and amplifier. The dependence of glass composition and dopant concentration on the spectroscopic and thermal properties is important for design of laser glasses. We investigated those important properties of the new glasses with different compositions doped with Er and ytterbium (Yb). The modified host glass is suitable for Yb

codoping due to their higher phonon energy to improve the pumping efficiency when using a 980nm laser as pump source. We also investigated only Yb doped PT glasses that are important for fabrication of diode pumped tunable, high power and short pulse lasers operating in the ~1μm. Direct writing of channel waveguides in glass using ultrafast laser pulses for fabrication of devices like waveguide laser and amplifiers has potential applications in telecommunications and optical signal processing. Writing channel waveguides by ultrafast laser in tellurite glass as such is challenging. Femtosecond laser writing experiments were performed on the modified tellurite glass doped with Er^{3+} ions. The broadband amplified spontaneous emission (ASE) sources or the so called superfluorescent sources have spatial coherence but their temporal coherence is very low. This makes such sources interesting for applications like optical coherence tomography, device characterization (in optical fibre communications), gyroscopes, and for fibre optic sensors. Fabrication of short, multimode fibre ASE sources using the new glass was also a subject of investigation of the thesis.

The first chapter is devoted to review the work done in the field as well as to present the experimental and theoretical tools used in the present work. The different glass systems and studies performed have been organized in the remaining five chapters.

PUBLICATIONS

Journals Papers:

1. P. Nandi, G. Jose, C. Jayakrishna, S. Debberma, K. Chalapathi, K. Alti, A. K. Dharmadhikari J. A. Dharmadhikari, D. Mathur, "*Femtosecond laser written channel waveguides in Er doped tellurite glass*", Optics Express, Vol. 14, No. 25, (2006) pp. 12145–12150.

2. P. Nandi and G. Jose, "*Ytterbium doped P_2O_5-TeO_2 glass for laser applications*", IEEE Journal of Quantum Electronics, Vol. 42, No. 11, (2006) pp. 1115–1121.

3. P. Nandi and G. Jose, "*Erbium doped phospho-tellurite glasses for 1.5µm optical amplifiers*", Optics Communications, Vol. 265, (2006) pp. 588–593.

4. P. Nandi and G. Jose, "*Spectroscopic properties of Er^{3+} doped phospho-tellurite glasses*", Physica B, Vol. 381, (2006) pp. 66–72.

5. G. Medhi, P. Nandi, S. Mohan and G. Jose, "*Silver nanocluster formation in silicate glass by single step ion-exchange*", Materials Letters, Vol. 61, Issues 11-12, (2007) pp. 2259-2261.

6. P. Nandi and G. Jose, "*Yb: Phospho-tellurite - A New Laser Glass*", Optoelectronic Materials and Devices, edited by Yong Hee Lee, Fumio Koyama, Yi Luo, Proc. Of SPIE, Vol. 6352, (2006) pp. 635222-1 – 635222-8.

7. P. Nandi and G. Jose, '*Structural analysis of thermal and optical properties of Er doped Na_2O- P_2O_5-TeO_2 glasses*', to be communicated.

8. P. Nandi and G. Jose, *'Rare earth doped short length glass fibre as broadband superfluorescent source '*, to be communicated

Conference Papers:

1. P. Nandi J. Thomas, R. Philip, G. Della Valle, S. Taccheo, G. Sorbello, P. Laporta, G.Jose, '*Optical nonlinearity in silver-sodium ion exchanged planar waveguides*', Photonics-2004, Kochi, India (December 2004).

2. P. Nandi, L. Irimpan, P Radhakrishnan, V.P.N. Nampoori and G. Jose, '*Spectroscopic properties of Ag-Na ion exchanged, Er-Yb codoped phosphate glasses*', NLS-2005, Mumbai, India (January 2005).

3. P. Nandi, S. Mohan, G. Medhi and G. Jose, '*Nanocluster Formation in Silicate Glass by Single Step Ion-Exchange*', OMTAT-2005, Cochin, India (October 2005)

4. Purnananda Nandi, Sabitha Mohan, Gin Jose, '*Spectroscopic properties of erbium doped phospho-tellurite glasses*', ICOL-2005, Dehradun, India (December 2005)

5. P. Nandi and G. Jose, '*Yb: Phospho-tellurite – a new laser glass*', APOC06, Guwangju, Korea (September 2006)

Contents

Chapter 1

Introduction

After the first demonstration of laser using ruby crystal as a gain medium by Maiman [1] in 1960 , a number of methods and materials have been proposed and successfully used for production of lasers. Lasers are now widely used in various fields of work like industry, medical, defense, scientific research and most importantly in modern optical communication systems. The applicability of a laser or optical amplifier is determined by its efficiency, output power, wavelength, wavelength tunability and versatility. The core to the development of a new laser is the design and fabrication of the gain medium. There exist a variety of different gain media such as semiconductors, gases, organic dyes and crystals/glasses doped with the transition metal ions [2]. Among the transition metal ions the rare earths (RE) occupy an important place in solid state lasers. It was Snitzer [3] who demonstrated the first laser using the rare earth ion by doping neodymium (Nd^{3+}) in a barium crown glass. Since then a large number of host glasses and crystals doped with different rare earth ions have been used for laser and amplifier application.

Crystals like yttrium aluminium garnet (YAG), is advantageous as a laser host because of their good thermal conductivity, higher emission cross-sections and lower threshold

pump power. They have lower tendency for Q-switching instability in passively mode locked lasers. But, glasses as laser active medium have some application specific advantages over crystals. They have much broad amplification bandwidth due to inhomogeneous broadening of laser transitions of active ions and therefore offers larger wavelength tunability. The broad bandwidth of laser glasses is favourable for ultrafast pulse generation. Moreover glasses are less costlier and easier to fabricate. In addition to applications in bulk lasers, doped glasses are also used in the fabrication of microchip lasers [4] and microsphere lasers [5, 6]. Doped glasses can be drawn into optical fibres for fibre lasers and amplifiers [7, 8]. Active integrated optical devices can also be fabricated using RE doped glass substrates [9].

Types	Pumping Optical @ nm	Lasing at (nm)	σ_e (x$10^{-20} cm^2$)	τ_f (μs)
Crystals [10]				
Nd:YAG	Lamp/ 808 DP	1064	28	230
Yb:YAG	940 DP	1031	2	951
Er:YAG	600-800/ 980DP	2940	2	100
Glasses[11]				
QX/Nd	Lamp	1054	3.8	353
QX/Yb	975 DP	1032	0.4	2000
QX/Er	975 DP	1535	0.8	7900

Table 1.1: Solid State Lasers, DP=Diode pumped.

The favorable conditions of a gain medium are very important from the point of an optical material scientist for designing a laser and amplifier material. The host must have good transparency in the amplification wavelengths. It must have an efficient pump absorption, absorption cross-section and emission cross-section. A suitable upper state lifetime is required, long enough for Q-switching applications, short enough for fast modulation of the power. A high quantum efficiency and absence of complex processes like excited state absorption, cross-relaxation, concentration quenching, fluorescence quenching via OH^- ion are

favorable. Low thermo-optic coefficient is required for weak thermal lensing in high power operations. Chemical stability is required for cutting and polishing to good optical quality in the required size and geometry. As an example some of the RE doped laser crystals and glasses commercially available are reported in the Table 1.1, along with their different laser parameters obtained from the product data sheet of the respective companies.

1.1 Rare earth doped photonic devices

In this section a discussion on the importance of the RE ions, erbium (Er) and ytterbium (Yb) doped glassy materials for applications in laser and amplifier is given.

1.1.1 Erbium doped fibre amplifier(EDFA)

Modern communication system relies to a great extent on broadband communication capability, with applications such as high-speed internet access, voice, video, multimedia broadcasting systems, and high-capacity data networking for remote storage and grid computing. Optical communication systems feature point-to-point transport capacities of many terabits per second over communication distance up to 10,000 km using a single, 125 μm thin optical fibre. Consequently, such systems find applications in nation wide fibre optic backbone networks and transcontinental submarine links. They are also massively entering the access network, with fibre-to-the-home deployments currently underway in several countries worldwide.

The attenuation of the light beam as well as the distortion in the optical signals as they are guided through the fibres are amazingly small, about 0.2 dB/km. So tens of kilometers can be bridged without amplifying the signal. The powerful laser signals, available for carrying the information made the systems more efficient by increasing the distance between the two amplifiers.

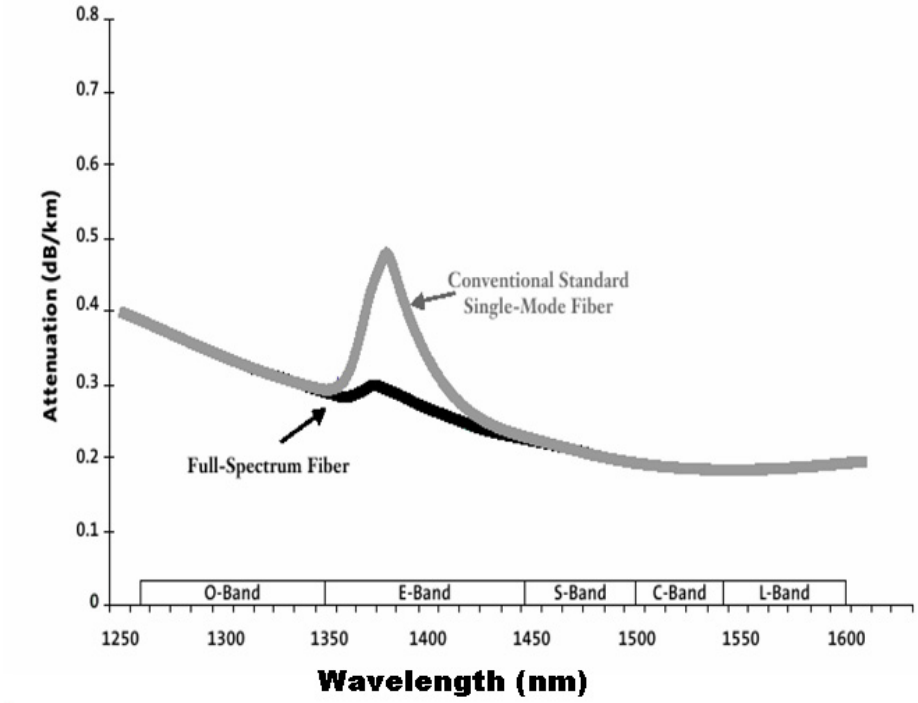

Figure 1.1: Loss of a full spectrum fibre of silica glass, where S Band is 1460-1530 nm, C Band is 1530-1550 nm, L Band is 1550 to 1610 nm [12].

Loss spectrum of a typical silica based optical glass fibre and the full spectrum fibre (developed by Corning Inc.) is shown in Fig. 1.1. A natural choice of the signal carrier wavelength is around 1550 nm (C-Band), which correspond to the lowest loss (∼0.2 dB/km) in the silica fibre, as shown in the figure. Another important aspect of this wavelength region is the availability of erbium doped fibre amplifier (EDFA), which can amplify signals in this low loss region. This is possible because of the coincidence of Er photoluminescence spectra with the low loss window of the silica fibre. The measured photoluminescence spectrum of an Yb-Er doped commercial phosphate glass and the different spectral bands are shown in the Fig. 1.2. An interesting and powerful aspect of an optical communication link is that many different wavelengths can be sent along a fibre simultaneously in the S, C and L bands. The technology of combining a number of wavelengths onto the same

fibre is known as wavelength division multiplexing (WDM) or dense wavelength division multiplexing(DWDM).

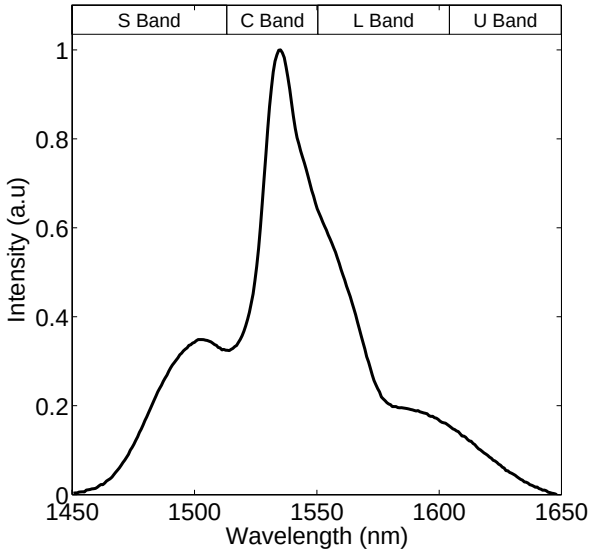

Figure 1.2: Photoluminescence (PL) spectrum of a erbium doped phosphate glass (Schott IOG), shows the emission at around 1535 nm.

The amplification is done in the optical domain by inserting EDFAs of required length in the main communication fibre which can amplify simultaneously all the WDM signals. Without the broad band EDFAs the optical signals at each wavelength would have to be separately amplified, or detected and then regenerated by a new transmitter, for each optical channel that could otherwise be amplified by single EDFA.

The demand for more and more transmission capacity leads to incorporating more and more channels in S, C and L bands. But silica based EDFA can amplify only in the C band. Tellurite based EDFA has been shown to amplify in C+L band [13]. Broad band amplification in the S+C+L bands by doping rare earth elements thulium and erbium has also been demonstrated [14].

1.1.2 Erbium doped waveguide amplifier (EDWA)

In recent years, considerable effort has been given on developing planar analog of EDFA known as erbium doped waveguide amplifier (EDWA). EDWA can be fabricated on a Er or Er-Yb doped glass substrates by methods such as ion-exchange, femtosecond (fs) laser writing and proton beam writing [15, 16, 17]. Other fabrication techniques of the channel optical waveguides are silica-on-silicon ($Si - SiO_2$) [18, 19], plasma enhanced chemical vapor deposition [20], flame hydrolysis [21], sol-gel [22] and thin film sputtering [23]. Er doped waveguide lasers are also demonstrated [24, 25]. Such devices may readily be integrated with other optical elements such as splitters and multiplexers/demultiplexers, all on the same substrate [26]. Among the different methods of fabrication of channel waveguides main advantage of fs laser writing are the simplicity of the setup, absence of the photolithographic steps (important for rapid device prototyping), and the unique capability of producing three-dimensional structures [27].

1.1.3 Fibre lasers

The fibre lasers have the guided wave approach and have many advantages over the bulk medium. Since the glass fibre core can be made only a few microns in diameter, the small mode field diameter of the waveguided pump light yields a much higher pump intensity in a fibre laser than in a bulk device, and therefore reduces lasing threshold. In a bulk gain medium, since the pump beam is divergent, there follows a relation between the optimum gain medium length and the pump spot size. However, for a fibre laser, the two parameters are independent. This added degree of freedom allows the doping density to be kept low to avoid unwanted processes like upconversion, cross-relaxation and concentration quenching [7]. In fibre form the gain medium can be of arbitrary length, yet compact. The small diameter of the fibre allows good heat dissipation, thus greatly reducing the

occurrence of heat related problems like thermal lensing, thermal gradient induced stress and reduced fluorescence at higher temperature. An all fibre laser cavity is much more robust to mechanical perturbations than a free space laser. Once components are spliced, there is no need for further alignments.

The fibre lasers, specially Yb and Er doped fibre lasers are growing very fast nowadays for high power and short pulse sources. Diode pumped high power Yb fibre lasers operated in cw mode is reported [28, 29, 30]. Er/Yb doped fibre lasers are reported to operate at ∼1550 nm in cw and pulsed mode [31].

1.2 Laser glasses

Different types of glasses are in use as RE doped active medium. By definition, glass is a non-crystalline solid which exhibits the glass transition. Glass transition happens in the temperature interval over which a given system gradually transforms upon cooling from a supercooled liquid state into the glassy state. Glasses are generally obtained by freezing in supercooled liquids at a sufficiently rapid rate to avoid crystallization. This process leads to the formation of a non-crystalline solid where the structural disorder of the liquid is retained in the solid state. Characteristics of a glassy material is the short range order and long range disorder [32]. Disorder is mainly in the spatial arrangements of atoms, ions and molecules. They do not exhibit three dimensional periodicity (translational symmetry), and the long range order of the crystalline state is destroyed. Glasses can be prepared by different methods as melt quenching technique, sol-gel process, physical vapour deposition, application of intense shock waves and mechanical alloying [33]. There are mainly two reasons why glasses have been chosen as the transmission medium for optical communication. There is no fixed melting temperature for glasses like crystalline solids,

rather there is a supercooled region of temperature of amorphous solid glass formation. So there is enough time for drawing fibre from glass preforms. Secondly, glass has a wide range of transparency with high refractive index and high mechanical strength and chemical durability. Other than fibres and lasers, glasses are potential candidate in display technology, and nonlinear medium for all optical switches [34, 35, 36].

Silicate glass has been most extensively studied as a laser host because of its excellent glass stability, chemical durability, and good fluorescence properties. Phosphate glass has been commercially used for its excellent thermal and spectroscopic properties [11, 37]. The tellurite glass which was proposed by Wang et. al [38] as a good host for lasers and amplifiers attracted renewed interest recently [39, 40, 41, 42, 43]. The main advantages of tellurite glasses are,

a reasonably wide transmission region (0.35 to 5 μm),

good glass stability and corrosion resistance,

a relatively low phonon energy among oxide glass formers,

high refractive index and high nonlinear refractive index.

The high nonlinear refractive index and the low phonon energy make the tellurite glass fibres uniquely suitable for nonlinear and laser applications. For example, the lower phonon energy results in a lower nonradiative transition rate between adjacent rare earth energy levels, leading to fluorescence and laser emission from additional energy levels that are not possible for silicate glasses. The longest fluorescent wavelengths that could be observed are about 2.8 μm, 2.2 μm, 4.4 μm, and 7.4 μm for tellurite, silica, fluoride and chalcogenide glasses, respectively. This is due to difference in the highest phonon energy for different glass hosts [38].

Different types of tellurite glasses are reported for rare-earth doping like Er^{3+}, Yb^{3+}, Tm^{3+} and Nd^{3+} [44, 45, 14]. Erbium doping is mostly studied in tellurite glass for

its application as a broadband optical amplifier. Tungsten-tellurite glasses were studied for broadband EDFA [46, 47, 48] and waveguide fabrication by ion exchange [49]. Spectroscopic properties of Er doped boro-tellurite [50] and germano-tellurite [41] glasses reported for 1.5 μm amplification. Er^{3+} doped Na_2O-Nb_2O_5-TeO_2 glasses were studied for optical waveguide laser and amplifier [39]. Zinc tellurite glasses doped with erbium and ytterbium are reported for the spectroscopic study [44, 40, 51, 52, 53].

Phosphotellurite (PT) glasses have attracted attention of many researchers due to the interesting properties that would result from mixed network formers. Here both TeO_2 and P_2O_5 are glass formers. Structural and electrical properties of PT glasses have been studied by various groups earlier [54, 55]. Nd^{3+} doped PT glass are studied for lasers [56]. The colour properties are investigated in $P_2O_5 - TeO_2 - ZnO$ system for their applications to optical filters [57]. Recently PT glasses containing heavy metal oxides are reported for the ultra broad band fibre Raman amplifiers [58]. But a detailed and systematic study of this potential glass host for Er^{3+}, Yb^{3+} doping has not been performed before. In this thesis the focus is on the investigation of the optical properties of Er and Yb doped PT glasses for fibre as well as planar integrated lasers and amplifiers.

1.3 Erbium doped glasses

1.3.1 Energy levels

Erbium (Er) is a transition metal of the rare-earth series. In a glass matrix, Er atoms assume the trivalent charge state with electronic configuration [Xe] $4f^{11}$ $5s^2$ $5p^6$, where [Xe] represents the closed shell configuration of Xenon. Spin-orbit interactions of the electrons in the 4f shell gives rise to a number of energy levels useful for laser transitions. This interaction is represented by Russell-Saunders coupling (or LS coupling) where L

(orbital angular momentum quantum number) and S (spin angular momentum quantum number) are vectorially added to form the total angular momentum J, and the states are labelled as $^{2S+1}L_J$ [59]. All these LS coupled levels are again Stark splitted in the central field approximation which gives rise to the broadening in absorption and emission spectra. More often, low temperature optical measurements of the stark splitting were used to deduce the nature of the ion site. This approach was applied to the Er^{3+} doped glasses using absorption spectra [60, 61]. The different LS coupled levels of Er^{3+} in silica host is shown in the Fig. 1.3 [8]. An illustration of various possible radiative and nonradiative transitions in an Er^{3+} doped system is depicted in the figure. For convenience, the lower most three energy levels of the Er^{3+} ions which are involved in a laser may be named as E_1 (ground state or zero energy state $^4I_{15/2}$), E_2 (intermediate state $^4I_{13/2}$), and E_3 (excited state $^4I_{11/2}$). In the following we discuss different processes in Er doped amplifier glasses.

Ground state absorption. In the absence of any electromagnetic energy in the medium, the ions reside at zero energy level. These ions can be excited and moved to the higher energy level E_3, through the absorption of an incoming photon if the photon energy hν (where h is a Planck's constant and ν is the frequency of incident light) is equal to the energy difference $E_3 - E_1$, which is equivalent to a pump wavelength of ∼980 nm in Fig.1.3. Other excitation pathways employing pump lasers with wavelengths ∼800 nm and ∼1450 nm are also possible [7]. However it depends on the properties of the active medium and available pump power.

Multiphonon relaxation. The excited ions subsequently decay to a more stable energy level, referred as metastable state, E_2, via a nonradiative relaxation. In crystals nonradiative relaxation corresponds to the emission and absorption of phonons. Although the absence of translational invariance in glasses means that the vibrational modes will not in general have a well defined wave-vector, for consistency these excitations are referred as

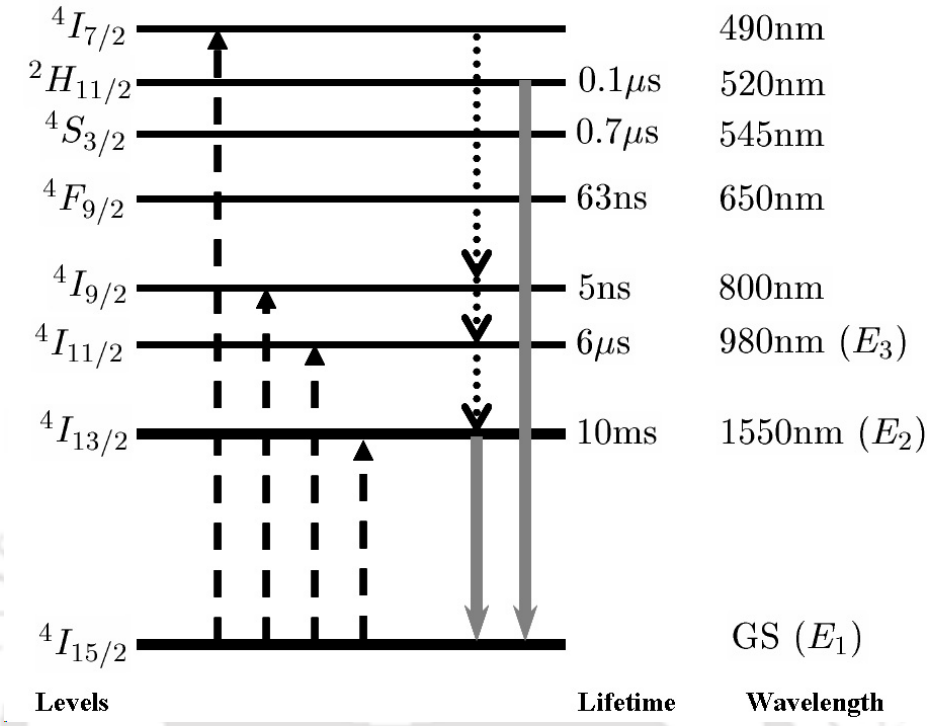

Figure 1.3: Different energy levels of Er doped silicate glass with the respective lifetimes. The dashed lines corresponds to the ground state absorption, dotted lines corresponds to the nonradiative relaxations and solid lines corresponds to the radiative transitions.

phonons [7]. The bulk phonon energy of different oxide glasses are given in order as Borate (1350-1480 cm^{-1}) > Phosphate (1100-1350 cm^{-1}) > Silicate (1000-1100 cm^{-1}) > Tellurite (600-800 cm^{-1})[38]. Therefore the lifetime of the level E_2 is different in the above glasses.

Photon emission. The ions in level E_2 can then return to the ground state by releasing their energy in the form of photons. This emission process may occur in two different ways called spontaneous emission and stimulated emission. Light produced by the spontaneous emission is called fluorescence. While in the case of stimulated emission, the ions are triggered by an existing single photon with energy equal to $E_2 - E_1$. The photons emitted in this process are an exact replica of the triggering photon in frequency, phase and polarization. These newly generated photons through the stimulated emission process add

more and more power to the initial triggering signal as it passes through the medium and results in optical amplification. In contrast, the spontaneous or random emission results noise in a fibre amplifier [62]. However the amplified spontaneous emission (ASE) in RE doped fibres is useful for broadband sources [63, 64].

Optical gain. The necessary requirement for realizing optical amplification is to maintain a population inversion between the states that are relevant to the stimulated emission process, i.e. the number of ions in the E_2 energy state should be greater than the number of ions in the ground state. This can be achieved by supplying sufficient optical power (pump power) at the appropriate wavelength (800/980/1480 nm) using an external energy source, often referred to as the pump. Another important factor for efficient optical amplification is how long the excited ions can stay in the metastable state until they get a chance to be triggered by a signal photon. This duration is referred as the fluorescence decay lifetime (τ_f) and defined as the exponential decay rate at which the excited ions decays from the metastable state to ground state. The emission cross-section (σ_e) together with lifetime determines the gain (G) of the amplifier, ie., $G \propto (\sigma_e \times \tau_f)$ [62].

Wavelengths, transitions and features of fibre lasers and amplifiers reported for Er^{3+} doped oxide and fluoride glass hosts are reported in Table.1.2. Important physical and spectroscopic properties of different oxide glass hosts are compared in Table.1.3.

Operating Range (nm)	Transition	Type of glass host Oxide	Fluoride	Type of Transition	Pump Wavelength (nm)
550	$^4S_{3/2} \rightarrow ^4 I_{15/2}$	Yes	Yes	UC, 3L	800/980
850	$^4S_{3/2} \rightarrow ^4 I_{13/2}$	No	Yes	3L	490
980-1000	$^4I_{11/2} \rightarrow ^4 I_{15/2}$	No	Yes	3L	–
1550-1600	$^4I_{13/2} \rightarrow ^4 I_{15/2}$	Yes	Yes	3L	800/980/1480
1720	$^4S_{3/2} \rightarrow ^4 I_{9/2}$	No	Yes	4L	–
2700	$^4I_{11/2} \rightarrow ^4 I_{13/2}$	No	Yes	ST	FL

Table 1.2: Er doped glass fibre lasers and amplifiers, where 3L= three-level; 4L= four-level; UC= up-conversion; ST=apparent self-terminating, FL=flash-lamp [7].

Parameters	Units	Tellurite	Al/Silicate	Phosphate
FWHM of 1.5 μm peak	nm	65	45	55
Half Maximum range	nm	1500-1565	1520-1565	1510-1565
Stimulated Emission Cross-section	$\times 10^{-21}$ cm^2	8.0	5.5	8.0
$^4I_{13/2}$ lasing level lifetime	ms	5	10	8
$^4I_{11/2}$ lifetime (calculated)	μs	20	1	1
Refractive Index	-	2.0	1.45	1.52
Bulk Phonon Energy	cm^{-1}	770	1100	1200
Glass Transition temperature T$_g$	^{o}C	250	700	450

Table 1.3: Properties of different Er doped glass hosts compiled from refs [46, 65].

1.3.2 Ion-Ion Interactions

Energy transfer is the transfer or sharing of energy between rare earth ions. This exchange may occur among rare earth ions of the same or different species, and it may be either beneficial or deleterious. $Yb^{3+} \rightarrow Er^{3+}$ energy transfer has been used since the earliest days of the solid state lasers to improve the pumping efficiency of devices [66, 67].The process of energy transfer between $Yb^{3+} \rightarrow Er^{3+}$ has been shown in Fig. 1.4(a). The mechanism involved is the absorption of the optical excitation by the donor (Yb^{3+}) and resonant radiative transfer of it to the activator ion (Er^{3+}). Radiative energy transfer involves one ion emitting a photon, which is then reabsorbed by another ion. In contrast $Er^{3+} \rightarrow Er^{3+}$ energy transfer is an important dissipative mechanism for fibre amplifiers at 1550 nm [7]. This process can distort the emission spectrum and cause radiation trapping. If two excited ions interact, one can transfer its energy to the other, leaving itself to the ground state and the other in the higher $^4I_{9/2}$ state. This is called *co-operative up-conversion* and it is an important gain limiting factor in heavily doped glasses. In oxide glasses the $^4I_{9/2}$ level quickly relaxes through the multiphonon relaxation back to the $^4I_{13/2}$ state, the net result of the process being to convert one unit of excitation of Er^{3+} to the $^4I_{13/2}$ level

into heat. These two processes of energy transfer between $Er^{3+} \rightarrow Er^{3+}$ has been shown in Fig. 1.4(b).

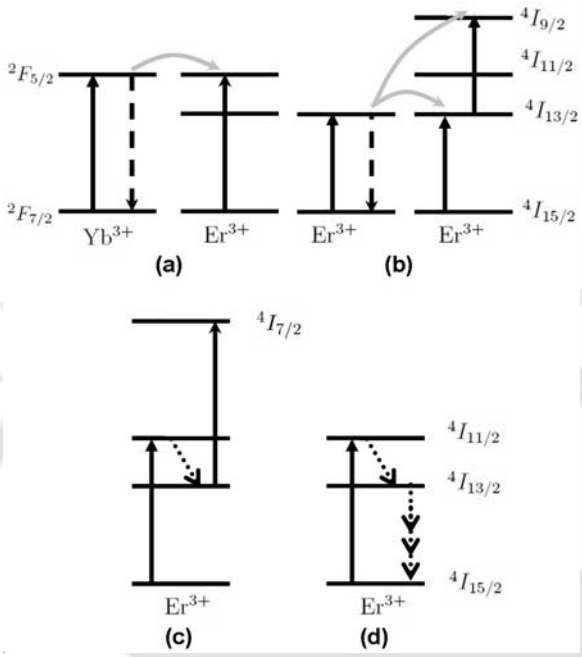

Figure 1.4: Different energy transfer mechanisms of Er and Er-Yb doped glass. (a) Yb-Er energy transfer, (b) Er-Er energy transfer and co-operative upconversion, (c) Pump ESA, (d) Fluorescence quenching. Solid lines correspond to the photon absorption, curved lines represent transfer of energy, dashed lines are relaxation to ground state via energy transfer and dotted lines correspond to the multiphonon relaxations.

Excited Sate Absorption (ESA) is an important gain limiting factor for low phonon energy hosts. In ESA, pump absorption occurs not from the ground state of the Er^{3+} ions, but from an excited level whenever there is an appropriate energy gap available for the absorption of a pump photon. Unlike co-operative up-conversion, since one ion is involved in ESA, it can occur only at high pump powers. The lifetime for the excited ions in the state where the ESA originates is also a factor that influences this effect. In the pump ESA, the excited ion in the pump state $^4I_{11/2}$ reabsorbs the pump photon and moves up to $^4I_{7/2}$ state, followed by a rapid relaxation to $^2H_{11/2}$. From this state, the ion then decays straight

to the ground state through the emission of photons at wavelengths around 520 nm (green light up-converted fluorescence) [7, 68]. The mechanism is described in Fig. 1.4(c).

The fluorescence quenching via nonradiative decay has been shown in Fig. 1.4(d). This can occur in glasses with high OH^- contents or in high phonon energy glasses. Another energy transfer mechanism which is deleterious is concentration quenching. It is the reduction in the quantum efficiency of an ion with increasing concentration of that ion. It can occur through energy transfer or via multiphonon relaxations. Another reason for the quenching is the clustering of the rare earth ions in the host matrix. Pure silica can incorporate only small amount of rare earths before microclustering occurs and ion-ion interaction appears. Phosphate and tellurite glasses are having higher rare earth solubility than silica. Approaches like addition of aluminium (Al) has found to reduce the clustering problem in silica glass[7, 68].

1.4 Yb doped glasses

Like erbium, ytterbium is also a transition metal of the lanthanides series with electronic configuration [Xe] $4f^{13}$ $5s^2$ $5p^6$. Since there are only two energy levels of the Yb^{3+} ions due to LS coupling, it is commonly believed that concentration quenching and multiphonon relaxation should not affect the luminescence properties [69]. The Yb^{3+} ions are of interest for the next generation high power lasers and also as sensitizer of the Er^{3+} ions in codoped glasses as discussed before.

Recently Yb^{3+} doped double cladding fibre lasers have received increasing attention because of their high power output at 1.06 μm [29]. Maximum output power reported recently is as high as 1.36 kW for a diode pumped Yb^{3+} doped fibre laser [28]. However, the cluster effect of Yb ions in silica fibre greatly reduce the concentration of Yb^{3+} ions in

the fibre. Usually, high Yb^{3+} doping concentrations can be realized in phosphate glasses [30]. It was shown recently that Yb-doped tellurite glasses have more advantages over some other laser glasses, being comparable to laser crystals like Yb:YAG, exhibiting high emission cross sections and long luminescence lifetimes [70, 52, 71].

1.4.1 Energy levels

Stimulated emission of Yb^{3+} involves transitions between Stark levels of the $^2F_{7/2}$ and $^2F_{5/2}$ electronic states at wavelengths in the range 1.01-1.06 μm [72]. These are the only levels of the $4f^{13}$ ground configuration; levels of excited configurations and charge transfer states are in the ultraviolet. Therefore, there is no excited-state absorption from the $^2F_{5/2}$ levels either at the lasing or the excitation wavelength. This is an attractive feature for optically pumped high-energy lasers in which there is a large inverted population density. Optical pumping is possible in Yb doped systems to directly excite into the $^2F_{5/2}$ level using diode lasers [73, 74].

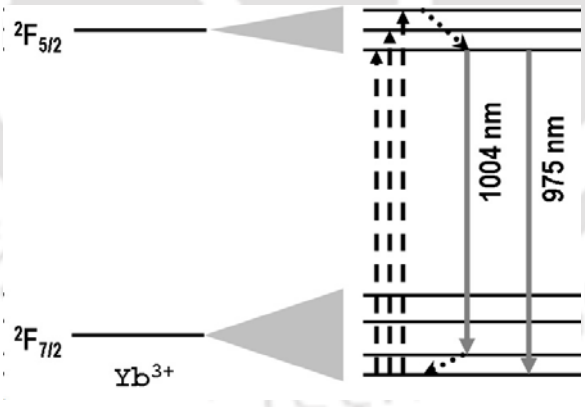

Figure 1.5: Stark splited energy levels of Yb^{3+} ions. The dashed lines represents the GSA, dotted lines are the phonon relaxations and solid lines are the radiative transitions.

Green luminescence has been reported in crystals [75] and glasses [76] doped with Yb due to cooperative luminescence effect. This is an upconversion process in which two

interacting ions in the excited state decay simultaneously to the ground state, emitting one photon at twice the energy of single ion transition [75, 67].

1.5 Research scheme for rare earth doped laser glasses

Rare earth ions such as Er, Yb, Nd, Ho, Tm and Tb doped in different glasses are investigated in the past. Tanabe gave a research scheme to comprehend optical phenomena of rare earth ions in glasses [77]. In the present thesis, the glass design aspect to optimize spectroscopic properties is schematically shown in Fig. 1.6. The steps followed is based on the procedure given in the references: [77, 56].

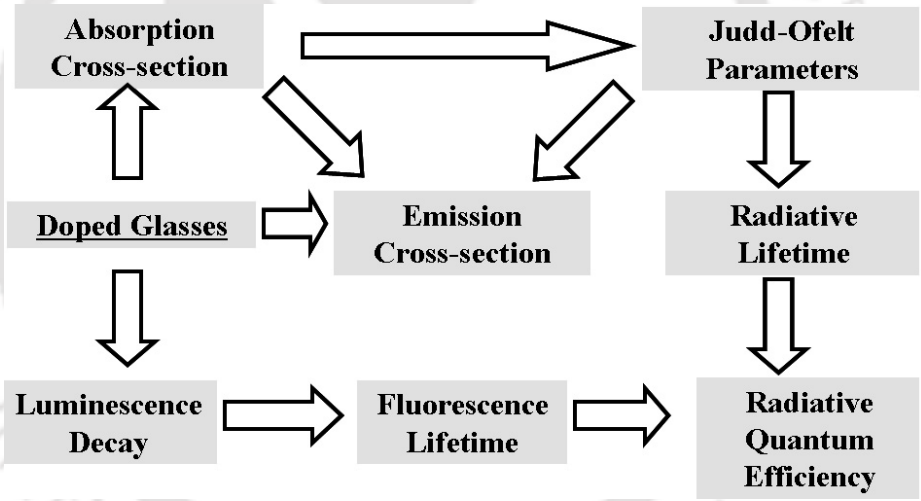

Figure 1.6: Research scheme for the spectroscopic study of rare-earth doped glasses.

1.5.1 Absorption cross-section

The absorption cross-section spectrum can be obtained from the measured absorption spectrum using the equation,

$$\sigma_a = \frac{2.303}{N \times d} E(\lambda) \tag{1.1}$$

where N is the number density of RE ions and d is the thickness of the sample. $E(\lambda)$ is the wavelength dependent absorbance.

1.5.2 Judd-Ofelt theory

For assessing a new glass as a laser host, it is important to measure the possible radiative transition rates between excited levels. Judd [78] and Ofelt [79], working independently, developed a quantum mechanical theory of RE ion doped in a medium which allowed estimates to be made of the electric dipole transition strengths between any pair of $|LSJ>$ manifolds. Judd-Ofelt (JO) analysis of a rare earth doped material essentially involves using the measured oscillator strengths P_{exp}, of all the observable transitions from the ground state to the excited manifolds, and using it to calculate the oscillator strengths of transition between two pairs of excited levels. The experimental *oscillator strengths* P_{exp} of the transitions are obtained from the measured absorption spectrum using the following equations,

$$P_{exp} = \frac{mc^2}{\pi e^2 N} \int \alpha(\bar{\nu}) d\bar{\nu} \tag{1.2}$$

$$\alpha(\bar{\nu}) = \frac{ln[I_0(\bar{\nu})/I(\bar{\nu})]}{d} = \frac{2.303 E(\bar{\nu})}{d} \tag{1.3}$$

where N is the number density of the RE ions, e the charge of the electron, $\bar{\nu}$ the wavenumber, $E(\bar{\nu})$ the absorbance, and d the sample thickness. The experimental oscillator strength contains electric-dipole and magnetic-dipole contributions. One has to subtract the magnetic dipole contribution from the experimental oscillator strength to obtain the electric-dipole contribution that can be equated with the calculated oscillator strength P_{cal}. The

magnetic-dipole contribution, P_{md}, can be obtained from the refractive index of the glasses and using the quantity, P' as reported in ref. [80].

According to Judd-Ofelt theory , the calculated oscillator strength is given by,

$$\begin{aligned} P_{cal}[(S,L)J;(S',L')J'] &= \frac{8\pi^2 mc}{3h\lambda(2J+1)}\frac{(n^2+2)^2}{9n} \\ &\times \sum_{t=2,4,6} \Omega_t |\langle (S,L)J \parallel U^{(t)} \parallel (S',L')J' \rangle|^2 \end{aligned} \tag{1.4}$$

where λ is the peak wavelength of the transition, m the mass of the electron, n the refractive index, Ω_t are called Judd-Ofelt intensity parameters and $\langle \parallel U^{(t)} \parallel \rangle$ are the double reduced matrix elements of unit tensor operators which are considered to be independent of the host matrix. The Judd-Ofelt intensity parameters Ω_t can be derived from the electric-dipole contributions of the experimental oscillator strengths using a least-squares fitting. The reduced matrix elements given in ref.[81] were used for the calculations given in the thesis. The Ω_t parameters are important for investigation of the local structure and bonding in the vicinity of rare earth ions in the glass.

Some important radiative quantities can be calculated using the values of Ω_t. The total spontaneous transition probability is given by [82, 59],

$$\begin{aligned} A[(S,L)J;(S',L')J'] &= A_{ed} + A_{md} \\ &= \frac{64\pi^4}{3h\lambda^3(2J+1)} \times [\frac{n(n^2+2)^2}{9} S_{ed} + n^3 S_{md}] \end{aligned} \tag{1.5}$$

where A_{ed}, A_{md} are the electric-dipole and magnetic-dipole spontaneous emission probabilities, respectively. The electric-dipole and magnetic-dipole line strengths, S_{ed}, S_{md}, are given as,

$$S_{ed} = e^2 \sum_{t=2,4,6} \Omega_t |\langle (S,L)J \parallel U^{(t)} \parallel (S',L')J' \rangle|^2 \tag{1.6}$$

$$S_{md} = \frac{e^2\hbar^2}{4m^2c^2} |\langle (S,L)J \parallel L + 2S \parallel (S',L')J' \rangle|^2 \tag{1.7}$$

The values of A_{md} were calculated using the values for RE in $LaF_3(A'_{md})$ and corrected for the refractive index difference [82]. The relationship is,

$$A_{md} = (\frac{n}{n'})^3 A'_{md} \tag{1.8}$$

where n, n' are refractive index of doped glasses and LaF_3, respectively.

The fluorescence *branching ratio* of transitions from initial manifold $|(S,L)J\rangle$ to lower levels $|(S',L')J'\rangle$ is given by,

$$\beta[(S,L)J;(S',L')J'] = \frac{A[(S,L)J;(S',L')J']}{\sum_{S',L',J'} A[(S,L)J;(S',L')J']} \tag{1.9}$$

1.5.3 Emission cross-section

The quantum efficiency of the RE doped laser material can be calculated if the radiative and measured fluorescence lifetime of the laser level is known.

The *radiative lifetime* of Er:$^4I_{13/2}$ state can be obtained from the JO analysis using Eq.(1.5). The calculated radiative lifetime τ_{JO} is,

$$\tau_{JO} = \frac{1}{\sum_{JJ'} A} \tag{1.10}$$

The Er fluorescence bands are asymmetric, therefore an effective bandwidth defined by

$$\Delta\lambda_e = \int I_e(\lambda) d\lambda \tag{1.11}$$

is determined from the normalized fluorescence intensity $I_e(\lambda)$. The peak stimulated emission cross-section $\sigma_e(J, J')$ is determined by using equations 1.5 and 1.11 [56].

$$\sigma_e(J, J') = \frac{\lambda_{peak}^4}{8\pi c n^2 \Delta\lambda_e} A(J, J') \tag{1.12}$$

where λ_{peak} is the peak emission wavelength, c is the velocity of light, n is the refractive index of the glass, A is the radiative transition probability at λ_{peak}.

The emission cross-section for an erbium system (three level system) can also be calculated from the absorption cross-section spectrum using the McCumber relation or reciprocity method [83].

Quantum efficiency is defined as $\eta = \frac{\tau_m}{\tau_{JO}}$, where τ_m is the measured lifetime and τ_{JO} is the radiative lifetime calculated from the JO analysis. Its a parameter of the efficiency of a rare earth host, more is the η, better is the host.

1.6 Bulk modification in transparent materials by an ultrafast laser

One of the most exciting applications of bulk modification of transparent materials using fs laser is the fabrication of 3D light guiding structures inside the bulk of the substrate critical components for future integrated optical chips. For the fabrication of waveguides, a localized, single-point modification, typically in the regime where positive index change are produced, must be extended to a line having the diameter of few microns. The technique is the so called micromachining. There are mainly two types of fs micromachining, longitudinal and transverse geometry shown in Fig. 1.7 (a) and (b) respectively. In longitudinal writing, the glass plate moves parallel to the focused beam. In transverse writing, the glass moves perpendicular to the irradiated laser. Transverse micromachining puts no limit on the length

of the waveguide, but the disadvantage is the asymmetry of the produced structure. Except for very high NA (numerical aperture) objectives, the focal radius is always much smaller than the confocal parameter, resulting in a waveguide with elliptical cross-section. To obtain waveguides with circular cross-section the beam can be shaped using an elliptical writing beam [84]. In a simpler setup by putting a slit in front of the focussing objective, however, at the expense of the energy loss of the laser beam, it has been demonstrated to write waveguides of circular cross-section [85]. The change in refractive index obtained depends on the pulse energy and writing speed (number of pulses applied at a given spot). Thus single mode or multimode waveguides can be produced by changing the writing parameters. Below 0.2 dB/cm propagation losses have been reported through the fs written channels [16] which is suitable for integrated optical applications . Using this technique, several devices have been demonstrated, 3D couplers and splitters [26], waveguide arrays [86] , Mach-Zehnder interferometers [87]. Channel waveguides written using ultrafast lasers in erbium-doped phosphate glasses for integrated amplifiers and lasers operating in the C-band have been demonstrated [88, 16]. As an application of void formation in transparent materials, 3D optical data storage has been reported, with the occurrence of a void representing a binary value of 1, and the absence of a void a binary 0 [89]. Gratings are fabricated inside a glass substrate by two beam interference of a single near field fs laser pulses [90].

There are different reasons cited for the refractive index change produced in dielectric medium under femtosecond(fs) laser irradiation. When an intense fs laser pulse is tightly focused inside the bulk of a transparent material, the intensity in the focal volume can become high enough to initiate nonlinear absorption. In this process optical energy is transferred to the material causing ionization of a large number of electrons. The ionized electrons, in turn, can cause permanent material modification by transferring energy to the lattice. In transparent materials the energy of a single photon within the laser pulse

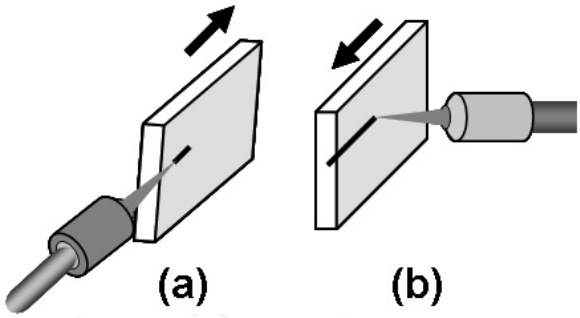

Figure 1.7: (a) Longitudinal (b) Transverse writing geometry of channel waveguides using a femtosecond laser.

cannot be absorbed (which is why they are transparent), so the material must simultaneously absorb more than one photon. This nonlinear absorption results in the creation of an electron-ion plasma that is localized to the focal volume. As the plasma recombines and its energy is dissipated, permanent structural changes can be produced inside the material. Because the nonlinear absorption allows energy to be dissipated into the bulk of a transparent material, these structural changes can be produced inside the sample without affecting the surface, allowing 3D structures to be fabricated by translating the laser focus through the sample [86].

Three types of structural changes were reported till now as a result of fs laser irradiation inside a transparent media. The refractive index changes observed at low energy are attributed to localized melting and rapid solidification of the glass [91]. Intermediate energy can induce birefringent refractive index changes inside the glass [92]. Strips consisting of alternating layers of nanometer scale voids and relatively undamaged material, termed 'nanograting', gives rise to birefringence in the structure [93, 94]. Voids produced at high energy are attributed to an explosive expansion of highly excited, vaporized material out of the focal volume and into the surrounding material, a process termed as microexplosion [95]. Other process are also known to occur during structural changes in the bulk

of the transparent material induced by fs laser irradiation. For example, E' colour centers (positively charged oxygen vacancies) and nonbridging oxygen hole centers formed in fused silica [96]. In multicomponent glasses, migration of components may also play a role in producing a refractive index change, even in the low energy regime where smooth refractive index profiles are produced [97].

Why ultrafast lasers?

Laser pulses of duration greater than picoseconds cannot be used for precision writing because of the following reasons: First, to reach the threshold peak intensity for optical breakdown, a large pulse energy is required. This high pulse energy causes the damage to the extend beyond the focal volume. In contrast, subpicosecond pulses achieve the same peak intensity at much lower energy. The excitation then remains confined to the focal volume, making it possible to deposit energy with submicrometer precision. Second, because the time it takes an excited electron to transfer the energy to the ions is of the order of a picosecond, thermal effects are not decoupled from the excitation. As a result, during the excitation of the electrons by the laser pulse, energy is transferred to the substrate which causes the region around the focal spot to heat up. Third, the occurrence of breakdown by long pulses tends to be random because the initial seed for breakdown is caused by impurities in the material. Subpicosecond pulses, on the other hand, generate the initial seed carrier density solely from multiphoton excitation, giving rise to an extremely steady and fairly material-independent breakdown threshold [98].

1.7 Superfluorescent fibre sources

Superfluorescent fibre sources (SFS) contains a high gain fibre medium which is optically pumped to sufficiently high level to excite the rare-earth ions in order to emit

superfluorescence output via amplified spontaneous emission (ASE) [63]. A spontaneously emitted photon in a rare-earth doped fibre can be amplified as it travels through an optical fibre and stimulates the emission of more photons from excited ions, photons that belong to the same mode of the electromagnetic field as the original spontaneous photon. The presence of spontaneous emission degrades the performance of the fibre amplifier by adding unwanted power near the signal wavelength in the form of noise. It robs photons that would otherwise participate in stimulated emission with the signal photons. Such spontaneously emitted photons subsequently get multiplied by the amplifier and travel along with the signal. It is usually refereed to as the amplified spontaneous emission. The temporal coherence of such a source is very low. The ASE noise power generated travels in both directions of the fibre due to its random nature of emission. Also, the ASE covers a broad spectral range. In the free ion the energy levels are sharp, but in solids, due to the Stark effect, each energy level splits into a manifold of energy sub levels. Therefore, the spontaneous emission of photons naturally originates over a wavelength range results in a broadband SFS and amplifiers.

A great amount of research has been carried out in Er doped SFS. Er doped SFS have potential advantage over the Nd counterparts for the reduction of Rayleigh backscattering and the improvements of the noise limit, because of their operational wavelength region in a low loss window of silica based fibres [99]. Er doped SFS pumped near 980 nm has been studied in four different configurations, SPF (single pass forward), SPB (single pass backward), DPF (double pass forward), DPB (double pass backward) to have more pumping efficiency, higher stable output and larger bandwidth [100]. High power SFS with stable single-transverse-mode output using a heavily doped multimode fibre is reported in an Er doped fibre with large core diameter and high numerical aperture [101]. Long period grating (LPG) has been used for multiwavelength fibre source [102], broadening the linewidth of Er-doped SFS [103] and compensate the dependence of mean wavelength of

ASE on temperature [104]. Er doped tellurite fibres can offer broad amplification bandwidth and high radiative transition efficiencies. They are now promising candidates for fabricating optical amplifiers by means of extending the amplification bandwidth of optical fibres to C+L bands beyond the range available from conventional Er doped silica fibre [105].

Because of the simple quasi-three-level energy structure, Yb ions doped glasses exhibits high quantum efficiencies, low nonradiative decay rate and long fluorescence lifetime (1-2 ms). Compared to Nd, Yb doped SFS offer greater conversion efficiency and generate emission at shorter wavelengths. Many of the complications which are well known for Er doped fibre SFS and amplifiers are avoided like excited state absorption (ESA) and concentration quenching by inter ionic energy transfer. High doping level of Yb are possible leading to high gain in a short length of fibre. Possibility of wide tuning and the prospect of scaling to the higher powers for Yb doped SFS are reported [64, 69]. Other than the doped fibres there are superluminscent diodes having disadvantages of short life time, low coupling into single-mode-fibres, poor spectrum stability with respect to temperature and operating mainly on 800 nm [99].

SFS were developed for navigation-grade fibre-optic gyroscopes (FOG) because they can produce stable and intense broadband light with the low degree of coherence required to detect small rotational rates [63, 106, 69]. Er doped SFS have been demonstrated as feasible light sources for spectrum-sliced WDMA optical communication systems [102]. SFS are also useful for spectroscopy, bio-medical imaging, passive component testing and sensing applications.

1.8 Conclusion

A review of rare earth doped optical materials and devices are given. The energy levels and different ionic interactions involved in erbium and ytterbium doped laser glasses are described. The theoretical and experimental tools adopted for the study of different doped phosphotellurite glasses described in this thesis is elaborated. The details of Judd-Ofelt theory have been discussed. The methods to calculate the quantities like oscillator strength, JO intensity parameter, radiative transition probability, branching ratio, radiative lifetime, quantum efficiency, absorption and emission cross section are defined. An introduction to the fabrication technique applicable to 2D/3D channel waveguides inside a transparent glass using fs laser and their advantages are presented. The applications of SFS and the different configurations of generating ASE sources using rare earth doped optical fibres are given as a prologue to the results given in Chapter 6.

Chapter 2

Spectroscopy of Er doped phosphotellurite glasses

Erbium doped phosphotellurite glasses with the alkali ions sodium and lithium were prepared and their physical and spectroscopic properties were studied in comparison to erbium doped sodium-tellurite glass. Differential scanning calorimetry of the glass samples show an increase in the glass transition temperature with the addition of phosphate (P_2O_5). From the infrared transmittance spectra we found that the maximum phonon energy of the phosphotellurite glasses is also high ($\sim$1290 cm^{-1}). Optical absorption spectrum of the phosphotellurite glasses showed a blue shift in the absorption edge comparing to the sample without phosphate. From the optical absorption spectra the Judd-Ofelt parameters (Ω_t), transition probabilities, branching ratios of various transitions and their radiative lifetimes were calculated.

2.1 Introduction

Erbium doped tellurite glasses have been given much attention nowadays for fabricating 1.5 μm broadband amplifiers for wavelength division multiplexed (WDM) optical communication systems. Erbium doped tellurite fibre amplifiers (EDTFA) are demonstrated with good gain in C and L bands [13]. The high refractive index and good transmittance over a wide wavelength region of $\sim$ 0.35-5 μm make them excellent host for erbium doped photonic devices. It was observed that tellurite glasses possess high second and third order optical nonlinearities making them potential candidates for nonlinear photonic devices [107, 108]. Different types of tellurite glasses have been studied for the fabrication of erbium doped waveguide amplifiers (EDWA) which are promising for metro-WDM network applications [109, 49]. Silicate and phosphate glasses were demonstrated good for fabrication of waveguide lasers and amplifiers in C-band [110, 24, 15]. Phosphate glasses have an advantage over silicate glasses in the device performance because of their high phonon energy and rare earth solubility. A major drawback of these glasses comparing to tellurite based glasses for amplifiers is their limited bandwidth, whereas the tellurite glasses have both higher bandwidth and higher absorption and emission cross-sections for the 1.5 μm emission of Er^{3+}. Because of the low phonon energy(< 800 cm^{-1}) of the tellurite glass, the lifetime of the $^4I_{11/2}$ level is high compared to the lifetime of this level in erbium doped phosphate and silicate glasses that have higher phonon energy. In a tellurite glass it results in the low pumping efficiency under 980 nm excitation because of excited state absorption from this level to higher levels such as $^4F_{7/2}$ and low nonradiative decay rate to the lasing level $^4I_{13/2}$. Consequently, the gain in the $^4I_{13/2}$ to $^4I_{15/2}$ transition band of Er^{3+} would be affected. To overcome this deficiency tellurite glasses with higher phonon energy have been demonstrated by adding tungsten and borate in tellurite glasses and increased phonon

energies of 920 cm^{-1} and 1335 cm^{-1} respectively are reported [46, 50]. The addition of the phosphate, because of its intermediate phonon energy (∼1200 cm^{-1}) in the tellurite glass is expected to decrease the lifetime of the $^4I_{11/2}$ level by multiphonon relaxation. Hence an increase in the pumping efficiency at 980 nm, and amplifier gain for $^4I_{13/2} \rightarrow^4 I_{15/2}$ transition at 1.5 μm is possible. Also with phosphate addition, because of their higher solubility of rare earth ions, high erbium concentration and codoping with ytterbium could be possible. Ytterbium codoping will enhance the pumping efficiency at 980 nm by energy transfer to erbium through cross relaxation.

2.2 Experiments

Erbium doped phosphotellurite glass samples were prepared using the conventional melt quenching technique. The high purity Na_2CO_3, Li_2CO_3, P_2O_5, TeO_2 and Er_2O_3 were used for the batch melting. Glasses were fabricated by a two step melting process at $\sim 800^oC$ in an electrical furnace. First, the batch was melted and quenched in a copper mold. It was then crushed, grinded and again melted. In the second step, the melt was transferred to a graphite mold and annealed for 1 hr below the glass transition temperature, and slowly cooled down to the room temperature. The glass samples were then polished to optical quality for the spectroscopic and refractive index measurements. The different

Given Sample ID	Compositions all in mole(%)	Density $[gm/cc]$	Refractive Index	N $[\times 10^{20}]$ $[ions/cc]$	T_g ^{o}C
NT	$19Na_2O$-$80TeO_2$-$1Er_2O_3$	4.83	2.10	4.06	252
NPT1	$19Na_2O$-$30P_2O_5$-$50TeO_2$-$1Er_2O_3$	3.92	1.96	3.42	340
NPT2	$19Na_2O$-$35P_2O_5$-$45TeO_2$-$1Er_2O_2$	3.65	1.94	3.18	333
LPT	$19Li_2O$-$30P_2O_5$-$50TeO_2$-$1Er_2O_2$	3.96	2.01	3.62	335

Table 2.1: Glass composition with their measured density, refractive index, Er^{3+} ions concentration and glass transition temperature T_g of the prepared samples.

glass compositions investigated in the present work are labelled and given in Table 2.1. The glass transition temperature T_g and refractive index n of the glasses were measured using a differential scanning calorimeter (Perkin Elmer DSC-7) and prism coupler (Metricon 2010) respectively. KBr pelletized samples were used for recording the transmittance in the infrared (IR) region using Perkin Elmer Spectrum I FTIR spectrometer. Absorption spectra in the ultraviolet-visible (UV-VIS) region were measured using dual beam spectrophotometer(Perkin Elmer Lambda 25) with 0.5 nm resolution. The absorbance of the glass samples in the NIR around 1.5 μm was taken using the Perkin Elmer Spectrum BX FTIR spectrometer with 1 cm^{-1} resolution. Density ρ of the glasses was measured using Archimedes' principle and Xylene as the immersion liquid. The fluorescence lifetime of the of erbium Er^{3+} : $^4I_{13/2}$ level of the glass samples is measured using an InGaAs detector and a 200MHz digital storage oscilloscope (Tektronics TDS 2024). The 980 nm laser diode (JDS uniphase) has been modulated by a waveform generator (Agilent 33220A) at the frequency of ∼10Hz. The fluorescence was detected by the photodetector and the decay was recorded with a digital storage oscilloscope (Tektronics TDS 2024). The schematic of the experimental setup is given in Fig. 2.1. All measurements were done at room temperature(∼ 300K).

2.3 Physical and thermal properties

The glass compositions, density, refractive index, and erbium ion concentration calculated from the density and weight percentage of the erbium oxide used initially for the batch melting of the prepared samples, are reported in Table 2.1. There is a decrease in the density and refractive index with the partial substitution of tellurite by phosphate. This was expected because the reported phosphate glasses have a refractive index ∼ 1.5 compared to ∼ 2.1 of tellurite glasses. Differential scanning calorimetric (DSC) graph given

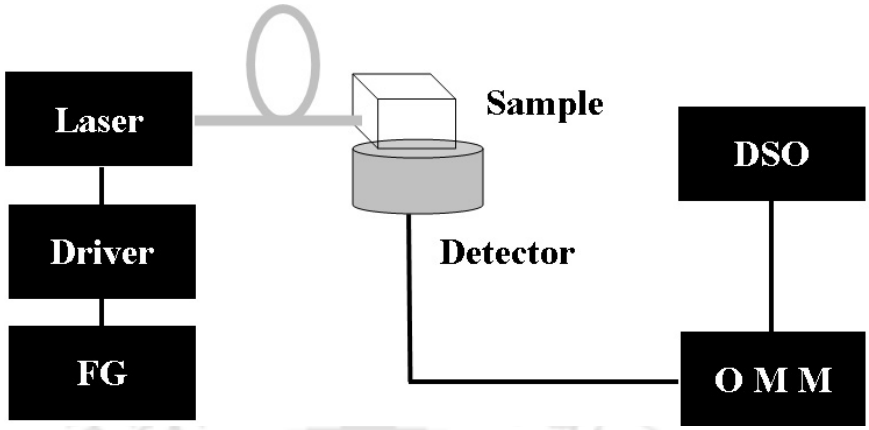

Figure 2.1: The schematic diagram of the lifetime measurement setup where 1 is the optical pumping of a fibre coupled 980 nm diode laser modulated by a function generator (FG), 2 denotes the sample and 3 represents an InGaAs detector connected to an optical multimeter (OMM) to the digital storage oscilloscope (DSO).

in Figure 2.2 show that the T_g values of the phosphotellurite glasses are much higher than that of the glass without phosphate (NT). The glass transition temperature T_g obtained from DSC measurement for all the samples are reported in Table 2.1. The results obtained with DSC shows that the T_g values of phosphotellurite glasses are much higher than that of the sodium tellurite glass (NT) (Table 2.1)making them suitable for planar waveguide fabrication by ion-exchange. This would be advantageous for the optical fibre fabrication using this glass.

2.4 Bulk phonon energy

In order to study the phonon energy of the new glass samples, we compared their infrared (IR) transmittance spectrum. The IR transmittance spectrum of all the glass samples are shown in Fig 2.3 for wavenumber $\bar{\nu}$, in the range 500 cm^{-1} to 1500 cm^{-1}. The observed absorption bands and the assignment of those bands to the vibrational bonds present in the glass matrix are given in Table 2.2. The highest phonon energy obtained

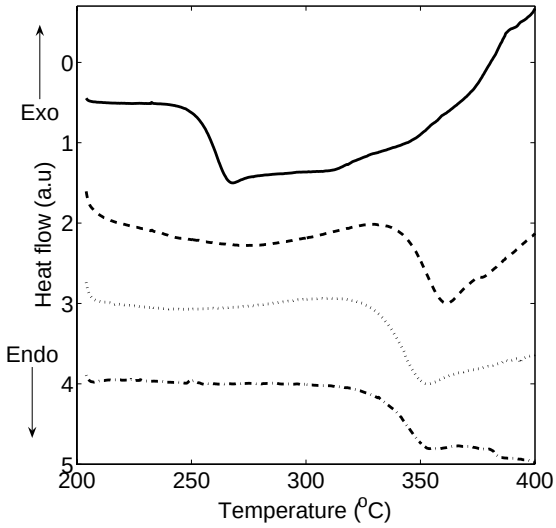

Figure 2.2: DSC scan of NT(solid), NPT1(dash), NPT2(dot) and LPT(dash-dot)

from the spectrum for all the samples are obtained from table.

The absorption band peaked at ∼634 cm^{-1} with a shoulder at ∼760 cm^{-1} of different tellurite vibrational bonds in NT became narrower in the NPTx (x =1,2) glass and in the LPT glass two well resolved peaks at ∼641 cm^{-1} and ∼739 cm^{-1} are observed instead. This band is due to the asymmetric stretching (as-s) of the vibrational bonds O-Te-O or Te-O^-, and group bonds of [TeO_6] [32]. The highest bulk phonon energy of the sample

Sample ID	phosphate		peaks	tellurite	peaks
NT	..	..	..	760(sh)	635(s)
NPT1	1290(s)	1096(s)	970(s)	..	642(s)
NPT2	1270(sh)	1093(s)	963(s)	..	634(s)
LPT	1290(sh)	1086(sh)	946(sh)	744(s)	640(s)
Vibrational Bonds	$^-$O-P-O$^-$ (as-s)	P-O-P (as-s)	P-O-P (as-s)	O-Te-O Te-O$^-$(as-s)	[TeO_6] (g)

Table 2.2: Peak transmittance wavenumber in cm^{-1} obtained from the IR spectra of NT, NPT1, NPT2 and LPT. as-s=asymmetric stretching, g=group, s=strong peak, sh=shoulder

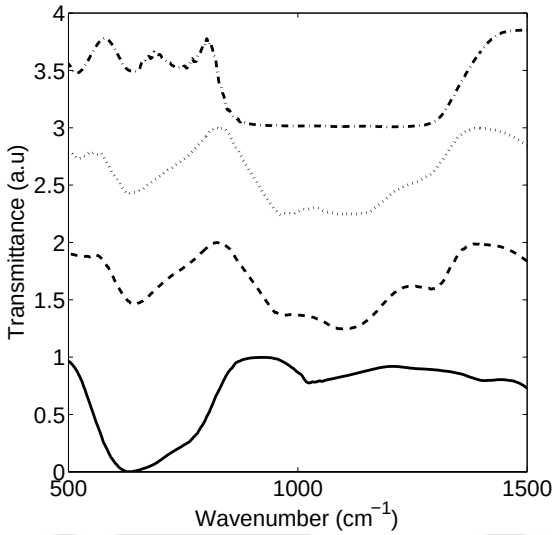

Figure 2.3: Infra-red transmittance spectrum of NT(solid), NPT1(dash), NPT2(dot) and LPT(dash-dot)

NT is ∼760 cm^{-1}. The bands due to the vibration bonds of P-O-P(as-s) peaked around ∼1100 cm^{-1}, ∼920 cm^{-1} and O-P-O(as-s) peaked around ∼1290 cm^{-1} are distinguishable in the spectrum of NPTx series. However these absorptions are overlapped in LPT and appears as single broad absorption band. Therefore the maximum phonon energy of the phosphotellurite glasses is obtained as ∼1290 cm^{-1} which is higher than that of the sodium tellurite (NT) glass and many other tellurite hosts, and less than only to boro-tellurite glass reported in literature [50]. The advantage of phosphate glasses over borate in terms of lower nonradiative decay from the lasing level $^4I_{13/2}$ to the ground level is immanent from Fig. 2.4 as reported in Ref.[7]. From the figure it is clear that there is a large probability of depopulation of the excited atoms in the lasing level E_2 via multiphonon relaxation in borate glasses because of there much higher phonon energy. However, it is worth mentioning that there is a substantial decrease in the nonradiative decay lifetime of the $^4I_{11/2}$ level of the Er^{3+} ions in NPTx and LPT comparing to NT. This would make 980 nm pumping

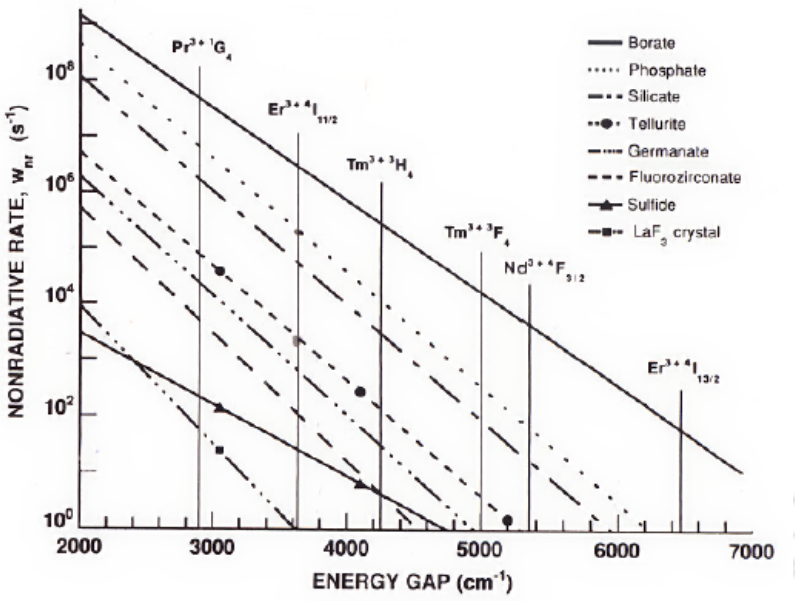

Figure 2.4: Nonradiative relaxation rate as a function of energy gap for the indicated glasses [7]

suitable for erbium doped amplifier and laser operating in the 1.5 μm fabricated using phosphotellurite glass.

Sample ID	Energy gap $\Delta E(cm^{-1})$	Highest Phonon Energy (cm^{-1})	Number of Phonon (p)	τ_{NR}
NT	3720	~ 760	5	$\sim 3ms$
NPT1	3695	~ 1290	3	$\sim 1\mu s$
NPT2	3695	~ 1270	3	$\sim 1\mu s$
LPT	3695	~ 1290	3	$\sim 1\mu s$

Table 2.3: Highest phonon energy and nonradiative lifetime(τ_{NR}) of $^4I_{11/2} \rightarrow ^4 I_{13/2}$ transition of all the samples.

2.5 Multiphonon relaxation

The multiphonon decay rate between $4f^n$ levels of rare earth ions in different types of glasses occur in a very similar way. The dependence of nonradiative decay rate from excited state to next nearest lower state $W_{NR}(T)$ on temperature T, and the number of phonons p is given by [111]

$$W_{NR}(T) \simeq A(1+n)^p exp[-\beta(p-2.4)] \tag{2.1}$$

and

$$n = (exp(\hbar\omega/KT) - 1)^{-1} \tag{2.2}$$

where $A \simeq 10^7 s^{-1}$, and $\beta \simeq 4.0$ for glasses. The values of A and β are obtained empirically for glasses as reported in the reference. The value of A approximately correspond to the $W_{NR}(0)$ at p=2.4 where $p = \Delta E/\hbar\omega$, is the number of phonons bridging the energy gap ΔE. $\hbar\omega$ is the maximum phonon energy of the RE host. The nonradiative decay lifetime $\tau_{NR} = \frac{1}{W_{NR}}$, of the $^4I_{11/2}$ level in oxide glass can be calculated using Eq.(2.1). The $^4I_{11/2} \rightarrow {}^4I_{13/2}$ energy gap ΔE, of Er^{3+} in each glass was obtained from the difference in peak absorption energies corresponding to $^4I_{15/2} \rightarrow {}^4I_{13/2}$ and $^4I_{15/2} \rightarrow {}^4I_{11/2}$ transitions and is reported in Table 2.3. The calculated number of phonons and nonradiative decay lifetime τ_{NR} for all the samples are also reported in the table. The number of phonons bridging the energy gap in phosphotellurite glasses has been decreased to three comparing to five in NT, and τ_{NR} value is $\sim 1\ \mu s$ for NPT1, NPT2 and LPT. This lower value of τ_{NR} would reduce the excited state absorption from $^4I_{11/2}$ under 980 nm excitation and hence the upconversion fluorescence around ~540 nm from the upper $^4S_{3/2}$ and $^2H_{11/2}$ levels of Er.

2.6 Absorption and emission cross-sections

The absorption cross-section of Er^{3+} ions in the samples around 980 nm and 800 nm is important because these are the conventional pump wavelengths of the Er doped glass lasers and amplifiers. The absorption cross-section spectrum of the samples in the 980 nm ($^4I_{15/2} \rightarrow {}^4I_{11/2}$) and 800 nm ($^4I_{15/2} \rightarrow {}^4I_{9/2}$) band is given Figs. 2.5 and 2.6 respectively. The peak absorption wavelength, experimental oscillator strength, absorption cross-section and effective bandwidth are given in Tables 2.4, and 2.5 for all samples together with the values reported in the literature for some other glasses. The peak absorption wavelength is shifted to 979 nm in phosphotellurite glasses from 976 nm in NT. The peak absorption cross-section around 980 nm is higher in NT, but the bandwidth is comparable in all four glasses. Peak cross-section at 980 nm for a phosphotellurite glass is less than that of the reported values of Phosphate L28 and Al/P Silica. However the bandwidth for this transition is higher in the present tellurite compositions than that of this glass. The 800 nm peak absorption cross-sections and bandwidths in the new glasses is less than that at 980 nm. The possibility of high excited state absorption from $^4I_{13/2} \rightarrow {}^2H_{11/2}$ due to the higher lifetime of the $^4I_{13/2}$ level in a phosphotellurite glass, the 800 nm pumping is not preferable in these glasses. The 980 nm absorption band has a rather flat top $\sim$ 10 nm width in NPTx and LPT comparing to the narrow peak of NT allowing more tunability to the pump wavelength. The higher cross-section at 980 nm together with the low nonradiative decay lifetime of the pump level of Na and Li, is advantageous for making amplifiers and lasers pumped by 980 nm laser diode. Absorption cross-section spectra is obtained from the measured absorption spectra using Eq.(1.1). The absorption cross-section spectrum of the glass samples for $^4I_{15/2} \rightarrow {}^4I_{13/2}$ transition is shown in Fig 2.7.

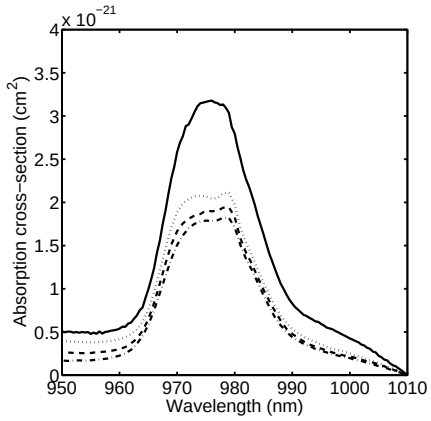

Figure 2.5: Absorption cross-section spectra around 980 nm for samples NT(solid), NPT1(dash), NPT2(dot) and LPT(dash-dot).

Sample ID	Peak Wavelength [nm]	Oscillator Strength $\times 10^{-6}$	$\sigma_a(peak)$ $\times 10^{-22}$ $[cm^2]$	Effective Bandwidth [nm]
NT	976	0.91	31.8	22.8
NPT1	979	0.54	19.4	22.6
NPT2	979	0.51	21.1	23.6
LPT	979	0.53	18.2	21.9
Al/P Silica[7]	978.6	0.64	31.2	16.6
Silicate L22[7]	980.8	0.20	9.5	22.1
Phosphate L28[7]	978.8	0.49	24.7	18.1

Table 2.4: The peak wavelength of absorption for $^4I_{15/2} \rightarrow ^4 I_{11/2}$ transition, Oscillator strength measured from the absorption spectra, peak absorption cross-sections σ_a and effective bandwidths of absorption spectrum $\Delta\lambda_a$ are listed for the samples NT, NPT1, NPT2, LPT and for few other glasses reported in literature

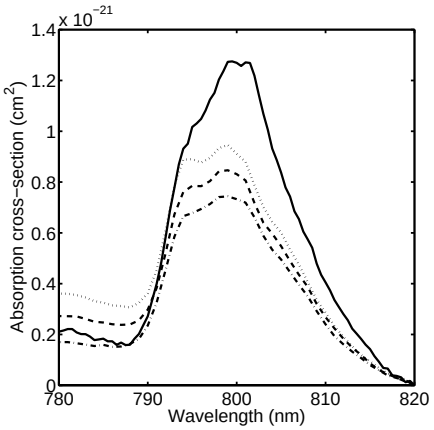

Figure 2.6: Absorption cross-section spectra around 800 nm for all samples NT(solid), NPT1(dash), NPT2(dot) and LPT(dash-dot).

Sample ID	Peak Wavelength [nm]	Oscillator Strength $\times 10^{-6}$	$\sigma_a(peak)$ $\times 10^{-22}$ $[cm^2]$	Effective Bandwidth [nm]
NT	799	0.38	12.70	16.7
NPT1	799	0.23	8.46	19.0
NPT2	799	0.23	9.46	19.4
LPT	799	0.20	7.44	18.4
Al/P Silica[7]	793.8	0.30	8.83	22.2
Silicate L22[7]	796.6	0.12	4.17	19.4
Phosphate L28[7]	798.6	0.25	10.7	15.2

Table 2.5: The peak wavelength of absorption for ${}^4I_{15/2} \rightarrow {}^4 I_{9/2}$ transition, Oscillator strength measured from the absorption spectra, peak absorption cross-sections σ_a and effective bandwidths of absorption spectrum $\Delta\lambda_a$ are listed for the samples NT, NPT1, NPT2, LPT and for few other glasses reported in literature

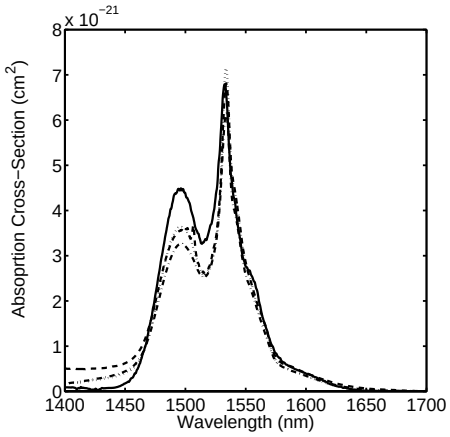

Figure 2.7: Absorption cross-section spectra of NT(solid), NPT1(dash), NPT2(dot) and LPT(dash-dot) plotted from wavelength λ= 1400 nm to 1700 nm

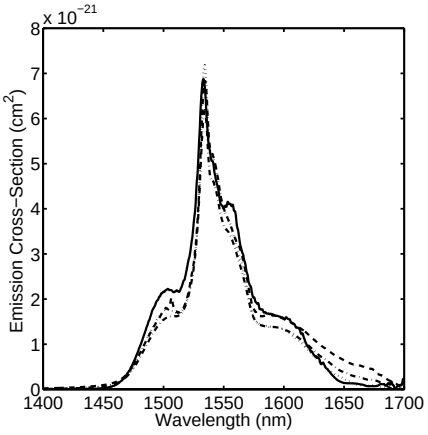

Figure 2.8: Emission cross-section of NT(solid), NPT1(dash), NPT2(dot) and LPT(dash-dot) plotted from wavelength λ= 1400 nm to 1700 nm

Stimulated emission cross-sections at 1.5 μm can be calculated using reciprocity method [83, 112, 113]. According to this, the absorption and emission cross-sections are related as,

$$\sigma_e = \sigma_a \exp[(\epsilon - h\nu)/KT] \tag{2.3}$$

where σ_a and σ_e are the absorption and stimulated emission cross-sections, ν is the photon

Sample ID	$\sigma_a(peak)$ $\times 10^{-21}[cm^2]$	Effective $\Delta\lambda_a[nm]$	$\sigma_e(peak)$ $\times 10^{-21}[cm^2]$	Effective $\Delta\lambda_e[nm]$
NT	6.8	58.3	6.9	58.7
NPT1	6.8	57.2	6.8	58.6
NPT2	7.2	50.8	7.2	49.7
LPT	6.2	55.4	6.2	55.8
Al/P Silica[7]	5.5	–	5.5	43.3
Silicate L22[7]	5.8	–	7.3	–
Phosphate[24]	6.6	–	6.6	46

Table 2.6: The peak absorption and emission cross sections $\sigma_{a,e}$ for ${}^4I_{15/2} \leftrightarrow {}^4I_{13/2}$ transition and effective bandwidths of absorption and emission spectrum $\Delta\lambda_{a,e}$ are listed for the samples NT, NPT1, NPT2, LPT and for few other glasses reported in literature

frequency, ϵ is the net free energy required to excite one erbium ion from ${}^4I_{15/2}$ ground state to the ${}^4I_{13/2}$ level at T K temperature, h the Plank's constant and k the Boltzmann constant. The value of ϵ taken using the method given by Miniscalco [114] and KT=200 cm^{-1} has been used for calculation. The emission cross-section spectra of the studied glasses for ${}^4I_{13/2} \rightarrow {}^4I_{15/2}$ transition are shown in Fig 2.8. The effective bandwidth $\Delta\lambda_{a,e}$ of the absorption and emission spectrum for the ${}^4I_{15/2} \leftrightarrow {}^4I_{13/2}$ transition of the Er ions are defined as,

$$\Delta\lambda_{a,e} = \frac{\int \sigma_{a,e}(\lambda)d\lambda}{\sigma_{a,e_{peak}}} \tag{2.4}$$

where $\sigma_{a,e}$ is absorption or calculated emission cross-sections and $\sigma_{a,e_{peak}}$ is the peak absorption or emission cross-section. Table 2.6 reports the absorption and emission cross sections of ${}^4I_{15/2} \leftrightarrow {}^4I_{13/2}$transitions at peak wavelength and effective bandwidths of absorption and emission cross section spectrum for all the samples in the 1.5 μm. The values reported in literature for Al/P Silica, Silicate L22 and phosphate are also given in table.

The peak absorption cross-section $\sigma_a(\times 10^{-21} cm^2)$ for NT, NPT1, NPT2 and LPT are 6.8, 6.8, 7.2, 6.2 respectively. Peak value of NPT1 is comparable to that of the NT and that of LPT is lower comparing to NPT1 and NT. The σ_a reported for NPT1 is higher com-

paring to Al/P Silica, Al-Silicate and phosphate glasses [7, 24]. The σ_e of phosphotellurite glasses are greater than that of reported glasses in the table except Silica L22. However the replacement of the alkali ion sodium by lithium in phosphotellurite glasses decreased the cross-sections. Even though the cross-sections for NT and NPT1 is almost same, by varying the phosphate/tellurite ratio this may change. The absorption and emission bandwidths reported in Table 2.6 shows that they all vary from 55 nm to 60 nm. In particular, the bandwidths for NPT1 and NT are almost equal. All four glasses studied in the present work have higher emission bandwidth comparing to the glasses and glass fibres reported in the table. It is apparent that the addition of phosphate is not changing the bandwidth of the Er^{3+} in the tellurite glass host largely, making them suitable candidates for broadband amplifiers operating in the C and L bands of optical communication.

The peak emission cross-sections and the bandwidths for all the sample are reported in Table 2.6. The effective bandwidths ($\Delta\lambda_{a,e}$) of NT, NPT1 and LPT are almost same however that of NPT2 is lower. So the bandwidth of the sodium tellurite glass has been retained with the addition of 30% phosphate. The absorption and emission cross-sections of NT, NPT1 and LPT differ very little, whereas that of NPT2 is slightly high. The phosphotellurite glass with 30% P_2O_5 is good for device fabrication as it preserves the bandwidth and cross-sections of sodium-tellurite glass and have higher phonon energy and T_g.

2.7 Judd-Ofelt analysis and quantum efficiency

The knowledge of the Judd-Ofelt (JO) intensity parameters $\Omega_t, (t = 2, 4, 6)$ of the Er^{3+} in phosphotellurite glass is important for the understanding of the relationship between the host glass and Er^{3+} emission properties. They are important for investigation

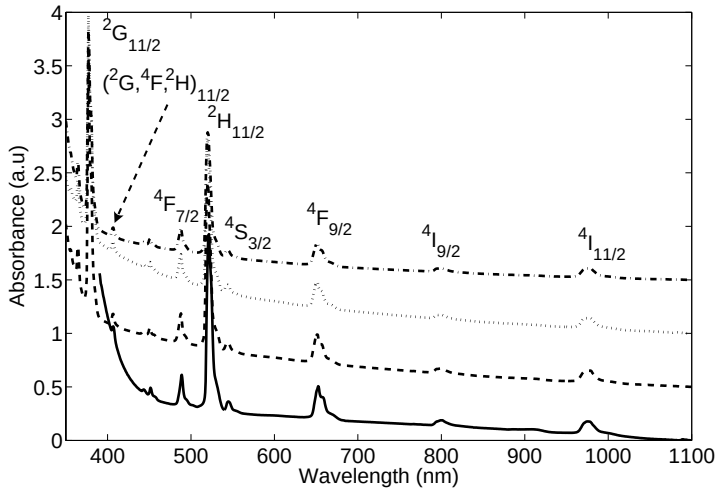

Figure 2.9: The room temperature absorption spectrum of the samples NT(solid), NPT1(dash), NPT2(dot) and LPT(dash-dot) in the wavelength range λ= 350 nm to 1100 nm. Transitions from $^4I_{15/2}$ of Er^{3+} corresponding to different absorption peaks is shown

of the local structure and bonding in the vicinity of rare earth ions. JO parameters can be derived from the electric and magnetic dipole contributions of the experimental oscillator strengths (P_{exp}) using a least-square fitting. The procedure given in Chapter 1 were followed for JO calculations. The UV-VIS absorption spectrum of the samples is shown in Fig 2.9 in the wavelength range 350 nm to 1100 nm. The absorption spectra of the samples (NPT1, NPT2, LPT) given in the figure indicates a blueshift of ∼60 nm the absorption edge of phosphotellurite glasses comparing to NT and other reported tellurite glasses [39, 40, 41, 42, 43]. The addition of P_2O_5 has clearly extended the transparency of the glass toward ultraviolet region. For Judd-Ofelt [78, 79] analysis, nine absorption bands corresponding to the absorptions from the ground state $^4I_{15/2}$ to the excited states $^4I_{13/2}$, $^4I_{11/2}$, $^4I_{9/2}$, $^4F_{9/2}$, $^4S_{3/2}$, $^2H_{11/2}$, $^4F_{7/2}$, $(^2G,^4F,^2H)_{9/2}$, $^4G_{11/2}$, respectively are taken into account. These transitions are labelled in the figure and the wavenumbers corresponding to the absorption peaks of the different transitions are used in the calculations.

Transition from to $^4I_{15/2}$	U(2)	U(4)	U(6)
$^4I_{15/2}$	–	–	–
$^4I_{13/2}$	0.0195	0.1173	1.4316
$^4I_{11/2}$	0.0282	0.0003	0.3953
$^4I_{9/2}$	0	0.1733	0.0099
$^4F_{9/2}$	0	0.5354	0.4618
$^4S_{3/2}$	0	0	0.2211
$^2H_{11/2}$	0.7125	0.4125	0.0925
$^4F_{7/2}$	0	0.1469	0.6266
$(^2G,^4F,^2H)_{9/2}$	0	0.0189	0.2256
$^4G_{11/2}$	0.9183	0.5262	0.1172

Table 2.7: Matrix elements $U^{(\lambda)}$ for Er^{3+}(aq) [80], where $U(\lambda) =< \psi J \parallel U^{(\lambda)} \parallel \psi' J' >$

The reduced matrix elements used in the calculation of JO parameters were taken from Ref.[81] and are given in Table 2.7. The JO parameters are then used to obtain the calculated oscillator strengths (P_{cal}). The P_{exp} and P_{cal} of different allowed transitions of Er^{3+} for all samples are given in Table 2.8. The values of P_{exp} and P_{cal} given in the table show only minor variations from sample to sample. The peak wavelength of transition from ground state for erbium ions in phosphotellurite glasses are different from that of NT. A measure of the accuracy of the fitted values of the JO parameters are given by the root-mean-square(rms) deviation $\delta_{rms} = [\sum_{i=1}^{n}(P_{cal} - P_{exp})^2 \frac{1}{q-p}]^{-1/2}$, where q is the number of spectral bands analyzed and p is the number of parameters sought, which is three in our case. JO parameters are then used to calculate the radiative lifetime of an emitting state using Eq(1.10). The values of the Judd-Ofelt intensity parameters Ω_t, rms deviation δ_{rms} are reported in Table 2.9. The rms deviation δ_{rms} is less for NPTx and LPT comparing to NT because of the inclusion of two more transitions ($^4I_{15/2} \rightarrow$ $(^2G,^4F,^2H)_{9/2}$ & $^4G_{11/2}$) in the calculation. The inclusion of these transitions were possible in these samples because of the increased transparency of the phosphotellurite glasses.

Sample ID	→	NT		→	NPT1	
Absorption $^4I_{15/2} \rightarrow$	Energy $[cm^{-1}]$	P_{exp} $\times 10^{-6}$	P_{cal} $\times 10^{-6}$	Energy $[cm^{-1}]$	P_{exp} $\times 10^{-6}$	P_{cal} $\times 10^{-6}$
$^4I_{13/2}$	6526	1.20	0.89	6520	0.84	0.69 $[P_{ed}]$
			0.65			0.62 $[P_{md}]$
$^4I_{11/2}$	10246	0.91	2.45	10215	0.54	1.72
$^4I_{9/2}$	12477	0.38	0.71	12516	0.23	0.37
$^4F_{9/2}$	15326	2.71	3.08	15361	1.44	1.76
$^4S_{3/2}$	18332	0.58	0.24	18382	0.39	0.22
$^2H_{11/2}$	19157	13.43	13.10	19231	8.41	8.56
$^4F_{7/2}$	20450	2.04	1.72	20492	1.47	1.19
$(^2G,^4F,^2H)_{9/2}$	..	..	..	24570	0.54	0.37
$^4G_{11/2}$	..	..	..	26525	15.41	15.19
Sample ID	→	NPT2		→	LPT	
Absorption $^4I_{15/2} \rightarrow$	Energy $[cm^{-1}]$	P_{exp} $\times 10^{-6}$	P_{cal} $\times 10^{-6}$	Energy $[cm^{-1}]$	P_{exp} $\times 10^{-6}$	P_{cal} $\times 10^{-6}$
$^4I_{13/2}$	6520	1.05	0.73	6520	0.94	0.71 $[P_{ed}]$
			0.65			0.62 $[P_{md}]$
$^4I_{11/2}$	10215	0.51	1.80	10215	0.53	1.61
$^4I_{9/2}$	12516	0.23	0.43	12516	0.20	0.38
$^4F_{9/2}$	15361	1.67	1.98	15361	1.56	1.82
$^4S_{3/2}$	18382	0.38	0.22	18382	0.35	0.22
$^2H_{11/2}$	19231	8.63	9.14	19231	7.73	8.09
$^4F_{7/2}$	20492	1.49	1.29	20492	1.42	1.23
$(^2G,^4F,^2H)_{9/2}$	24570	0.51	0.39	24570	0.53	0.39
$^4G_{11/2}$	26525	16.65	16.22	26525	14.68	14.35

Table 2.8: Experimental and calculated oscillator strengths of erbium ions for all the samples.

The parameters Ω_2, Ω_4 depends on the local symmetry of the Er^{3+} ions, and Ω_6 depends upon the local basicity of the rare earth sites [77]. The decrease in the Ω_2, Ω_4 parameters after adding phosphate is an indication of the local structure modification of the glass host which we also discussed before on the basis of IR spectra of the samples. The Ω_6 values are almost same for all four glasses. The replacement of Na^+ by Li^+ decreased the value of Ω_2 parameter. A comparison of τ_{JO} of phosphotellurite glasses with that of NT given in Table 2.9 show that the addition of phosphate increased the radiative lifetime of

Sample ID	Ω_2 ×	Ω_4 10^{-20}	Ω_6 $[cm^2]$	δ_{rms} $(\times 10^{-6})$	τ_{JO} ms	τ_r ms	τ_m ms	$\eta = \frac{\tau_m}{\tau_{JO}}$ %
NT	5.18	2.02	0.40	0.92	4.7	3.3	2.5	53
NPT1	3.84	1.24	0.39	0.56	6.1	4.1	4.0	66
NPT2	4.07	1.44	0.41	0.52	6.0	4.5	4.1	68
LPT	3.53	1.28	0.40	0.54	5.9	3.6	3.4	58

Table 2.9: Omega parameters of NT, NPT1, NPT2 and LPT

Transitions		Avg freq $[cm^{-1}]$	A_{ed} $[s^{-1}]$	A_{md} $[s^{-1}]$	β	τ_{JO} $[ms]$
$^4I_{13/2} \rightarrow$	$^4I_{15/2}$	6526	127.4	86.8	1	4.7
$^4I_{11/2} \rightarrow$	$^4I_{15/2}$	10246	188.4	..	0.795	4.2
	$^4I_{13/2}$	3720	29.1	19.4	0.205	
$^4I_{9/2} \rightarrow$	$^4I_{15/2}$	12477	518.6	..	0.915	
	$^4I_{13/2}$	5951	45.1	..	0.080	1.8
	$^4I_{11/2}$	2231	..	2.8	0.005	

Table 2.10: Calculated spontaneous radiative transition rates, branching ratios and lifetime of erbium ions in NT glass

the $^4I_{13/2}$ level of Er^{3+} in those glasses by ∼1 ms. However there is no appreciable change in the branching ratios. This indicates that higher rare earth doping levels are possible in phosphotellurite glasses comparing to many other tellurite based glasses. The spontaneous radiative transition probabilities (both electric dipole and magnetic dipole), the branching ratios and the lifetimes of different erbium levels of NT is reported in Table 2.10 and that of NPT1, NPT2 and LPT in Table 2.11, 2.12 and 2.13 respectively.

The radiative lifetime τ_r can also be calculated from absorption cross-section spectrum, which is reported to have less error than τ_{JO} [115]. For a simple two level system with 1 and 2 be the ground ($^4I_{15/2}$) and excited ($^4I_{13/2}$) state respectively, the radiative lifetime, τ_r, of the excited state is given by,

$$\tau_r = \frac{1}{A_{21}} \tag{2.5}$$

Transitions		Avg freq $[cm^{-1}]$	A_{ed} $[s^{-1}]$	A_{md} $[s^{-1}]$	β	τ_{JO} $[ms]$
$^4I_{13/2} \rightarrow$	$^4I_{15/2}$	6520	89.4	75.00	1	6.1
$^4I_{11/2} \rightarrow$	$^4I_{15/2}$	10215	135.4	..	0.793	5.7
	$^4I_{13/2}$	3695	18.58	16.76	0.207	
$^4I_{9/2} \rightarrow$	$^4I_{15/2}$	12513	247.4	..	0.863	
	$^4I_{13/2}$	5996	36.8	..	0.128	3.5
	$^4I_{11/2}$	2301	..	2.4	0.008	

Table 2.11: Calculated spontaneous radiative transition rates, branching ratios and lifetime of erbium ions in NPT1 glass

Transitions		Avg freq $[cm^{-1}]$	A_{ed} $[s^{-1}]$	A_{md} $[s^{-1}]$	β	τ_{JO} $[ms]$
$^4I_{13/2} \rightarrow$	$^4I_{15/2}$	6520	93.4	73.88	1	6.0
$^4I_{11/2} \rightarrow$	$^4I_{15/2}$	10215	139.2	..	0.794	5.7
	$^4I_{13/2}$	3695	19.8	16.5	0.206	
$^4I_{9/2} \rightarrow$	$^4I_{15/2}$	12513	281.9	..	0.876	
	$^4I_{13/2}$	5996	37.7	..	0.117	3.1
	$^4I_{11/2}$	2301	..	2.4	0.007	

Table 2.12: Calculated spontaneous radiative transition rates, branching ratios and lifetime of erbium ions in NPT2 glass

Transitions		Avg freq $[cm^{-1}]$	A_{ed} $[s^{-1}]$	A_{md} $[s^{-1}]$	β	τ_{JO} $[ms]$
$^4I_{13/2} \rightarrow$	$^4I_{15/2}$	6520	92.3	75.9	1	5.9
$^4I_{11/2} \rightarrow$	$^4I_{15/2}$	10215	135.0	..	0.789	5.9
	$^4I_{13/2}$	3695	19.81	16.96	0.211	
$^4I_{9/2} \rightarrow$	$^4I_{15/2}$	12513	259.0	..	0.863	
	$^4I_{13/2}$	5996	38.4	..	0.127	3.3
	$^4I_{11/2}$	2301	..	2.4	0.008	

Table 2.13: Calculated spontaneous radiative transition rates, branching ratios and lifetime of erbium ions in LPT glass

where A_{21} is the spontaneous emission probability between two states (Einstein A Coefficient). A_{21} can be calculated using wavenumber dependent absorption cross-section, given by

$$A_{21} = \frac{g_1}{g_2} 8\pi c n^2 \bar{\nu_b^2} \int \sigma_a(\bar{\nu}) d\bar{\nu} \tag{2.6}$$

where g_1, g_2 are the degeneracies of state 1 and 2, c is the velocity of light, n is the refractive index of the medium, $\bar{\nu_b}$ is the barycenter of the absorption band. In the calculations for the transition $^4I_{13/2} \rightarrow^4 I_{15/2}$ the barycenter of NT, NPT1, NPT2 and LPT are taken as 6606 cm^{-1}, 6595 cm^{-1}, 6597, and 6595 cm^{-1} respectively. The obtained values of τ_r are given in Table 2.9. Calculated τ_r value for phosphotellurite glasses are higher than that of NT. It is reported that the uncertainty of τ_r calculated using Eqs. (2.5) and (2.6) are at least one order of magnitude less than those of τ_{JO} [115].

The quantum efficiency of the reported glass samples are obtained using $\eta = \frac{\tau_m}{\tau_{JO}}$ and the values are given in Table 2.9. τ_m is the measured lifetime of $^4I_{13/2}$ given in the table. The quantum efficiency of the phosphotellurite glasses are higher than that of NT glass, which indicates that they are better host for the high concentration erbium doping without concentration quenching for the amplification at 1550 nm under 980 nm pumping. NPT1 and NPT2 have almost same quantum efficiency. It was also observed that the physical, thermal and spectroscopic properties in NPT1 is better than other samples. Therefore the phosphate concentration of 30% is the best among the investigated samples for laser applications.

2.8 Conclusion

Erbium doped phosphotellurite glasses and sodium tellurite glass has been made by melt quenching technique. The physical properties of the glasses like density, refractive

index and glass transitions temperature has been measured and reported. The T_g of the phosphotellurite glass is found to be higher than the many other tellurite glasses. The addition of phosphate in the tellurite glass has increased the phonon energy of the tellurite glass up to 1290 cm^{-1}. The absorption spectra shows that there is a blueshift of the absorption edge of phosphotellurite glasses comparing to NT. Thus the transparency range of the tellurite glass in the UV-VIS has been increased and three more Er^{3+} absorption peaks included in JO calculation. The Ω_2, Ω_4 parameters of phosphotellurite glasses has been decreased comparing to NT, but Ω_6 does not show any considerable change. Spontaneous radiative transition probabilities A_{ed}, A_{md}, branching ratios β and the lifetimes τ_{JO} of different erbium levels has been calculated. The absorption and stimulated emission cross-sections $\sigma_{a,e}$, effective bandwidths $\Delta\lambda_{a,e}$, lifetime τ_r of the 1.5 μm transition has been calculated from the absorption spectra. The peak absorption and emission cross-sections of all samples vary little. The calculated radiative lifetime of the phosphotellurite glasses is high comparing to sodium tellurite glass. The physical, thermal and spectroscopic properties of erbium doped phosphotellurite glasses suggests that they can be potential candidate for fibre as well as integrated optical amplifiers and lasers at $\sim$1.5 μm under 980 nm optical pumping.

Chapter 3

Structural analysis of thermal and optical properties

Different series of phosphotellurite glasses were prepared by varying the glass composition. Differential scanning calorimetric measurements show the glass transition temperature T_g decreases with the decrease in the Na_2O concentration. An analysis based on FTIR spectra is used to explain the behaviour of T_g. The fluorescence bandwidth increases with the increase in concentration of sodium as well as erbium. The decrease in bandwidth with addition of phosphate in tellurite is discussed on the basis of the analysis of fluorescence spectra. We have observed the decrease in $TeO_{3+\delta}$ and TeO_3 units present in the glass compared to tellurite glass. A model is proposed for the structure of Er doped phosphotellurite glasses. We have optimized the Er_2O_3 concentration for this glass and have found that 0.25 Er concentration is having highest emission cross-section (σ_e) and emission lifetime (τ_f). Addition of Yb_2O_3 has increased the τ_f but σ_e has decreased. Gain ($\sim \sigma_e \times \tau_f$) is higher for Er-Yb codoped glasses.

3.1 Introduction

Rare earth (RE) ions played the role of a probe for local structural variations in glasses because of the unique spectroscopic properties resulting from the optical transitions in the intra 4f shell. Many rare earth ions including erbium has been used to spectroscopically investigate the structure of different glasses [59]. As we know the laser transitions in rare earth doped glasses greatly depend on the local environment, the design of glass host demands understanding of the structural factors affecting the efficiency of the laser transition. Since the erbium (Er) doped glass fibres have been used widely in optical communication systems as amplifier it is important to understand the factors affecting in particular the gain and gain bandwidth of Er-doped glasses. In Chapter-1 Er-doped phosphotellurite glasses with improved properties such as glass transition temperature, phonon energy, fluorescence lifetime and quantum efficiency were demonstrated comparing to many reported tellurite glass. The reported decrease in fluorescence bandwidth and increase in glass transition temperature need better understanding based on structure. There are reports on the study of the structure of P_2O_5-TeO_2 glasses using different tools [54, 56, 55, 116]. An analysis of the fluorescence and infrared spectra is expected to provide some important information on the modifications in the local structural units in this mixed glass former system. These two spectroscopic methods are used in this chapter to investigate the structure of the glass to interpret observed changes in two important parameters, T_g and fluorescence bandwidth, with glass composition.

The thermal and optical properties of PT glasses are further studied by varying Na_2O and Er_2O_3 concentrations. One objective of this study is to find the suitable Na_2O concentration having higher T_g for waveguide fabrication. The Er_2O_3 concentration is then varied to check the concentration quenching and to find the optimum glass composition

Sample ID	Compositions in mole%	T_g (^{o}C)	n @ 633 nm	N_{Er} ($\times 10^{20}$	N_{Yb} -ions/cc)
0Na	$30P_2O_5 - 69.9TeO_2 - 0.1Er_2O_3$	398	2.01	0.30	–
5Na	$A - 64.9TeO_2 - 0.1Er_2O_3$	381	2.00	0.30	–
10Na	$10Na_2O - 30P_2O_5 - 59.9TeO_2 - 0.1Er_2O_3$	354	2.00	0.30	–
15Na	$15Na_2O - 30P_2O_5 - 54.9TeO_2 - 0.1Er_2O_3$	346	2.00	0.28	–
0.25Er	$A - 64.75TeO_2 - 0.25Er_2O_3$	379	2.00	0.76	–
0.5Er	$A - 64.5TeO_2 - 0.5Er_2O_3$	375	2.00	1.54	–
1Er	$A - 64TeO_2 - 1Er_2O_3$	379	2.00	3.20	–
2Er	$A - 63TeO_2 - 2Er_2O_3$	383	2.00	6.46	–
1.5Yb	$A - 63.25TeO_2 - 0.25Er_2O_3 - 1.5Yb_2O_3$	376	2.00	0.80	4.80
1.75Yb	$A - 63TeO_2 - 0.25Er_2O_3 - 1.75Yb_2O_3$	381	2.00	0.80	5.61
NPT1	$19Na_2O - 30P_2O_5 - 80TeO_2 - 1Er_2O_3$	340	1.96	3.42	–
NT	$19Na_2O - 80TeO_2 - 1Er_2O_3$	252	2.10	4.06	–

Table 3.1: where $A = 5Na_2O - 30P_2O_5$. Glass compositions with physical properties like T_g the glass transition temperature, n the refractive index measured at 633 nm, and the Er and Yb ion concentrations in the glasses are reported.

with high emission cross section (σ_e), fluorescence bandwidth ($\Delta\lambda$), fluorescence lifetime τ_f and high quantum efficiency for the Er^{3+} :$^4 I_{13/2} \rightarrow^4 I_{15/2}$ transition. In Er-doped glasses, ytterbium codoping has been attractive because of its good absorption cross-section at 980 nm, which improve the pumping efficiency for erbium lasing transition through energy transfer [117, 118, 119, 110]. It is well known that Yb^{3+} :$^2 F_{7/2} \rightarrow^2 F_{5/2}$ ground state absorption (GSA) wavelength ($\sim$ 980 nm) matches with that of Er^{3+} :$^4 I_{15/2} \rightarrow^4 I_{11/2}$ GSA. In planar waveguide lasers and amplifiers Yb-Er co-doped glass has been in general the obvious preference [24, 15]. The effect of Yb-Er codoping on the fluorescence properties under 980 nm excitation is also studied in the phosphotellurite glass.

3.2 Experiment

Erbium doped and Yb-Er codoped sodium phosphotellurite glass samples are made by melt quenching technique as discussed in section(2.2). High purity chemicals

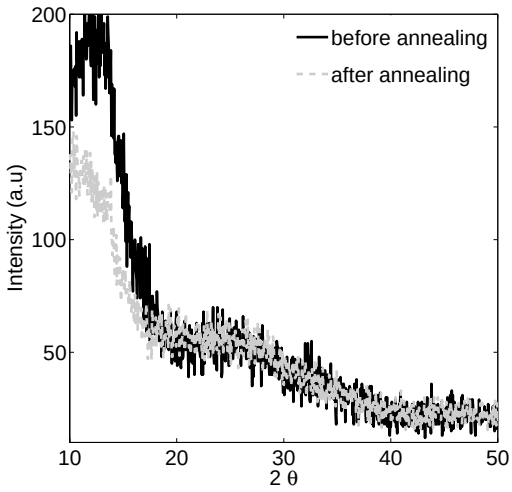

Figure 3.1: XRD pattern of a sample before and after the annealing.

like Na_2CO_3, P_2O_5, TeO_2, Er_2O_3 and Yb_2O_3 are used for the batch melting. The composition of glasses prepared for the study are reported in Table 3.1. NT and NPT1 are glass compositions reported in Chapter-2. The density, refractive index, ionic concentrations of erbium (N_{Er}) and ytterbium (N_{Yb}) in each glass are given in the table. The glass transition temperature T_g, measured using the differential scanning calorimeter (DSC) for all the samples are also reported. The crystallization peaks were not observed in the DSC measurement for the glass samples in the temperature range 300-550^{o}C. The powder X-ray diffraction (XRD) pattern of the glasses annealed at $\sim 510^oC$ for half an hour confirmed the absence of crystallization. A plot of XRD measurement is given in Fig. 3.1 for 1.75Yb. Absorption spectrum and the fluorescence lifetime of the samples are measured. The room temperature fluorescence spectra of the samples are recorded in an optical spectrum analyzer (Agilent 86142B) using a cw 980 nm laser diode (JDS uniphase) as the excitation source. The schematic of the fluorescence measurement setup is shown in Fig. 3.2.

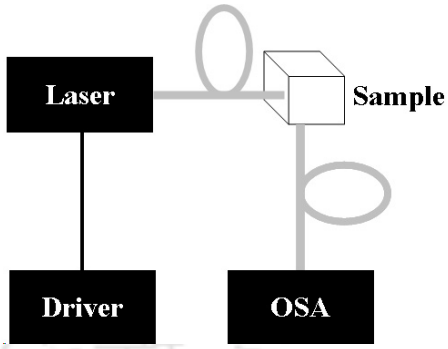

Figure 3.2: Measurement setup used to record the fluorescence lineshape of the doped glasses.

3.3 Glass transition temperature

The glass transition temperature in the mixed glass former system like $P_2O_5{-}TeO_2$ follows an interesting structural dependency. We will discuss this below in the light of IR and DSC results obtained. Before that it is apt to mention the results of Neov et al. presented in an excellent study on the structural aspects of $P_2O_5 - TeO_2$ glasses [54]. According to them in $P_2O_5 - TeO_2$ glasses, when the P_2O_5 content is more than 20%, more and more of the PO_4 units gets into tellurite chains deforming the immediate environment around Te atoms. This conclusion was based on the radial distribution function (RDF) they calculated from neutron diffraction data obtained for the glass. It is worth mentioning that the glass transition temperature, T_g of pure TeO_2 glass is 304^{o}C, whereas the addition of an alkali modifier like Li_2O to the TeO_2, T_g decreases it to 250^{o}C [120]. We observed the same trend for the glass sample NT. It is known that the addition of Na_2O leads to the conversion of TeO_4 trigonal bipyramids (tbp) to TeO_3 trigonal pyramids (tp) with nonbridging oxygens (NBO) [121]. So how to increase the T_g beyond the maximum achievable in pure tellurite glass which is required in many photonic device applications. The phosphate addition is proved to be a practical solution.

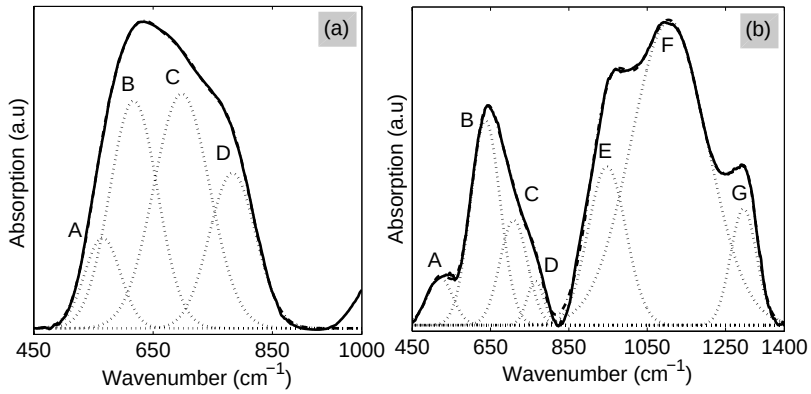

Figure 3.3: (a) IR absorption spectra with peak fit of Sample NT, (b) IR absorption spectra with peak fit of Sample NPT1, where dotted lines are the gaussian fits with the original data plotted in solid lines and dot-dashed lines are the fit to the experimental data.

It can be seen from Table 3.1 that the T_g has increased from 252^{o}C (NT) to 340^{o}C (NPT1). Both glasses contain equal wt% of sodium. We compared the IR spectrum of the NT an NPT1 glasses to understand the influence of phosphate addition on the tellurite glass network. The IR absorption bands for NT and NPT1 glasses are shown in Fig. 3.3(a) and (b) respectively. Depending on the already reported band peaks for tellurite and phosphotellurite glasses we fitted with multiple gaussian peak fitting equation to the IR absorption data and found 4 bands for NT glass and 7 bands for NPT1 glass and they are given in Table 3.2. It is observed that with the addition of phosphate (30%) in tellurite host, both height and bandwidth of bands D and C decreases with respect to B. The C/B ratio has been decreased from 1.04 in NT to 0.51 in NPT1 and the decrease of D/B ratio is from 0.69 to 0.24. This means $TeO_{3+\delta}$ and TeO_3 polyhedra are present in less number in the NPT1 glass network with respect to TeO_4 tbps. This is due to rapture of the glass network by PO_4 tetrahedra incorporated in the chains. The band A in NPT1 glass result

Band ID	Peak cm^{-1}	Height (a.u)	FWHM cm^{-1}
Sample-NT			
A	565	0.30	75
B	617	0.74	100
C	698	0.77	117
D	783	0.51	97
Height Ratio	A/B=0.41	C/B=1.04	D/B=0.69
Sample-NPT1			
A	521	0.16	80
B	637	0.68	95
C	710	0.35	88
D	765	0.16	54
E	948	0.52	121
F	1106	1.00	243
G	1296	0.38	83
Height Ratio	A/B=0.24	C/B=0.51	D/B=0.24

Table 3.2: IR band peaks obtained from deconvoluted spectra. Band A corresponds to the Te-O-Te / Te-O-P vibrations. Band B corresponds to the vibration of continuous TeO_4 tbps in the glass network. Band C corresponds to vibration of Te-O_{NBO} in $TeO_{3+\delta}$ and Te=O_{NBO} in TeO_3. Band D corresponds to the stretching vibration of Te-O_{BO} in $TeO_{3+\delta}$ and TeO_3. Band E corresponds to the asymmetric stretching of P-O-P bridge. Band F corresponds to the vibration of $(PO_4)^{3-}$ polyhedra. Band G corresponds to the $(PO_3)^{2-}$ and $(PO_2)^{-}$ terminal group vibrations.

from both -Te-O-Te- and -Te-O-P- bonds vibrations, and got resolved better than that in the NT glass. The decrease in the ratio A/B is indicative of braking of the chains of -Te-O-Te- and -Te-O-P-. Based on these observation it can be inferred from the IR spectroscopy that the addition of P_2O_5, does not favour formation TeO_3 tp units with NBOs. Therefore the increase of T_g of the NPT1 glass can be attributed to the decrease of TeO_3 units in NPT1 glass compared to NT and also the preferential stability of PO_4 units.

With the increasing amount of P_2O_5 in the tellurite glass two types of bonding is realized as given in ref. [54] and they are depicted in Fig. 3.4. The PO_4 tetrahedra influence glass structure formation considerably stronger than TeO_4 units. In this aspect while the deformation of PO_4 is insignificant, the TeO_4 units suffer a strong deformation.

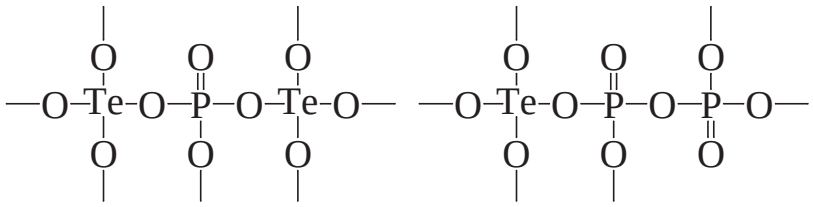

Figure 3.4: Two types of structural units present in P_2O_5:TeO_2 glass [54].

The P atoms distribute themselves between tellurite chains and layers having a marked tendency to preserve their own co-ordinational bonding. It could be concluded that both methods of bonding stimulate the creation of NBO ions of the type [Te-O], while the NBO ions to which the PO_4 group contributes, are predominantly of the [P=O] type. In this context it is appropriate to look at some other reported tellurite systems with mixed glass formers. Addition of glass former doesn't develop TeO_3 tp units with NBOs in germano-tellurite(GT) [55]. In tungsten tellurite (TT) glass, simultaneous presence of TeO_3, TeO_4 units occur along with clusters of WO_6 octahedral [122].

From the data given in Table 3.1 for xNa series, the decrease in the glass transition temperature with increase in the sodium concentration support the argument on the induced structural changes in TeO_2 glass with alkali addition. This will be a major concern in deciding the alkali concentration in the tellurite glass especially when designing glasses for integrated optics. The concentration of sodium was chosen to be 5 mole% for investigating the glasses by varying RE concentration, because of its highest T_g among the sodium containing glasses. The variation of rare earth concentration in the range reported in table has negligible effect on the $T_g(380\pm5^oC)$. We do not observe any crystallization for this glasses against devitrification, which is beneficial for fibre drawing from these glasses.

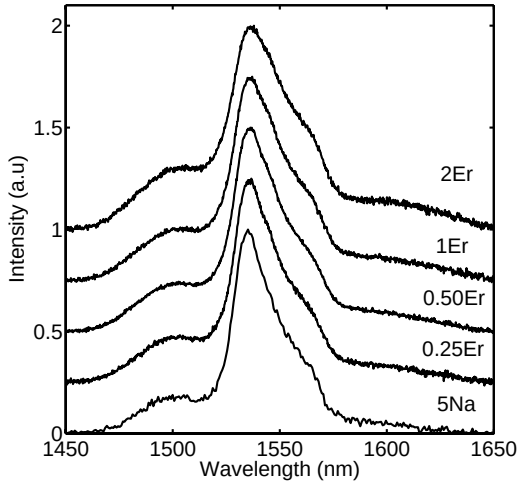

Figure 3.5: Fluorescence spectra for samples having different Er ion concentration.

3.4 Fluorescence bandwidth

The Er fluorescence bands are asymmetric, therefore an effective bandwidth defined by $\Delta\lambda_e = \int I_e(\lambda)d\lambda$ is calculated from the normalized fluorescence intensity, $I_e(\lambda)$. The fluorescence spectra given in Fig. 3.5 shows that the fluorescence bandwidth ($\Delta\lambda_e$) increases with the concentration of erbium. The ytterbium codoping also increased the bandwidth as evident from Fig. 3.6, both 1.5Yb and 1.75Yb glasses shows higher bandwidth comparing to 0.25Er glass without Yb. The variation of $\Delta\lambda_e$ values for samples with Na_2O and Er_2O_3 concentration is shown in Figs. 3.11(a) and (b) (values for all the samples are reported in Table 3.5).

In order to study the structural factors influencing the bandwidth we analyzed the fluorescence spectrum obtained for glasses by varying their compositions. The peak-fit analysis of room temperature fluorescence spectra show that the Stark transitions have different heights and widths. For two glass samples with the different Er concentrations

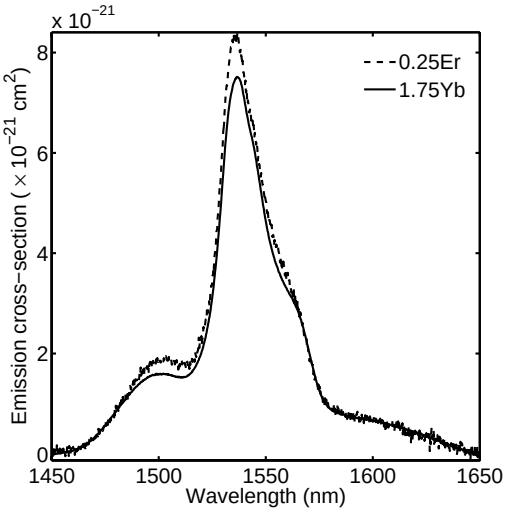

Figure 3.6: Comparison of emission cross-section spectra of two sample 0.25Er and 1.75Yb.

0.1 mole% and 2 mole%, the fitted curve showing the Stark components is depicted in Figures 3.7 (a) and (b). It is reported that inhomogeneous broadening can result from the structural disorder of the glass that causes differences in the ligand electric field at various sites of Er ions and depends on the composition of the glass host [123]. In the present analysis we considered homogeneous broadening and the individual Stark transitions are fitted using gaussian. The Stark components that contribute to the spectrum resolved by peak fit show that 7 peaks fits the curves completely. However, it was observed that on increasing the Er concentration from 0.1 to 2 mole% the different fitted peak wavelengths are almost same but the height and width are different. In particular the height and width of the peak around 1562 nm (peak 6) has increased, while that of 1552 nm (peak 5) peak decreased with more and more Er incorporation. The observed number of peaks is same that observed in the case of zinc-tellurite glasses [123], however the peak positions and heights are different in 0Na and 2Er glass samples.

The variation of the various Stark transitions with the phosphate addition was

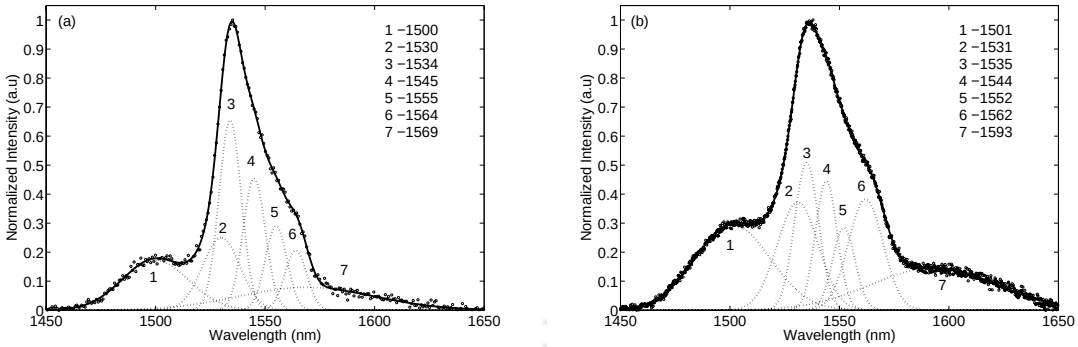

Figure 3.7: The fitted spectral components of the overall emission for the (a) 5Na and (b) 2Er glass samples.

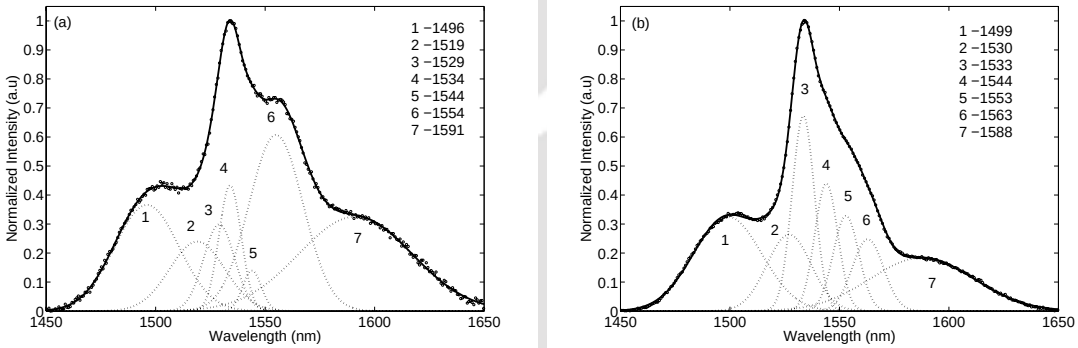

Figure 3.8: The fitted spectral components of the overall emission for the (a) NPT1 and (b) NT glass samples.

studied by comparing the deconvoluted fluorescence spectrum of tellurite (NT) and phosphotellurite (NPT1) glasses. This would provide some information on the origin of bandwidth decrease with the addition of phosphate in tellurite glass. The calculated bandwidth reported for these two samples in the previous chapter is slightly different from that obtained from measured fluorescence spectra which is used in this section for detailed study. The fluorescence bandwidth is 73 nm for NT glass while that of NPT1 is 54 nm. Figure 3.8(a) and (b) shows that the peak at 1554 nm (peak 6) of NT is much stronger than NPT1 glass. In fact the broad peak-6 in NT has been resolved into two peaks (5 and 6) in NPT1. This

is responsible for the smooth downfall of the fluorescence line shape of the NPT1 glass.

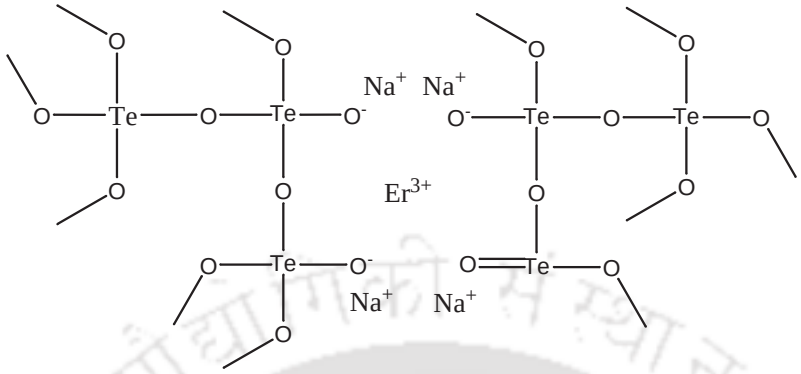

Figure 3.9: Schematic diagram of the local environment of Er in a phosphotellurite glass with 30% P_2O_5.

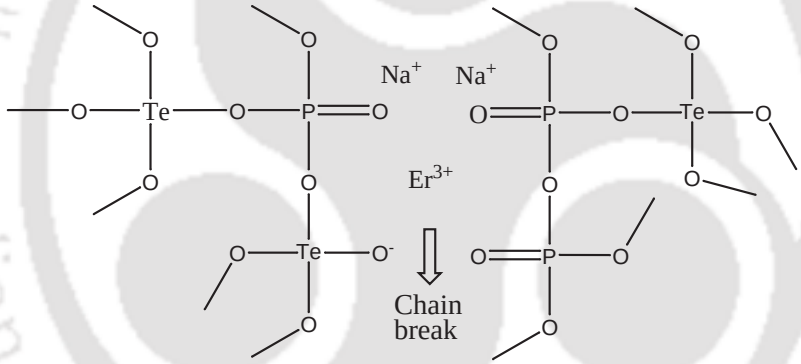

Figure 3.10: Schematic diagram of local environment of Er in a sodium tellurite glass.

In general mixed glass former systems the bandwidth shows markedly different trends. The Er doped tungsten-tellurite glass is reported to have higher emission bandwidth (85 nm) [46]. However, boro-tellurite (BT) showed lower emission bandwidth [50] than tellurite glass NT used in the present study. Addition of glass former doesnt develop TeO_3 tp units with NBOs in germano-tellurite [54], boro-tellurite and phospho-tellurite (PT) glasses . However in TT glass the addition of tungsten develops more TeO_3 tp units [122].

Therefore fluorescence bandwidth decreases in BT and PT whereas it increases in TT glass with the addition of second glass former/intermediate glass former. It was already given in the previous section that the addition of P_2O_5 do not favour the formation of $TeO_{3+\delta}$ units from the analysis of the IR spectra of the glass. So higher the presence of TeO_3 tp units in the tellurite glass, higher will be the fluorescence bandwidth of Er^{3+} :^{4} $I_{13/2}$ $\rightarrow^4$ $I_{15/2}$ transition under 980 nm excitation. This is the reason for decrease of bandwidth in NPT1 glass compared to NT glass. This also explains the shorter fluorescence bandwidth in BT and PT.

It is also observed that addition of more and more of Na_2O increases the bandwidth (Fig. 3.11(a)). The reason for this is the breaking of the glass network and formation of more $TeO_{3+\delta}$ and TeO_3 polyhedra. In highly doped glasses rare-earth ions also acts as a modifier in the glass network as well as there will be clustering of Er ions. This may contribute to the increase in the bandwidth with Er^{3+} ion concentration. Based on the above considerations a possible schematic structure of the Er doped Na_2O-P_2O_5-TeO_2 glass with $\sim$ 30 mole% P_2O_5 (NPT1) is shown in Fig. 3.10. The structure proposed for NT glass is depicted in Fig. 3.9. The comparison of the two structures shows that the addition of phosphate into the sodium tellurite glass changed the local environment of Er^{3+} ions. The PO_4 units which participate in the network formation raptures the -Te-O-Te- chain in P_2O_5-TeO_2 glass [54]. Therefore the local ligand field of Er^{3+} ions are more under the influence of PO_4 tetrahedra and the terminal groups PO_3 and PO_2. So the bandwidth decrease in PT glass is culmination of the two factors,

the formation of TeO_3 and $TeO_{3+\delta}$ units

the formation of PO_4 tetrahedra and the terminal groups PO_3 and PO_2 which also leads to the breaking of tellurite network.

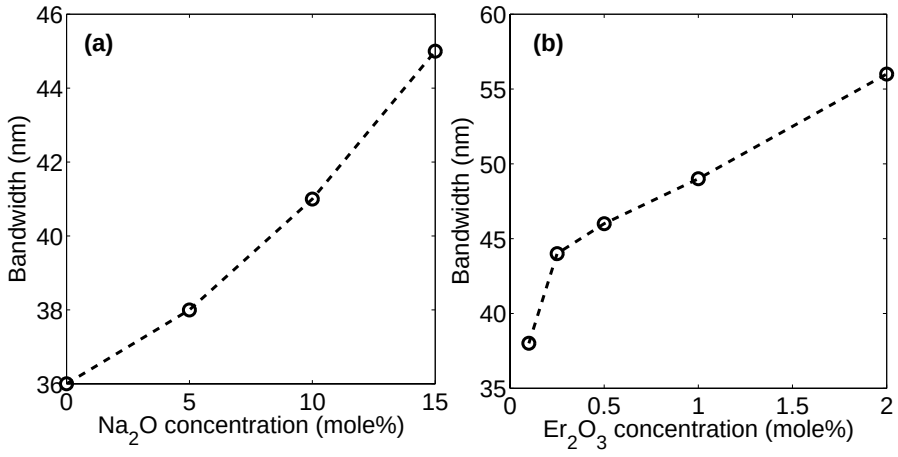

Figure 3.11: Fluorescence bandwidth variation is compared with increasing concentration of (a) Na_2O and (b) Er_2O_3.

3.5 Radiative properties

The absorption spectra in the wavelength range 300 nm-1100 nm were recorded using a dual beam spectrophotometer with 0.1 nm resolution. The absorption spectra of the sample 1.75Yb for different ground state absorption (GSA) has been labelled and shown in Fig. 3.12 as a representative of the samples used in the present work. The eight absorption bands corresponding to the absorptions from the ground state $^4I_{15/2}$ to the excited states $^4I_{11/2}$, $^4I_{9/2}$, $^4F_{9/2}$, $^4S_{3/2}$, $^2H_{11/2}$, $^4F_{7/2}$, $(^2G,^4F,^2H)_{9/2}$, $^4G_{11/2}$, respectively are taken into account for Judd-Ofelt(JO) [78, 79] analysis. For Yb codoped glasses we excluded the GSA around 980 nm from the JO calculation because of the overlap of both Er and Yb transitions. The JO intensity parameters $\Omega_t(t = 2, 4, 6)$ are found from a least square fit to Eq.(1.4) to the integrated absorption band strengths in the 300-1100 nm region and are tabulated in Table 3.3. A notable change in the JO parameters of the samples reported in

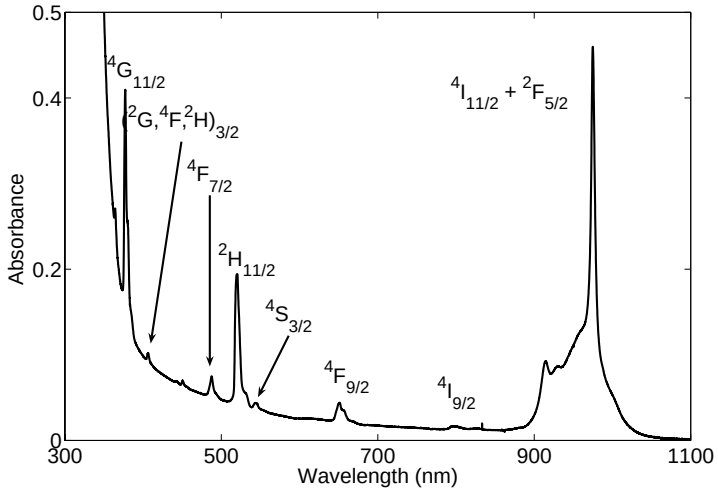

Figure 3.12: Absorption spectra of the 1.75Yb glass sample.

Table 3.3 is the decrease in Ω_2 with the increase in Er^{3+} concentration. The Ω_2 parameter in the Judd -Ofelt analysis is an indication of the extent of covalent bonding between the rare earth ion and the surrounding ligand atom. An increase in the value of Ω_2 represents stronger covalent bonding with the host matrix. Generally it is noted that Ω_2 is higher in glasses than in crystals [124]. In glassy systems the dopants are randomly distributed over nonequivalent sites with a distribution in the crystal fields. A large number of impurity sites will thus occupy sites with noncentrosymmetric potential, which is known to contribute significantly to Ω_2 [124]. The larger values of Ω_2 parameter in glassy hosts arise from this random distribution of dopant sites and lower site symmetry. This suggests the decrease in Ω_2 in phosphotellurite glass is indicative of weaker covalent bonding in the samples with the Er addition. Using the Ω_t parameters the radiative lifetime (τ_{JO}) of $^4I_{13/2}$ to $^4I_{15/2}$ transition was calculated for all samples and reported in Table 3.3.

The absorption cross-sections of the transition Er^{3+} :^{4} $I_{15/2}$ $\rightarrow^4$ $I_{11/2}$ and Yb^{3+} :^{2} $F_{7/2}$ $\rightarrow^2$ $I_{5/2}$ corresponding to the pump absorption band at 980 nm in samples with

Sample ID	Ω_2 ($\times 10^{-20} cm^2$)	Ω_4 ($\times 10^{-20} cm^2$)	Ω_6 ($\times 10^{-20} cm^2$)	$\tau_{JO}(13/2)$ (ms)
0Na	4.19	1.39	0.21	7.4
5Na	4.10	1.54	0.28	6.8
10Na	4.17	1.39	0.25	7.1
15Na	4.76	1.80	0.36	6.1
0.25Er	6.56	2.52	0.46	5.0
0.5Er	4.18	1.40	0.22	7.1
1Er	4.06	1.41	0.25	6.9
2Er	3.38	1.21	0.24	7.2
1.5Yb	3.95	0.61	0.56	5.4
1.75Yb	4.36	0.68	0.54	5.4
NPT1	3.94	1.31	0.37	6.4
NT	5.18	2.02	0.40	4.7

Table 3.3: The JO intensity parameters and radiative lifetime to ground level reported for all glasses.

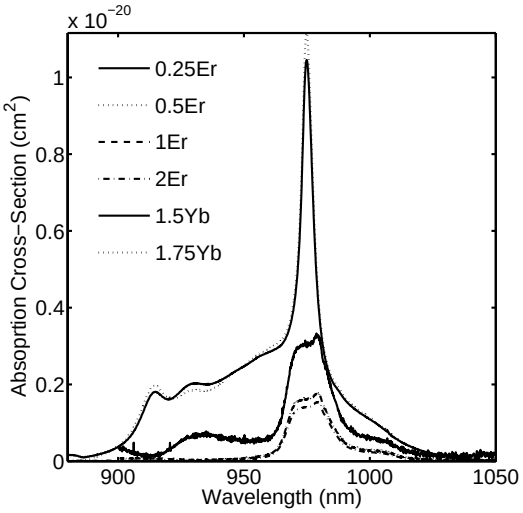

Figure 3.13: Absorption cross-section spectra around 980 nm.

Sample ID	λ_a (nm)	Oscillator strength $\times 10^{-6}$	σ_a $(\times 10^{-21} cm^2)$	$\Delta\lambda_a$ (nm)
0Na	979	0.45	1.92	26.0
5Na	979	0.61	2.12	30.3
10Na	978	0.59	2.13	29.3
15Na	978	0.58	2.36	24.4
0.25Er	979	1.19	3.33	33.3
0.5Er	979	0.47	1.80	25.4
1Er	979	0.51	1.76	25.3
2Er	979	0.49	1.54	23.7
1.5Yb	975	–	10.46	25.6
1.75Yb	975	–	11.12	24.6
NPT1	979	0.54	1.94	22.6
NT	976	0.91	3.18	22.8

Table 3.4: Peak absorption wavelength λ_a, oscillator strength of Er^{3+} :^{4} $I_{15/2}$ $\rightarrow^4$ $I_{13/2}$ transition, absorption cross-section of that transition and effective absorption bandwidth $\Delta\lambda_a$ for all the samples.

different RE concentrations are shown in Fig. 3.13. The absorption cross-sections were calculated using Eq.(1.1). The values of absorption cross-section, bandwidth and oscillator strength of Er^{3+} :^{4} $I_{15/2}$ $\rightarrow^4$ $I_{11/2}$ transition is reported in Table 3.4. From the figure and data given in the table it can be seen that the magnitude of absorption cross-section is maximum for samples co-doped with Yb. The value of absorption cross-section for 1.75Yb is an order of magnitude greater than that of only Er doped samples. It is expected that pumping efficiency of Er-Yb codoped glass amplifiers would be higher than that of only Er doped glasses near the threshold due to transfer of energy from Yb to Er resonantly at the pump wavelength. Other significant trend observed is the decrease in peak absorption cross-section with the increasing Er concentration.

The emission cross-section spectrum of the samples are obtained from the fluorescence spectrum using Eq.(1.12). We used the radiative lifetime obtained using JO analysis (see Table 3.3) in the calculation. The peak stimulated emission cross-section σ_e is found

Sample ID	λ_p (nm)	$\Delta\lambda_e$ (nm)	τ_f (ms)	σ_e ($\times 10^{-21} cm^2$)	$\sigma_e \times \tau_f$ ($\times 10^{-21} cm^2$-ms)	η %
0Na	1534	36	2.7	6.9	18.6	36
5Na	1534	38	2.8	7.0	19.6	41
10Na	1534	41	3.3	6.3	20.8	46
15Na	1534	45	2.8	6.7	18.8	46
0.25Er	1535	44	3.3	8.4	27.7	66
0.5Er	1535	46	2.4	5.6	13.4	34
1Er	1535	49	1.5	5.4	8.1	22
2Er	1535	56	1.0	4.6	4.6	14
1.5Yb	1534	45	3.9	7.7	30.0	72
1.75Yb	1535	46	4.2	7.5	31.5	78
NPT1	1533	54	4.1	5.5	22.6	64
NT	1534	73	2.5	4.9	12.3	53

Table 3.5: Luminescence properties such as $\Delta\lambda_e$ the fluorescence effective bandwidth, τ_f is the measured lifetime of Er^{3+} :$^4 I_{13/2} \rightarrow ^4 I_{15/2}$ transition, peak emission cross-section σ_e, $\sigma_e \times \tau_f$ and quantum efficiency η.

from the calculated emission cross-section spectrum and reported in Table 3.5. The highest emission cross-section among all samples is obtained for 0.25Er and equal to $8.4 \times 10^{-21} cm^2$. Addition of Yb decreased the emission cross-section of the Er doped glass @ 1535 nm as shown in the table and in Fig. 3.6.

The fluorescence lifetime τ_f of all the samples were measured and it is reported in the Table 3.5. The fluorescence decay of the sample 1.75Yb is shown in the logarithmic scale and are fitted with a straight line to obtain the measured lifetime (τ_f) of fluorescence for $^4 I_{13/2} \rightarrow ^4 I_{15/2}$ transition in Fig. 3.14. The dependence of fluorescence lifetime on RE concentration is depicted in Fig. 3.15. Measured lifetime recorded is highest for 1.75Yb. Addition of Yb has increased the measured lifetime and quantum efficiency of the glass. The lifetime is expected to be more than what reported. The observed lower value may be attributed to the residual hydroxyl groups present in the glass. The optical gain variation for Na_2O and Er_2O_3 concentrations are shown in Figs. 3.16(a) and (b). The best gain obtained

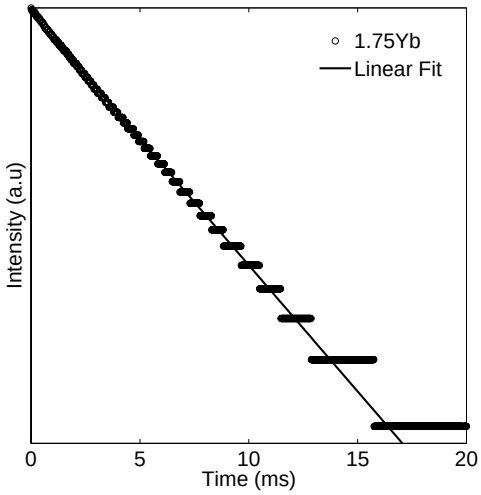

Figure 3.14: Fluorescence decay of ${}^4I_{13/2} to {}^4I_{15/2}$ transition with the linear fitting (solid line) to obtain the measured lifetime.

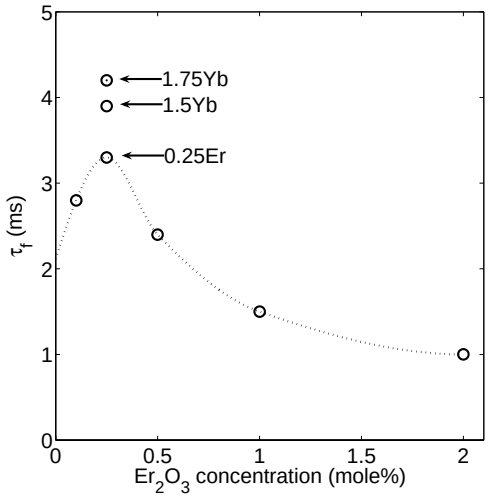

Figure 3.15: Comparison of measured lifetime τ_f with increasing Er concentration, and the effect of Yb-Er codoping on lifetime is shown.

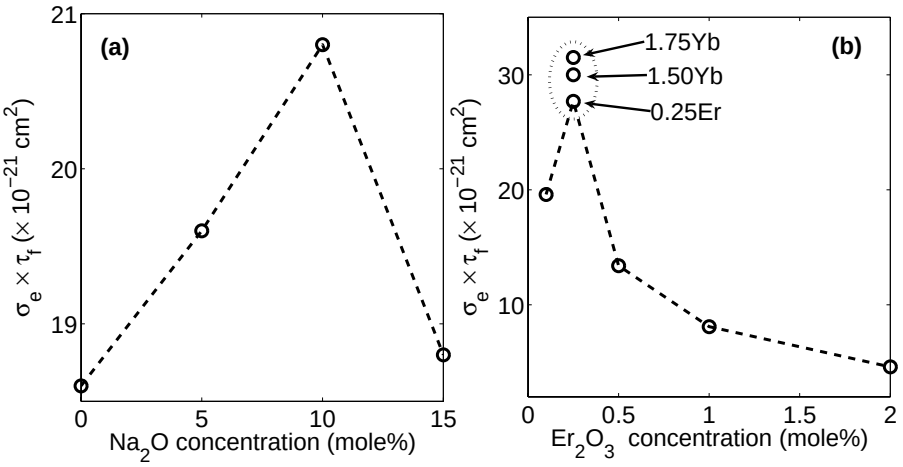

Figure 3.16: Gain variation is compared with increasing concentration of (a) Na_2O and (b) Er_2O_3.

is for 0.25Er, however it increases with increasing Yb concentration. The quantum efficiency as high as 82% is obtained in 1.75Yb (Table 3.5).

3.6 Conclusion

The thermal properties are studied by varying the Na_2O concentration to optimize the T_g. The glass transition temperature as high as 398^{o}C is reported. The dependence of glass transition temperature on glass composition is analyzed using IR spectra. We observed a decrease in the fluorescence bandwidth of the Er doped NPT1 glass than NT. We studied the IR spectrum to identify different vibrational bands and found that $TeO_{3+\delta}$ and TeO_3 units are less in the NPT1 glass compared to NT glass. We modelled a probable structure of Er doped NPT1 glass with the help of existing models for phosphotellurite glass having high P_2O_5 content. We conclude that decrease in $TeO_{3+\delta}$ and TeO_3 units in TeO_4 chains

decreases the bandwidth. This is common for all the tellurite glasses modified by another glass former like P_2O_5 and B_3O_3. We have studied the spectroscopic properties of different Er_2O_3 concentrations to optimize the rare earth concentration. We observed that 0.25Er is the best concentration, having highest gain and higher bandwidth. Then we codoped Yb with Er as a sensitizer, which increases the lifetime but there is a decrease in the σ_e.

Chapter 4

Yb doped glasses for laser

Ytterbium doped sodium phosphotellurite glasses were fabricated with different P_2O_5 *:* TeO_2 *ratio, and* Yb^{3+} *concentrations. Physical properties of the new Yb hosts are favorable for laser applications. The glasses show high absorption and emission cross-sections and higher lifetime of* Yb^{3+}*:* $^2F_{5/2} \rightarrow ^2 F_{7/2}$ *transition. The emission cross-sections are calculated using two different methods and compared. The laser parameters of these* Yb^{3+} *doped glasses are better than many reported glasses and crystals making them potential to fabricate high power laser and broadband optical amplifier in the wavelength region around*$\sim$*1* μm*.*

4.1 Introduction

The ytterbium doped glasses and crystals are of interest for fabrication of diode pumped tunable, high power and short pulse lasers [125, 28, 126, 127, 45]. Ytterbium has been used as sensitizer of erbium ions in silicate, phosphate and tellurite glass based amplifiers and lasers [7, 62]. Ytterbium-doped fibre amplifiers (YDFA's) offer high output power and excellent power conversion efficiency over a broad wavelength range from ∼975 nm to ∼1100 nm. The absence of many well known complexities like ESA (Excited State Absorption) and concentration quenching is an added advantage of YDFA. Hence higher level of Yb doping is possible, leading to high gain in short length of fibre or planar waveguide. There is also a wide range of possible pumping wavelength (∼860 nm to ∼1064 nm), allowing a variety of pumping schemes [73]. The spectroscopic properties of Yb:glass has also been studied in the context of laser induced fluorescent cooling or optical refrigerant [128].

Dependence of absorption and emission cross-sections and lifetime of the lasing level of Yb^{3+} on many glass compositions like borate, phosphate, silicate has been studied extensively in the past[129, 131, 45, 130]. In recent years, a few Yb doped tellurite glass hosts has been studied for laser applications[52, 70, 53]. Addition of phosphate in a tellurite host has demonstrated increased glass transition temperature and phonon energy [132]. Phosphate (P_2O_5) glasses show good spectroscopic and lasing properties for the $^2F_{5/2}$ to $^2F_{7/2}$ transition of ytterbium ions. P_2O_5 is also a good glass former but the drawback of a phosphate glass is that it is having low emission cross-section [45]. A P_2O_5:TeO_2 glass host is therefore expected to have better emission cross-section and lifetime for Yb: $^2F_{5/2} \rightarrow ^2 F_{7/2}$ transition.

In this chapter we report the spectroscopic properties of the ytterbium doped phospho-tellurite (PTY) glasses. The absorption and emission cross-sections of the new

glasses are studied. The emission cross section spectra is calculated from the measured absorption cross-section spectra using the reciprocity method (RM) [133] and integral method of reciprocity (IMR) [134]. The fluorescence decay lifetimes and other relevant laser parameters of the glasses with two different phosphate concentrations and varying Yb concentrations are investigated in detail.

4.2 Experimental procedure

Ytterbium doped sodium phospho-tellurite glass sample are made using the melt quenching technique. High purity chemicals, Na_2CO_3, P_2O_5, TeO_2 and Yb_2O_3 are used for the batch melting. Glasses are fabricated by a two step melting process at $\sim 800^oC$ in an electrical furnace. The melt was then quenched at $\sim 300^oC$ to form the glass samples. The samples are annealed for 1 hr below the glass transition temperature, and slowly cooled down to the room temperature. The glass samples are then polished to optical quality for the spectroscopic and refractive index measurements.The samples are transparent and disk shaped having thickness ranging from 1.2 mm to 1.5 mm with diameter ∼10 mm. The density of the glass is measured using the Archimedes' principle and Xylene as the immersion liquid. The glass transition temperature (T_g) is measured by differential scanning calorimeter at a heating rate of 10 ^oC/min. The mechanical strength of the glass is studied by measuring the microhardness using a Buehler Micromet 2100 automated microhardness tester. The refractive indexes are obtained using the prism coupler at 633 nm. Absorption spectra is recorded using a dual beam spectrophotometer with 0.1 nm resolution. The lifetime of the PTY glasses (of $^2F_{5/2}$ level) is measured using an InGaAs detector and a 200MHz digital storage oscilloscope. A fibre pigtailed laser diode (JDS uniphase, tunable in the wavelength range ∼970-980 nm) is used as the excitation source. The laser diode has

been modulated by a waveform generator at the frequency of 50Hz. The room temperature fluorescence spectra are recorded on an optical spectrum analyzer using the same laser diode as the excitation source.

Given Sample ID	Compositions Yb in wt(%) others in mole(%)	ϱ $(\frac{gm}{cc})$	N (10^{20}) $(\frac{ions}{cc})$	T_g (^oC)
30PT1Y	A-1Yb_2O_3	3.92	1.20	365
30PT3Y	A-3Yb_2O_2	4.05	3.71	368
30PT5Y	A-5Yb_2O_2	4.16	6.36	362
35PT1Y	B-1Yb_2O_2	3.64	1.11	353
35PT3Y	B-3Yb_2O_2	3.72	3.41	358

Table 4.1: Glass composition with their measured density, Yb^{3+} ions concentration and glass transition temperature T_g are given for all the samples, A=10Na_2O-30P_2O_5-60TeO_2, B=10Na_2O-35P_2O_5-55TeO_2

4.3 Physical and thermal properties

Density of the glasses are reported in Table 4.1. The refractive indexes measured is 2.0 for all glasses. The ytterbium ion concentration in each glass is calculated from the density and the weight percentage of the Yb_2O_3 used initially for the batch melting. Different ionic concentrations of Yb^{3+} are given in the table for all the samples. The glass transition temperature T_g and the onset of crystallization temperature T_x are obtained from the differential scanning calorimetric measurements. The relative error for T_g is estimated to be $\pm 5\%$. The excess heat capacity ΔC_p at the glass transition is defined as the difference between the specific heat values of the glass and supercooled liquid. Glasses exhibiting a small ΔC_p at T_g show a strong resistance to structural degradation in the liquid state called 'strong glass'. On the other hand, glasses exhibiting large ΔC_p at T_g were termed as 'fragile glass'. From the DSC curve we have calculated ΔC_p for all glasses, and it is rather low, varying from 0.25 J/gm-^{o}C to 0.29 J/gm-^{o}C. The microhardness measurement method

involves the use of a diamond micro indenter of a square pyramid (Vicker's) shape. The Vicker's hardness number is defined as, HN=$\frac{force}{area}$ (Kg/mm^2). The size of the indentation is in the range of 18 to 20 microns under 50 gm load for our glasses. The VHN is 299.3 for 30PT5Yb, which is the highest among all the samples used in the present study. It has been observed that microhardness increases with the increase inYb concentration. Further, from a comparison of the VHN of 30PT3Yb (284.5) and that of 35PT3Yb (273.8), it is inferred that the microhardness value decreased with the increase in P_2O_5 concentration.

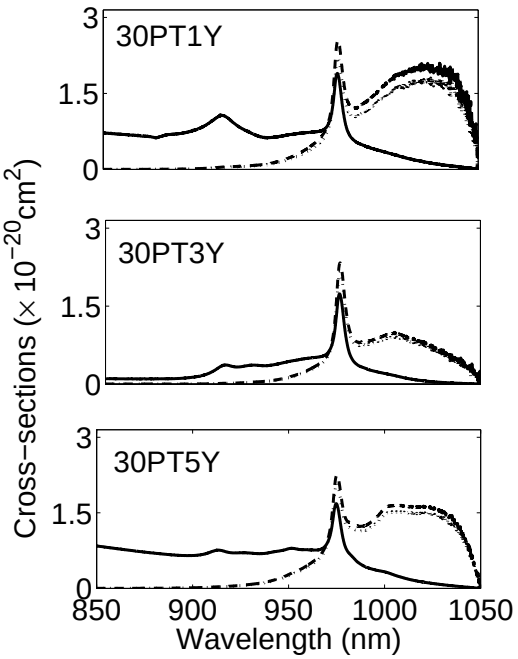

Figure 4.1: Absorption cross-section spectra (solid line) and stimulated emission cross-section spectra calculated by reciprocity method(RM)(dash line) and integral method of reciprocity(IMR)(dotted line) are shown for the samples 30PT1Yb, 30PT3Yb, 30PT5Yb.

4.4 Spectroscopic properties

The absorption cross-section spectra and emission cross-section spectra for 30PT1Y, 30PT3Y, and 30PT5Y are shown in Fig 4.1 and that of 35PT1Y and 35PT3Y are shown in Fig 4.2. The residual absorption band due to the scattering observed in Fig 4.1, 4.2 in the lower wavelength region. This is due to small amount of inhomogeneities present in those glass samples. This can be removed by improving the melt quenching process of the glass fabrication. From the absorption spectra and the measured lifetime we calculated the spectroscopic parameters relevant to ytterbium doped laser materials. The absorption cross-section spectra is obtained from the measured absorption spectra using the following equation,

$$\sigma_a = \frac{2.303}{N \times d} E(\lambda) \tag{4.1}$$

where N and d are the number density of Yb^{3+} ions and thickness of the sample. $E(\lambda)$ is the wavelength dependent absorbance. The relative error in the calculation of σ_a is 10%. The integrated absorption cross-section (Σ_a), and mean wavelength ($\bar{\lambda}$) are defined as,

$$\Sigma_a = \int \sigma_a(\lambda) d\lambda \tag{4.2}$$

$$\bar{\lambda}_{a,e} = \frac{\int \lambda \sigma_{a,e}(\lambda) d\lambda}{\int \sigma_{a,e}(\lambda)} \tag{4.3}$$

where the subscript a, e corresponds to absorption and emission respectively.

Stimulated emission cross-sections σ_e can be calculated from the absorption cross-section σ_a spectra using reciprocity method (RM) [133, 83, 135, 114]. According to this, the absorption and emission cross-sections are related as,

$$\sigma_e(RM) = \sigma_a \frac{g2}{g1} \exp[(E_{ZL} - \frac{hc}{\lambda})/KT] \tag{4.4}$$

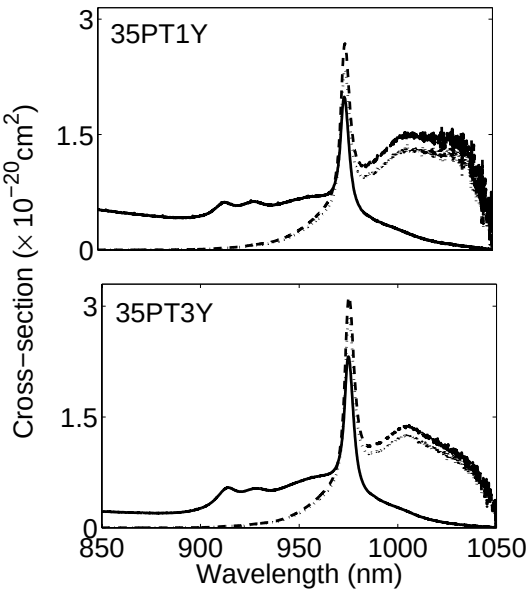

Figure 4.2: Absorption cross-section spectra (solid line) and stimulated emission cross-section spectra calculated by reciprocity method(RM)(dash line) and integral method of reciprocity(IMR)(dotted line) are shown for the samples 35PT1Yb, 35PT3Yb.

where λ is the photon wavelength, E_{ZL} (zeroline energy) is the net free energy required to excite one ytterbium ion from $^2F_{7/2}$ ground state to the $^2F_{5/2}$ level at T K temperature, h the Plank's constant and k the Boltzmann constant. The zeroline energy E_{ZL} is the absorption energy corresponding to the peak absorption wavelength λ_p.

It is also possible to determine the stimulated emission cross-section from the absorption cross-section spectra and the radiative lifetime of the Yb^{3+} ions by a slightly modified procedure called integral method of reciprocity (IMR)[134]. This method do not require the knowledge of the electronic structure of the ytterbium ions in the glass matrix. According to IMR the emission cross-section is,

$$\sigma_e(IMR) = \sigma_a \times \frac{3\exp(-\frac{hc}{\lambda kT})}{8\pi n^2 \tau_{rad} c \int \lambda^{-4} \exp(-\frac{hc}{\lambda kT}) d\lambda} \tag{4.5}$$

Sample ID	λ_p (nm)	σ_a (10^{-20}) (cm^2)	Σ_a (10^{-19}) (cm^3)	$\bar{\lambda}_a$ (nm)	τ_{rad} (ms)
30PT1Y	974.9	1.26	5.66	952.8	1.19
30PT3Y	974.9	1.16	3.19	959.5	2.11
30PT5Y	974.9	1.12	5.26	954.2	1.28
35PT1Y	974.9	1.33	4.70	956.7	1.43
35PT3Y	974.9	1.55	4.50	958.7	1.50

Table 4.2: Peak absorption wavelength λ_p, peak absorption cross-section σ_a, integrated absorption cross-section Σ_a, mean absorption wavelength $\bar{\lambda}_a$ and radiative lifetime obtained from the absorption spectra are listed for all the samples.

Sample ID	σ_e(RM) (10^{-20}) (cm^2)	σ_e(IMR) (10^{-20}) (cm^2)	τ_f (ms)	σ_e(RM) $\times\tau_f$ (cm^2 ms)	I_{min} ($\frac{kW}{cm^2}$)
30PT1Y	1.70	1.47	1.26	2.14	1.79
30PT3Y	1.55	1.44	1.15	1.79	2.14
30PT5Y	1.50	1.39	0.94	1.41	2.70
35PT1Y	1.79	1.56	1.17	2.09	1.84
35PT3Y	2.09	1.90	0.96	2.01	1.92

Table 4.3: The peak emission cross-section calculated from the reciprocity method σ_e(RM) and integral method of reciprocity σ_e(IMR), measured lifetime τ_f, product of σ_e(RM) and τ_f, and minimum pump power are reported for all five samples.

Radiative lifetime τ_{rad} is obtained from the absorption spectra, using the data on the structure of electron levels of the ground state and excited state multiplets participating in the transition $^2F_{5/2}$ to $^2F_{7/2}$[134],

$$\tau_{rad} = \frac{3\lambda_p^4}{8\pi n^2 c}\frac{g_2}{g_1}\frac{1}{\int \sigma_a(\lambda)d\lambda} \tag{4.6}$$

where λ_p is the peak absorption wavelength, n is the refractive index of the glass, c is the velocity of light, g_1 and g_2 are the excited state and ground state multiplets of Yb^{3+}. Values of λ_p, $\sigma_a(peak)$, Σ_a, $\bar{\lambda}_a$ and τ_{rad} obtained for all five samples are reported in Table 4.2. The absorption and stimulated emission cross-section spectra (both σ_e(RM) and σ_e(IMR)) of the sample 35PT3Y are shown in Figs 4.1 and 4.2. The peak emission cross-sections (σ_e(RM)

and σ_e(IMR)) are given in Table 4.3 for all glasses. The propagation error for σ_e(RM) is estimated to be 10% and that of σ_e(IMR) about 15%. The measured fluorescence spectrum of two samples with same Yb concentration and different phosphate concentration is given in Fig 4.3. Fluorescence decay lifetime of $^2F_{5/2}$ level of Yb^{3+} is measured as described in the experimental procedure. All the decays are recorded by averaging over 128 measurements, and fitted with a single exponential decay equation to obtain the fluorescence lifetime, τ_f. The fluorescence decay curves for all the samples are shown in the Fig 4.4 and the measured fluorescence decay lifetimes are given in Table 4.3. The error in the measured fluorescence lifetime is 5%.

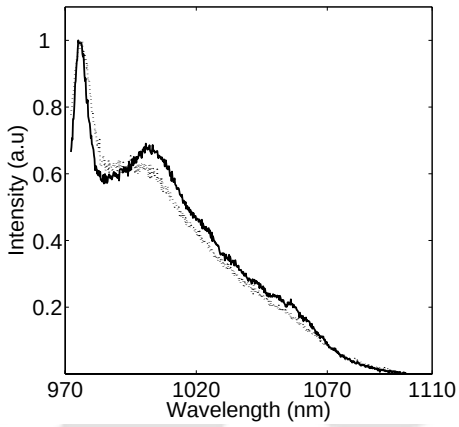

Figure 4.3: Recorded emission spectrum of 30PT3Y (solid) and 35PT3Y (dotted) under 970 nm laser excitation

4.5 Laser performance parameters

Among the important parameters that determine the viability of laser operation, such as absorption cross-section and emission cross-section, there is the minimum pump intensity, I_{min} that takes into account the pump saturation intensity, I_{sat} and the β_{min}

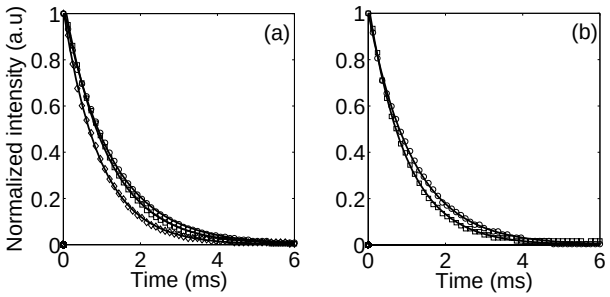

Figure 4.4: Measured fluorescence decay data for 30PT1Y (circle), 30PT3Y (square), 30PT5Y (diamond) in (a) and 35PT1Y (circle), 35PT3Y (square) in (b). Solid lines indicate the fitting of those data to a single exponential decay.

parameters as below [133, 74].

$$\beta_{min} = \frac{\sigma_a(\lambda_0)}{\sigma_a(\lambda_0) + \sigma_e(\lambda_0)} \tag{4.7}$$

where $\sigma_a(\lambda_0)$ and $\sigma_e(\lambda_0)$ are the absorption and emission cross-sections at the extraction wavelength, λ_0 ~1000 nm. β_{min} is defined as the minimum fraction of Yb ions that must be excited to balance the gain exactly with the ground state absorption at λ_0.

Another important parameter that characterize the pumping dynamics is the pump saturation intensity I_{sat}, which requires an accurate measure of the absorption cross-section at laser pump wavelength, λ_p, and the emission lifetime, τ_f, of the Yb^{3+}.

$$I_{sat} = \frac{hc}{\lambda_p \tau_f \sigma_a(\lambda_p)} \tag{4.8}$$

where $\frac{hc}{\lambda_p}$ is the pumping energy and $\sigma_a(\lambda_p)$ is the peak absorption cross-section at $975nm$. I_{min} is the parameter which evaluates the minimum absorbed pump intensity required to reach laser threshold in a loss-less oscillator. I_{min} takes into account both the absorption

and emission properties of the active medium and is defined by,

$$I_{min} = \beta_{min} \times I_{sat} \tag{4.9}$$

The laser parameters obtained for the glasses is given in Table 4.3. In Table 4.4 we have shown some of the already reported laser parameter values of Yb doped glasses and crystals elsewhere. The emission cross-section for the glasses studied in the present work and that of some reported glasses are give in Fig 4.5 with the the minimum pump intensity.

In Fig 4.6 we have plotted the minimum pump intensity (kW/cm^2) verses $\sigma_e \times \tau_f$ ($\times 10^{-20}$ cm^2 ms). Position of our glasses in these figures show their potential for laser fabrication.

4.6 Discussion

Phospho-tellurite is a new class of glass investigated for Yb^{3+} doped amplifiers and lasers. The physical and optical properties of this glass can be discussed in comparison with those reported for phosphate and tellurite glasses. The difference between the onset of crystallization temperature and glass transition temperature ($T_x - T_g$) has been used as a measure of glass forming ability and potential to fabricate preform for fibre drawing. It is reported that rare earth addition decreases ($T_x - T_g$) in P_2O_5- TeO_2 glasses [38]. In the present work it is observed that the T_g remains almost same with Yb addition in the two composition of glasses with different P_2O_5: TeO_2 ratio(Table 4.1). The T_g of the glass has been decreased by $\sim 10^oC$ when the P_2O_5: TeO_2 weight ratio of the glass is increased from 0.50 to 0.64. The transition corresponding to T_x is not observed in DSC curves of any of the present glass samples. We confirmed this by recording the XRD pattern before and after the annealing a glass sample at 500^oC for half an hour. The XRD pattern did not show any crystalline peak. The rather high T_g of these glasses are favourable for planar waveguide

fabrication by ion-exchange. The refractive index of the samples are higher than that of phosphate glasses and close to the values reported for tellurite glasses. The higher value of refractive index would increase the oscillator strength of the lasing transition.

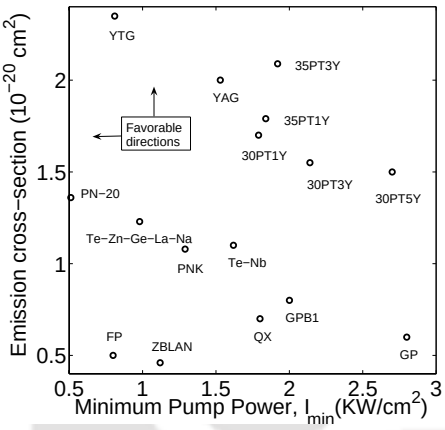

Figure 4.5: Comparison of different Yb:hosts reported and glasses in the present study with respect to emission cross-section and I_{min}. The dotted line with arrows shows the trend with glass composition for PTY glasses

The absorption and emission cross-section spectra are studied with varying the Yb concentration and P_2O_5: TeO_2 composition of the glass. The room temperature absorption cross-section spectra shows poorly resolved stark structure in the lower wavelength side(below 975 nm). The absorption lineshape shows some changes when the phosphate component is increased in the glass. This is clear from a comparison of the absorption spectra for samples 30PT1Y and 35PT1Y given in Figs 4.1 and 4.2. If we compare the spectra for glasses with different Yb concentration, the absorption line of 30PT1Y is different from that of 30PT3Y and 30PT5Y Fig 4.1. The absorption band at ∼910 nm observed for 30PT1Y has been weakened and changed into less resolved stark absorption bands in the glasses with higher concentration of ytterbium as well as for glasses with 35% phosphate. It has been reported that the lineshape depends on the glass composition, ie., both on glass

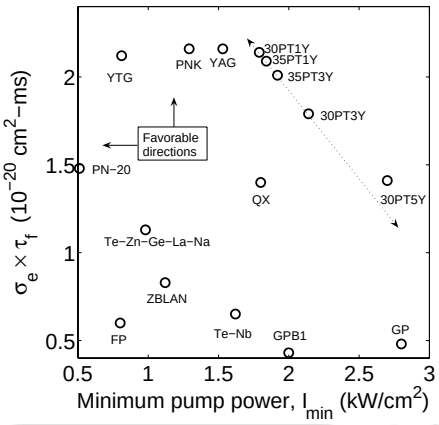

Figure 4.6: Comparison of $\sigma_e\tau_f$ vs. I_{min} for different reported Yb:hosts and glasses studied in this thesis

former and modifier[129]. It is due to the change in local structural environment of Yb ions that the 30PT1Y and 35PT1Y show different lineshapes in the lower wavelength side of peak absorption. The change in the absorption lineshape in the 30PTxY series is due to the modifier effect of ytterbium ions in the glass network. In both cases the effect is inhomogeneous broadening of the absorptions from stark levels of $^2F_{5/2}$ to $^2F_{7/2}$. The absorption cross-section at the peak wavelength of 975 nm is the highest for 35PT3Y comparing to all other compositions studied. The emission cross-section is calculated using the RM and IMR method. The value of the cross-sections differ in the two methods. A comparison σ_e(RM) and σ_e(IMR) (Table 3) show that the former is greater than the latter in all glasses. RM and IMR are equivalent in many ways and the difference in the obtained cross-sections are within the error involved in the methods. The emission cross-sections calculated by the two methods have large errors in the wavelength region above $\sim$ 1040 nm where the absorption cross-section is very close to zero. This has been reported previously and also evident from Eq.(4.4) and (4.5) due to the exponential factor which dominates at higher wavelengths. Therefore the lineshape obtained in this region by RM or IMR method has no relevance (see

Fig 4.1,4.2). The change in the lineshape of the emission cross-section in this region has relation to the dopant concentration or glass composition. In the calculation of the emission cross-section we have used the absorbance data available upto 1050 nm zeroed at this wavelength, therefore there is an abrupt fall to zero of the cross-section at this wavelength. From the measured fluorescence spectra (Fig 4.3) we can see that the emission intensity approach zero only at ∼1100 nm. In order to get the emission cross-section above ∼ 1040 nm we need to apply the Fuchtbauer-Ladenburg relation[136]. As a measure of accuracy we compared the radiative lifetimes obtained using RM and IMR methods. The τ_{rad} using RM is more close to the measured lifetime values comparing to those obtained by IMR. So, we can say that RM is sufficient for obtaining the emission cross-section spectra in the wavelength region were absorption is not very low. However as mentioned before the IMR method would be useful when electronic structure of the ytterbium ions in the host is unknown. Laser parameters I_{min}, σ_e, and $\sigma_e\tau_f$ together provide a good spectroscopic measure of the overall usefulness of the laser medium for the pulse or the cw operation. From the laser operation point of view, it is favorable to have higher emission cross-section for greater gain, longer emission lifetime in order to permit high inversion density, and higher absorption cross-section at pump wavelength for efficient diode laser pumping. I_{min} is to be small to minimize the threshold for an Yb-laser material engaged in an oscillator type configuration, and also to offer the best extraction efficiency at the laser wavelength[74, 137]. All these parameters for different hosts reported are given in Table 4.4. The I_{min} is calculated using the σ_e(RM). The measured lifetime is highest for 30PT1Y comparing to other samples. The lifetime decreases with increasing Yb concentration in the glass. Increasing the phosphate also decreases the fluorescence lifetime as evident from the table. The fluorescence spectrum for two samples with different P_2O_5: TeO_2 ratio is given in the Fig 4.3. The broad emission peak at 1004 nm in 30PT3Y has changed to a shoulder of the broadened 975 nm

emission of 35PT3Y. The local structural variations induced by the increased phosphate content influence the laser transition.

Glasses/ Crystals	σ_e (10^{-20}) (cm^2)	λ_{em} (nm)	τ_f (ms)	$\sigma_e \times \tau_f$ (cm^2 ms)	I_{min} $(\frac{kW}{cm^2})$
QX [45]	0.70	1018	2.00	1.40	1.80
PN-20 [74]	1.36	1019	1.09	1.48	0.51
PNK [130]	1.08	1016	2.00	2.16	1.29
FP [138]	0.50	1020	1.20	0.60	0.80
YTG [52]	2.35	1024	0.90	2.12	0.81
YAG [133]	2.00	1031	1.08	2.16	1.53
Te-Nb [71]	1.10	1028	0.59	0.65	1.62
GP [139]	0.60	1009	0.80	0.48	2.80
GPB1 [139]	0.80	1021	0.54	0.43	2.00
ZBLAN [74]	0.46	1001	1.81	0.83	1.12
Te-Zn-Ge-La-Na [53]	1.23	1008	0.92	1.13	0.98

Table 4.4: Laser parameters of some reported Yb doped glasses/crystals

The emission cross-section of the PTY glasses are higher than the phosphate glasses like QX [45], PN-20 [74] and comparable to other tellurite hosts like YTG [52]. However the measured lifetime of the $^2F_{5/2}$ level is highest among the reported tellurite hosts given in Table 4.4. It is apparent from the Fig 4.6 that 30PT1Y glass is the best among the new glasses reported in the present work, and is comparable to the YTG, PNK glasses and YAG crystals. I_{min} is also comparable to QX, Te-Nb, YAG and lower than GP. Further optimization of the PTY glass composition would result in better Yb glass hosts for lasers and amplifiers.

4.7 Conclusion

Different ytterbium doped sodium-phospho-tellurite(PTY) glasses are fabricated for the present study. Physical and spectroscopic properties of those glasses are measured

and discussed. The glass studied is having higher T_g ($\sim 365^oC$) than ordinary tellurite glass and high refractive index (n $\sim$ 2) than the phosphate glasses. The absorption and emission cross-sections ($\sigma_{a,e}$) measured are higher than those of phosphate glasses whereas the excited state lifetime (τ_f) is higher than the reported tellurite glasses. Comparing the laser parameters already reported in different glass hosts, we conclude that PTY glasses are potential host as laser and amplifier at $\sim$1 μm region under diode pumping at 970 nm.

Chapter 5

Femotosecond laser-written channel waveguides in tellurite glass

We have prepared and characterized a new, erbium-doped tellurite glass that has high glass transition temperature. Addition of phosphate is found to increase the phonon energy. The peak emission cross section is 6×10^{-21} cm^2 *at 1537 nm and the fluorescence lifetime of the* $^4I_{13/2} \rightarrow ^4 I_{15/2}$ *transition is 4.1 ms. We have written 2-D channel waveguides in this glass using focused, 45-fs pulses from an amplified Ti:sapphire laser at different laser energies and writing speeds. Migration of atoms towards the periphery of the waveguides occurs, leading to refractive index changes. Channels show waveguiding at 1310 nm which is promising for the fabrication of integrated lasers and broadband amplifiers.*

5.1 Introduction

Micromachining within glass substrates by means of femtosecond laser pulses has potential application in the fabrication of optical integrated circuits [86]. The ready availability of high power and low pulse-width laser technology has led to increasing interest in fabricating channel waveguides by this technique [27]. Such laser writing opens new vistas for fabrication of 3-D waveguides inside transparent glass substrates, which is not possible using conventional ion-exchange and photolithographic processes [26]. Channel waveguides written using ultrafast lasers in erbium-doped phosphate glasses for integrated amplifiers and lasers operating in the C-band have been demonstrated [88, 16]. Waveguide writing in Bismuth doped silicate glass was reported for broadband amplification [140]. Extension of the method to tellurite-based glasses has been less successful: there is one report on longitudinal writing of relatively short waveguides and positive refractive index change in niobium tellurite glasses using 130 fs pulses [141]. In contrast, it has also been reported that only negative refractive index change is induced by ultrafast laser irradiation of tellurite glass, making waveguiding impossible [142]. Moreover, surface damage during photolithographic processing has hindered fabrication of ion-exchanged channel waveguides in Er-doped tellurite glass [109]. On the other hand, tellurite glasses that are doped by rare earth elements like thulium and erbium are strong candidates for broadband amplification in the S-C-L bands [14]. Tellurite, as a host of Er-doped glass, has the disadvantage of having a small phonon energy, which enhances the upconversion process and decreases gain at 1550 nm under 980 nm pumping. Addition of P_2O_5 in TeO_2 increases the phonon energy as well as the glass transition temperature in a phosphotellurite (PT) host doped with erbium [143].

The channel waveguide writing in an erbium-doped tellurite glass modified by phosphate and aluminum addition is shown. The physical and spectroscopic properties of

this glass are studied to assess its suitability for 1550 nm amplification under 980 nm excitation. Centimeter-long channels have been written by us inside the glass using ultrashort (45 fs) laser pulses. Migration of La and P atoms occurs from the center towards the periphery of such channels; the resulting modulation of Te:P ratio across the irradiated region may be responsible for a net positive refractive index change across each channel.

5.2 Experimental procedures

Tellurite glass doped with 0.25 mole% erbium was made by us using the melt quenching technique. High-purity chemicals like TeO_2, P_2O_5, Al_2O_3, La_2O_3, and Er_2O_3 were used for batch melting. A two-step melting process at $\sim 1100^oC$ was performed before quenching. The melt obtained after the second step was quenched at $\sim 350^oC$ to form the transparent glass. The glass was annealed for 1 hour below the glass transition temperature, and slowly cooled down to room temperature. Polished glass was used for spectroscopy, refractive index measurement and waveguide writing using a femtosecond laser.

The refractive index was measured using a prism coupler at 633 nm (Table 5.1). The erbium ion concentration (N) in the glass was calculated from the density and the weight percentage of the Er_2O_3 used initially for batch melting. The glass transition temperature (T_g) was measured using a differential scanning calorimeter at a heating rate of 10 ^oC/min. The glass transition temperature T_g obtained from the measurement is indicated in Table 5.1.

The absorption spectrum in the wavelength range 400-1100 nm was recorded using a dual-beam spectrophotometer with 0.1 nm resolution. Room temperature fluorescence spectrum was recorded in an optical spectrum analyzer using a cw 980 nm laser diode as the excitation source. The fluorescence decay of the glass (from Er^{3+} : $^4I_{13/2}$ level)

was measured using an InGaAs detector and a 200 MHz digital storage oscilloscope by modulating the laser diode at ∼10Hz.

The spectral broadening due to self phase modulation of the laser is observed on transmitting unfocused laser light, of energy 343 μJ, through the glass sample. The spectrum was recorded by a fibre-coupled spectrometer (Ocean Optics) over the wavelength range 750-880 nm. Using this data the nonlinear index of refraction, n_2, of the glass was deduced.

Properties	Parameters	Values	Units
Physical	Refractive index, n, @633 nm	2.0	
	Glass transition temperature, T_g	411	^oC
	Excess heat capacity, ΔC_p	0.2	J/gm-^oC
	Density	3.75	gm/cc
	No. of Er^{3+} ions, N	7.2×10^{19}	ions/cc
JO Analysis	Ω_2	3.4×10^{-20}	cm^2
	Ω_4	1.0×10^{-20}	cm^2
	Ω_6	0.2×10^{-20}	cm^2
	Radiative lifetime, τ_r	7.9	ms
Fluorescence	Peak wavelength	1537	nm
	Emission cross-section	6×10^{-21}	cm^2
	Fluorescence lifetime	4.1	ms
	Fluorescence linewidth	41	nm

Table 5.1: Physical properties, Judd-Ofelt (JO) parameters, radiative lifetime and fluorescence properties of the tellurite glass.

In the waveguide writing experiment we used a Ti:sapphire laser operating at 806 nm wavelength with a pulse duration of 45 fs and 1 kHz repetition rate. The laser was tightly focused inside the transparent tellurite glass using a microscope objective (25X, NA=0.45), and the glass was translated transversely to the focused beam at three different writing speeds. The schematic diagram is shown in Fig. 5.1

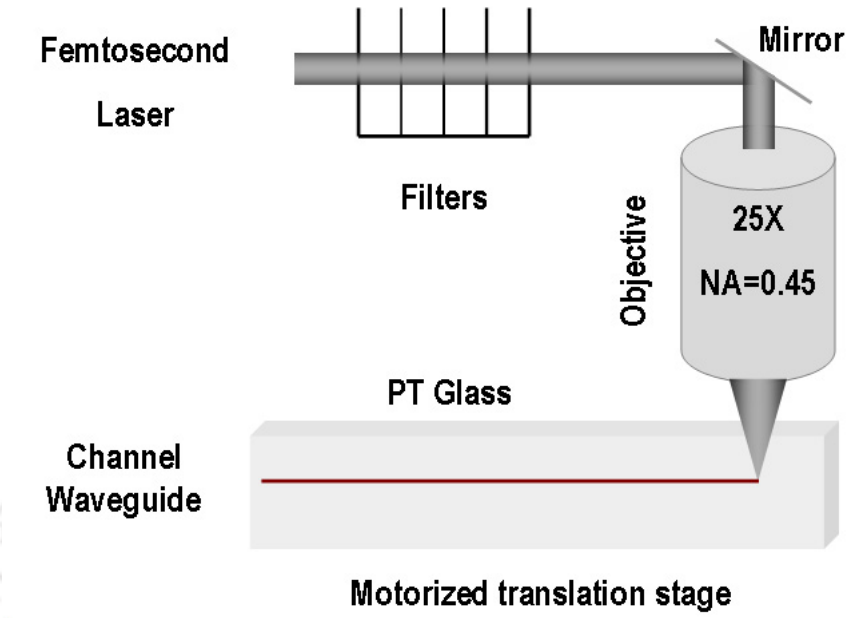

Figure 5.1: Schematic of the femtosecond laser writing experiment.

5.3 Results and discussion

5.3.1 Bulk glass properties

The composition of the glass that we prepared is $67TeO_2 - 30P_2O_5 - 1Al_2O_3 - 1.75La_2O_3 - 0.25Er_2O_3$ (all in mole %); the physical and spectroscopic properties that we measured are summarized in Table 5.1. The refractive index is higher compared to that of phosphate glasses. The glass transition temperature is seen to have increased compared to the phosphotellurite glass [143]. Addition of Al_2O_3 and La_2O_3 into the glass matrix is responsible for this enhancement. The absorption spectrum in the UV-VIS region is shown in Fig. 5.2. The absorption peaks are labelled with respect to transitions from the ground level ($^4I_{15/2}$) to various upper levels of erbium. Oscillator strengths of these transitions were used to calculate the JO intensity parameters (Ω_t) of the erbium doped glass [78, 79]. The parameter Ω_2 shows a decrease compared to the earlier reported glass [143], indicative of

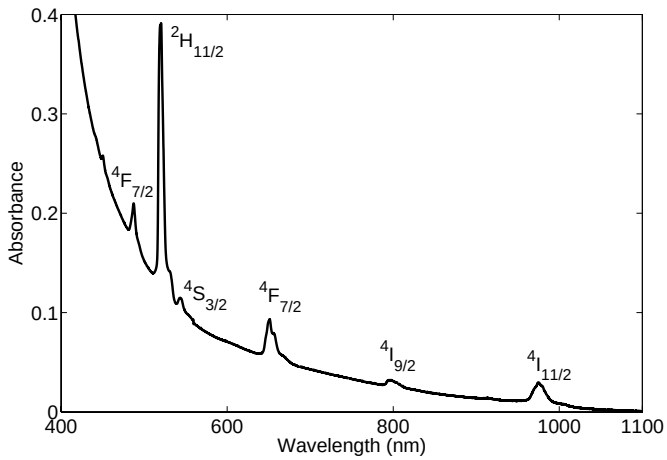

Figure 5.2: Absorption spectrum of the erbium-doped glass.

the formation of less Er covalent bonds upon addition of aluminum and lanthanum oxides.

The emission cross-section of the glass was obtained from the emission spectrum using standard procedures [56]. The radiative lifetime obtained from the JO analysis was used in the calculation of the spectrum. A typical emission cross-section spectrum is depicted in Fig. 5.3(a) and yields a cross-section of $6\times10^{-21}cm^2$ at 1537 nm. The fluorescence decay, shown in Fig. 5.3(b), yields a lifetime of 4.1 ms.

In order to deduce the nonlinear refractive index n_2, of the glass we used the self phase modulation (SPM) phenomena that generates spectral broadening in the 750-880 nm wavelength region. SPM was induced using an unfocussed, 45 fs laser pulse of energy 343 μJ. The peak wavelength of the incident laser pulse was measured to be 806 nm, with 26 nm bandwidth. After passing through a glass sample, the peak laser wavelength shifted to 805 nm and bandwidth increased to 31 nm. From the spectral broadening one can calculate the nonlinear refractive index n_2 [144]. The extent of Stokes broadening is obtained by,

$$\Delta\omega_{-} \simeq \omega_0 \, Q \tag{5.1}$$

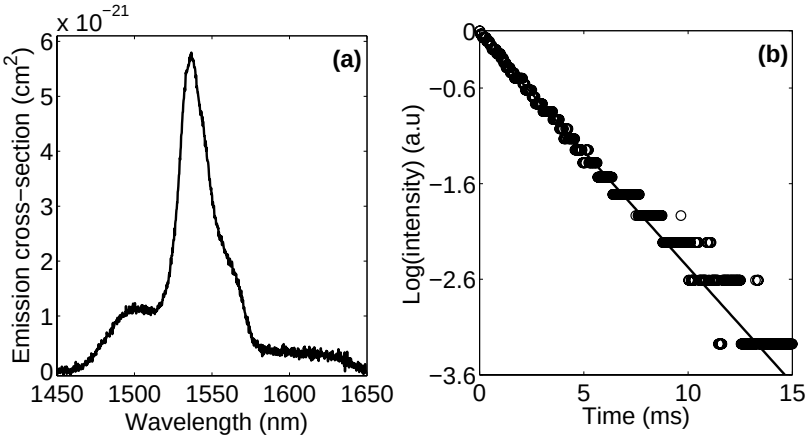

Figure 5.3: (a) Emission cross-section spectrum of the erbium-doped glass; (b) fluorescence decay data for the $^4I_{13/2} \rightarrow {}^4I_{15/2}$ transition. The fit (solid line) to the data yields a lifetime of 4.1 ms.

with $Q = \Delta n_{max}\ l_{eff}/c\ T$ where $T \sim 45$ fs and l_{eff} =1 cm. Δn is the induced refractive index change, c is the velocity of light and $\Delta\omega_-$ is the stokes broadening observed. The calculated Δn is then used to find n_2 using the relation $\Delta n = n_2\ I$ where I is the intensity of the laser. The broadening calculated from the Fig. 5.4 allows us to deduce the value of n_2 to be 6×10^{-20}m^2/W, which is about an order of magnitude less than that reported for tellurite glass [38]. We note that there is an overlap of the broadened light output (Fig. 5.4) with the $^4I_{9/2}$ state (Fig. 5.2). However, the product of sample length (0.1 cm) and absorption coefficient at 800 nm for the $^4I_{9/2}$ state (0.2 cm-1) is small enough to ensure that this overlap did not seriously affect the n_2 value that is deduced by us.

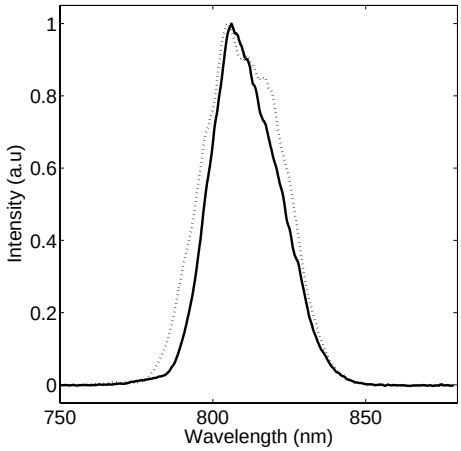

Figure 5.4: Spectrum of the incident laser pulse (solid line) and the spectrum of the light that is transmitted through our glass sample (dotted line).

5.3.2 Channel waveguides

Channels were fabricated in the glass using procedures described in the experimental section. Fig. 5.5(a) shows the top view of three channels in a typical glass sample photographed using optical microscope. Each of these channels were written using 3 μJ laser energy at constant writing speed of 0.01 cm/s (top channel), 0.02 cm/s (middle channel), and 0.03 cm/s (bottom channel). Many other writing experiments were performed using different laser energies and writing speeds, but the essential morphological features remained the same as shown in Fig. 5.5(a).

We used the transverse writing geometry without any beam shaping. The channels show good continuity under microscope inspection and are separated by $\sim$ 50 μm. They are formed at a distance of 500-800 μm below the surface of the glass. The width of the channels lies in the 4-8 μm range and each channel is 1 cm long. We have imaged the cross section of the channels under white light illumination and a slight ellipticity is noted. While transverse micromachining puts no limits on the length of the waveguide.

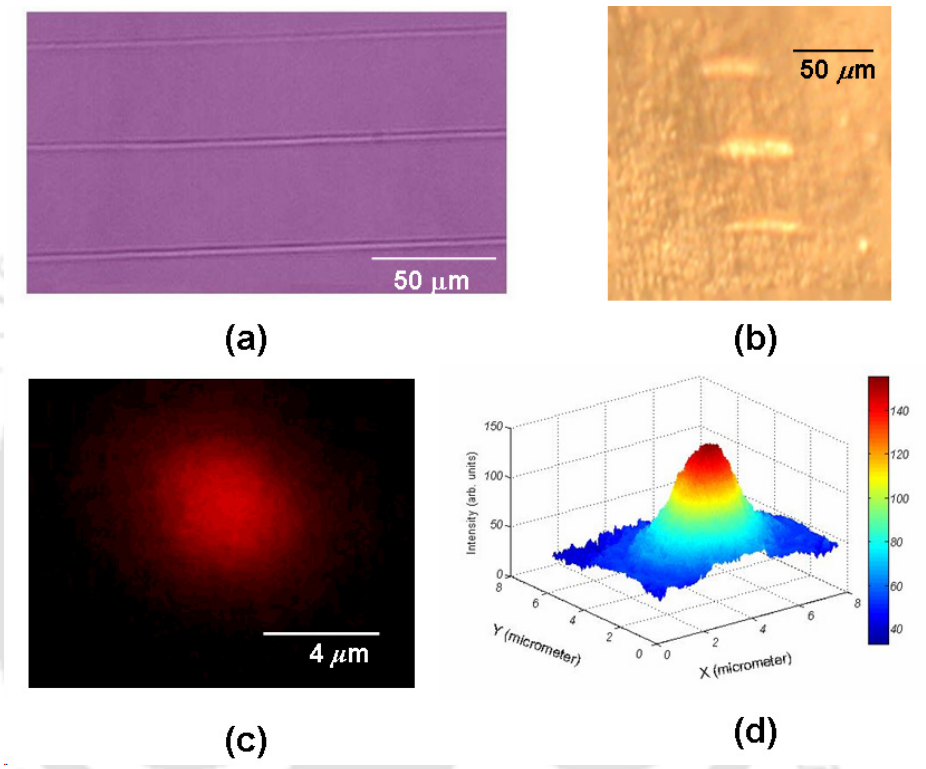

Figure 5.5: . (a) Laser-written channels observed through an optical microscope at writing speeds of 0.01 cm/s (top channel), 0.02 cm/s (middle channel), and 0.03 cm/s (bottom channel) with 3 μJ energy. (b) Cross-sectional side images of the waveguides shown in (a). (c) Mode-profile image of channel-transmitted 1310 nm laser light. (d) Intensity profile of the channel output depicted in (c). Horizontal lines in (a), (b), and (c) denote the indicated scale lengths.

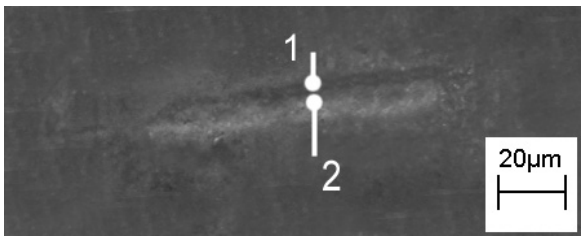

Figure 5.6: SEM picture of a channel face from the side. Te/P ratio at 1 (near the edge of the channel) is 1.4 and that at 2 (middle of the channel) is 3.0. Average Te/P ratio of the bulk glass outside the channel is found to be 1.9.

The cross-section of the waveguide in this geometry is expected to be elliptical because the structural modification is localized over the confocal (Rayleigh) range. To minimize ellipticity necessitates a transverse circular focal volume and this can only be achieved if the laser beam is shaped using either beam-shaping optics or slits [84, 85]. No beam shaping was carried out in the present work.

We also noted that there was a certain amount of ablation of the glass at the channel end faces. It has been reported that explosive expansion of ionized material (microexplosion) can take place in a tellurite glass under femtosecond laser irradiation [18][97]. However, in the present glass the lowering of the n_2 value (increase in the bandgap) compared to previously studied tellurite glasses has resulted in lower nonlinear absorption. Moreover, the higher glass transition temperature and the structural modification introduced by phosphate addition seems to favour waveguide formation. These facets are indicated in the side images of the waveguides that we depict in Fig. 5.5(b). The images shown in Fig. 5.5(a,b) are indicative of a refractive index profile that is quite complex. More detailed studies are clearly warranted.

The channel written glass was edge polished for efficient light coupling; light was launched into the channels by butt-coupling the fibre output from a 1310 nm laser source. Optical guidance was clearly observed. In Fig. 5.5(c) we show a mode-profile image (through

a 45X microscope objective) of the guided 1310 nm laser beam through the channel laser-written at a speed of 0.02 cm/s. The 3-D intensity profile of this channel output, shown in Fig. 5.5(d), indicates a net positive change in the refractive index, contrary to a previously reported result in tellurite glasses [142]. We made loss measurements at 1310 nm; estimated propagation losses are < 2 dB/cm. We also measured atomic concentrations of different components across the channels that we wrote, using scanning electron microscopy with X-ray microanalysis (LEO 1430VP). The SEM picture of one of the channels is shown in Fig. 5.6. A decrease in La and P atomic concentrations at the center of the channel and a migration of these atoms towards the periphery of the channels is observed in the analysis. The Te/P ratio near the edge of the channel (position 1 in figure) is 1.4 and that at middle of the channel(position 2) is 3.0. The average Te/P ratio of the bulk glass outside the channel is found to be 1.9. The modulation of Te:P ratio across the irradiated region can lead to a positive refractive index change [132] across each channel.

5.4 Conclusion

An erbium-doped tellurite glass with new composition has been designed, fabricated and its physical and spectroscopic properties characterized. Channels have been written inside this glass with focused, 45 fs laser pulses at 806 nm wavelength, using different energies and by varying substrate translation speeds. Our laser-written channels guide light of 1310 nm wavelength with estimated propagation losses of < 2 dB/cm. We believe this to be the first report of waveguiding in ultrashort-laser-written channels in erbium-doped tellurite glass. We attribute the positive index change under laser irradiation to the modification of the glass upon addition of phosphate. This introduces significant increase in the glass transition temperature and decrease of the nonlinear index of refraction. The re-

sults obtained in present work are promising for the fabrication of erbium doped integrated amplifiers and lasers based on tellurite glasses.

Chapter 6

Superfluorescent fibre source

Short length, air-clad, multimode fibres were fabricated using high concentrations Yb and Yb-Er doped phosphotellurite glass. Superfluorescent fibre sources are obtained by optically pumping the fibres using a 980 nm diode laser. Yb doped fibre shows superfluorescence in 1000-1100 nm wavelength region, whereas Yb-Er codoped fibre shows amplified spontaneous emission (ASE) in both 1000-1100 nm (due to Yb^{3+} ions) and 1450-1650 nm (due to Er^{3+} ions) wavelength regions. The recorded ASE spectra are compared for different fibre lengths and pump powers. We observed change in the ASE spectral shape and peak ASE wavelength with the increasing fibre length is discussed.

6.1 Introduction

Superfluorescent fibre sources (SFS) are low-coherence light sources with high-spectral power density over broad wavelength range. A rare-earth doped fibre optically pumped to a sufficiently high level can generate significant superfluorescent output via amplified spontaneous emission (ASE) [63].

Er doped SFS are of great interest for several applications such as wavelength division multiplexed (WDM) optical networks and fiber-optic gyroscopes (FOG) [145]. Er doped SFS were demonstrated for interferometric sensor applications [146]. ASE source was used to generate super-continuum of 956 nm with a spectral density of over -10 dBm/nm [147]. In general, an incoherent broadband optical source with low spectral ripples and high power intensity in ASE spectrum is required for better performance. The ASE from Er^{3+} ions in silica glass covers the spectral range 1520–1560 nm (C-band) for the transition from $^4I_{13/2}$ to $^4I_{15/2}$ [8]. Watt-level L band Er doped SFS are reportedly used in a critical geometry [148]. Er doped tellurite glass fibres are reported for broadband amplification of Er doped fibres [13]. Erbium doped tellurite fibre (EDTF) has much better gain flatness and broader amplification range [105]. The potential for ultra-short length, broadband EDTF amplifiers are reported [149]. Tellurite glass fibre doped with thulium and erbium is reported for broadband emission in the S-C-L bands [14].

Because of the simple quasi-three-level energy structure [64], ytterbium ions doped glasses exhibits high quantum efficiencies, low nonradiative decay rate and long fluorescence lifetime (1-2 ms) [150]. Usually high Yb^{3+} doping can be achieved in glasses and crystals. Possibility of wide tuning and the prospect of scaling to the higher powers for Yb doped SFS are reported [64, 151]. Yb-doped SFS with 3 dB bandwidth of 42 nm and output power of 2 W is demonstrated [152]. Yb doped tellurite based SFS demands more attention for

high power and broad bandwidth applications.

The objective of this chapter is to fabricate and study spectroscopic properties of the Yb doped and Yb-Er codoped phosphotellurite(PT) glass suitable for SFS. The characteristics of the ASE spectrum of doped phosphotellurite glass fibre were investigated using fibres of different lengths and pump powers.

6.2 Experimental procedures

Two phosphotellurite glasses doped with ytterbium and erbium is fabricated and their physical and spectroscopic parameters are obtained as described in the earlier chapters. Bulk samples made were of the following compositions (all in mole%),

1. $25P_2O_5$-$74.6TeO_2$-$0.4Yb_2O_3$ (FY)

2. $25P_2O_5$-$74.25TeO_2$-$0.25Yb_2O_3$-$0.25Er_2O_3$ (FYE)

For the fabrication of the fibre the above compositions were chosen excluding sodium. The refractive index, glass transition temperature, density and number of Yb^{3+} and Er^{3+} ions/cc present in the glass matrix were obtained by the procedure described previously [section 2.2]. The absorption spectra of the polished glass samples in the NIR region were recorded. The emission spectra was obtained under 970-980 nm optical pumping using a diode laser. The modulated laser beam was used for the lifetime measurements as described earlier.

Air cladded, multimode fibres of high RE doping concentrations and short lengths were pulled from the preformed glasses heated to a temperature of $\sim 550^oC$. A commercial silica fibre was used to pull the doped fibres from the glass melt. The light guidance through the fibre was tested by coupling the fibre to the output of a He-Ne laser. The fibres were inspected under an optical microscope to to check the cross-section and the uniformity

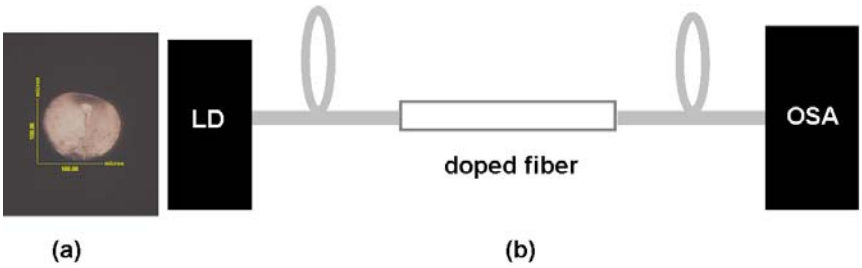

Figure 6.1: (a) The cross-section of one of the fibres fabricated is also given. (b) The schematic of the experimental setup for ASE measurement shown.

along its length. End face of one of the fabricated fibres is shown in Fig. 6.1(a). The fibres which are uniform throughout the length and of diameter ∼90 μm were used for ASE generation. The value of the numerical aperture of the fibres were ∼1.7. The schematic of the experimental setup used for the ASE measurement is shown Fig. 6.1(b). The doped fibre was pumped using a laser diode which is tunable in the wavelength range 970-980 nm. The output fibre from the laser diode was butt coupled to the doped fibre. The output from the doped fibre was fed to OSA through a standard single mode fibre. The single pass forward ASE light produced by different pump powers were measured using the OSA.

6.3 Results and discussion

6.3.1 Bulk glass properties

The physical and spectroscopic properties were found for both the glasses. The important properties of the Yb doped glass named FY is reported in Table 6.1. The procedure to obtain those parameters is discussed in Chapter-4. The calculated absorption and emission cross-section spectra of the Yb^{3+} ions in the wavelength region 900-1100 nm is shown in Fig. 6.2(a). The emission cross-section spectrum is obtained from the absorption cross-section spectrum using reciprocity method given in Chapter-4. The measured

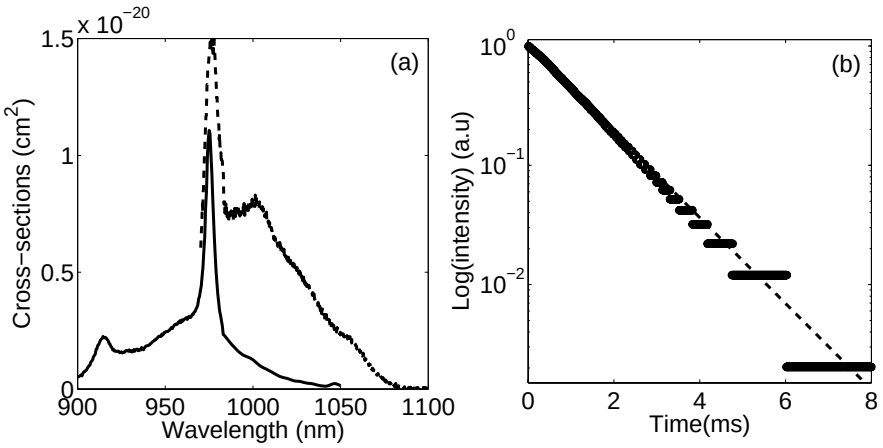

Figure 6.2: (a) Absorption (solid line) and emission (dashed line) cross-section spectra of the Yb doped bulk glass sample, (b) Fluorescence decay under 970 nm excitation.

fluorescence decay is given in Fig. 6.2(b).

The properties of Yb-Er doped glass named FYE was measured using methods discussed in previous chapters. The important parameters are given in Table. 6.2. The emission cross-section spectrum and measured fluorescence decay used to calculate the life-time is shown in Fig. 6.3(a) and (b) respectively. Emission cross-section spectrum was obtained from the measured fluorescence spectrum using Eq.(1.12) and using measured lifetime.

6.3.2 Yb doped fiber ASE

We used the Yb doped PT glass fibre for generating ASE. ASE spectra were obtained with three different fibre length 36 cm, 26 cm and 10 cm using the pump laser at a wavelength 980 nm and pump power 200 mW. It is shown in Fig. 6.4. From the figure it is observed that the wavelength corresponding to peak ASE intensity vary with the fibre

Properties	Parameters	Values	Units
Physical	n @633 nm	2.01	
	T_g	391	^oC
	ΔC_p	0.192	J/gm-^oC
	Density	3.70	gm/cc
	No. of Yb^{3+} ions, N	1.1×10^{20}	ions/cc
Absorption	σ_a @ 975 nm	1.11×10^{-20}	cm^2
	σ_a @ 980 nm	0.40×10^{-20}	cm^2
	σ_a @ 1001 nm	0.12×10^{-20}	cm^2
Fluorescence	σ_e @ 975 nm	1.51×10^{-20}	cm^2
	σ_e @ 1001 nm	0.83×10^{-20}	cm^2
	τ_f	1.12	ms
Laser parameters	Gain ($\sigma_e \times \tau_f$) @ 975	1.69×10^{-20}	cm^2-ms
	Gain ($\sigma_e \times \tau_f$) @ 1001	0.93×10^{-20}	cm^2-ms
	I_{min}	1.90	kW/cm^2

Table 6.1: Physical, spectroscopic properties, and Laser parameters of the bulk glass having the composition $25P_2O_5$-$74.6TeO_2$-$0.4Yb_2O_3$ (FY). n is refractive index, T_g glass transition temperature, ΔC_p excess heat capacity, σ_a absorption cross-section, σ_e emission cross-section, τ_f fluorescence lifetime and I_{min} is the parameter which evaluates the minimum absorbed pump intensity required to reach laser threshold.

length. Also there is change in the spectral lineshape and peak ASE wavelength. The peak ASE wavelength for 10 cm, 26 cm and 36 cm fibres are 1024 nm, 1033 nm and 1044 nm respectively. The FWHM of the observed ASE spectra for 36 cm, 26 cm and 10 cm fibres are 49 nm, 54 nm and 64 nm respectively. For the fibre with 10 cm length the residual pump power is visible in the given ASE spectrum. However, the pump is absent in the spectrum of 26 cm and 36 cm long fibres. The bandwidth of the ASE spectrum decreases with the length of the fibre for a given pump power. Whereas the FWHM does not show any considerable change with the pump power. This can be seen from Fig. 6.5 in which we have plotted pump power vs. FWHM for different fibre lengths. The overall shifting of the spectrum towards the higher wavelength side can be explained on the basis of the absence of pump in the spectrum of the longer fibres mentioned before. In the case of fibre of length 10 cm the pump power is available throughout its length and therefore the forward ASE

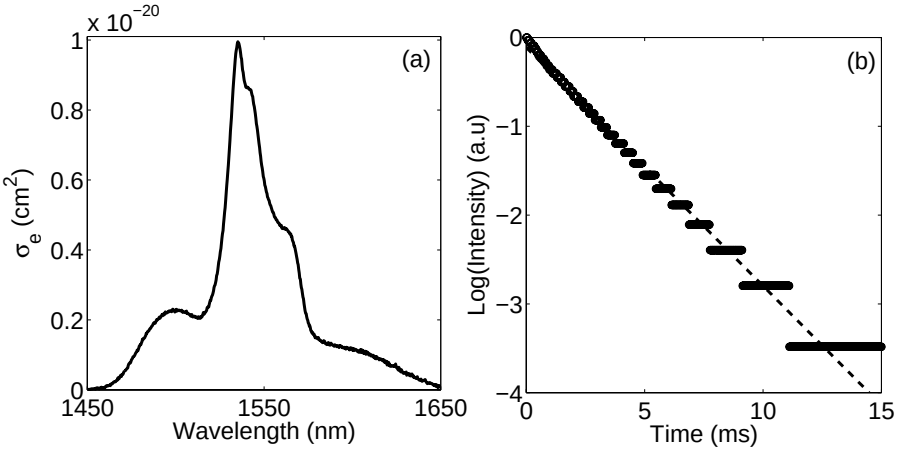

Figure 6.3: (a) Absorption and emission cross-section spectra of the Er-Yb doped bulk glass sample, (b) Fluorescence decay under 980 nm excitation.

generated in the fibre gets amplified as it propagates through the fibre. This can be verified by looking at Fig. 6.6. The lineshape remains the same with the increasing pump power and the residual pump intensity was visible in all the spectra shown in the figure. In the case of longer fibres of length 26 cm and 36 cm the forward ASE generated at the input and amplified to the point where there was enough pump to produce spontaneous emission. Since the given pump power is not sufficient to propagate till the fibre end the ASE would be reabsorbed in the fibre as it propagates beyond the point where the pump is absent. Since the absorption cross-section is higher on the lower wavelength side (below ∼1000 nm) the reabsorption is more prominent in this region.

In a short Yb doped fibre FWHM reported here is higher than that reported in a commercial ASE source [153]. The bandwidth could be increased to ∼70 nm by optimizing the fibre length and pump power in a single pass forward configuration. The performance of the proposed ASE sources could be improved further by choosing different

Properties	Parameters	Values	Units
Physical	n @633 nm	2.00	
	T_g	386	^oC
	ΔC_p	0.125	J/gm-^oC
	Density	3.75	gm/cc
	No. of Er^{3+} ions, N	4.5×10^{19}	ions/cc
	No. of Yb^{3+} ions, N	4.6×10^{19}	ions/cc
Fluorescence	σ_e @ 1535 nm	9.95×10^{-21}	cm^2
	Effective Bandwidth	50	nm
	Fluorescence lifetime	3.7	ms
	Gain @ 1535	36.82×10^{-21}	cm^2-ms

Table 6.2: Physical, and fluorescence properties of the bulk glass having the composition $25P_2O_5$-$74.25TeO_2$-$0.25Yb_2O_3$-$0.25Er_2O_3$ (FYE).

pump wavelengths, fibre parameters and system configurations [151, 100]. Such short length fibres are also promising for lasers and amplifiers.

6.3.3 Yb-Er doped fiber ASE

In this section we investigated the characteristics of ASE produced in air clad, shortlength multimode fibres codoped with Yb and Er. We fabricated four fibres having lengths 25 cm, 15 cm, 10 cm, and 5 cm. The forward ASE output intensity has been recorded using the setup shown in Fig. 6.1(b). The fibre was pumped at 980 nm. The ASE spectrum obtained in the OSA from 950 nm to 1700 nm for 25 cm fibre is shown in the Fig. 6.7. The figure shows the ASE spectrum produced in the fibre individually by Yb^{3+} and Er^{3+} ions.

The observed ASE in the wavelength range 1000 nm-1100 nm is produced by Yb^{3+} ions and the wavelength range 1450 nm-1650 nm is produced by Er^{3+} ions. Therefore in a Yb-Er codoped fibre the simultaneous generation of ASE due to Yb and Er is possible using a single pump laser of wavelength 980 nm. The peak power of the ASE increases with the increase of pump power for both the Yb and Er amplification regions. The peak ASE

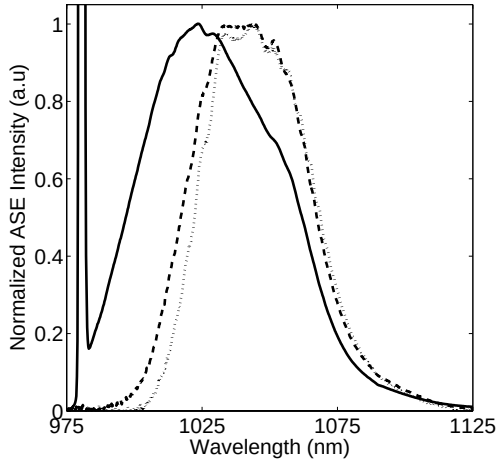

Figure 6.4: Normalised ASE of the Yb doped fibre of different lengths 10 cm(solid line), 26 cm(dashed), 36 cm(dotted).

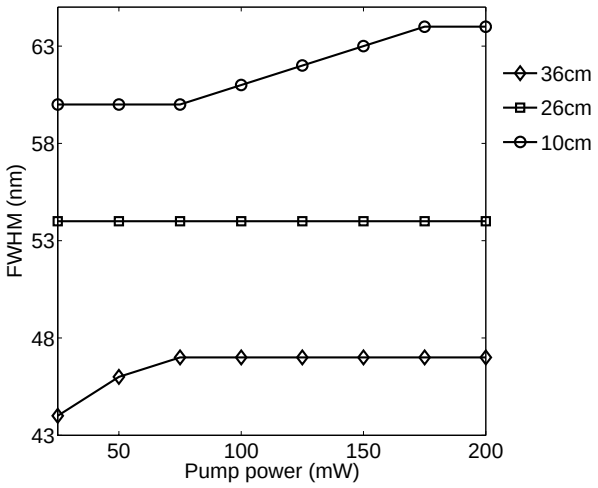

Figure 6.5: The variation of FWHM of the obtained spectra with pump power shown for different fibre lengths.

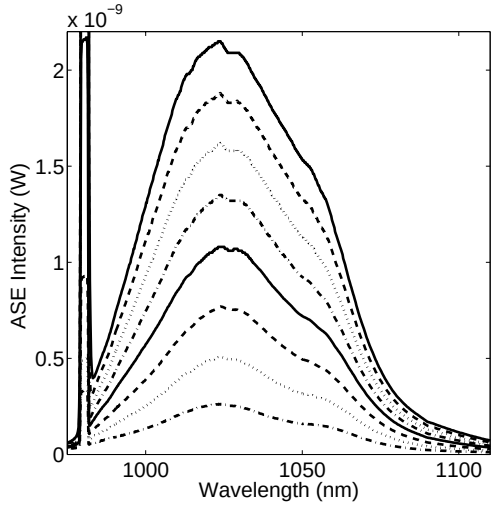

Figure 6.6: ASE spectrum obtained with increasing 980 nm pump power for 25mW to 200mW having interval of 25mW.

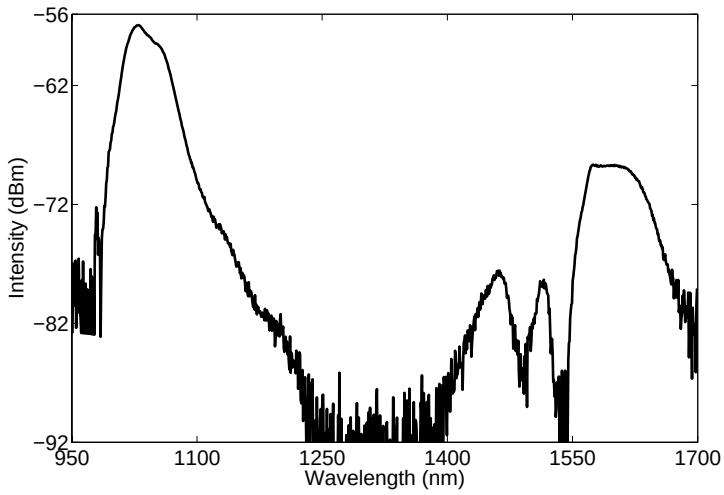

Figure 6.7: ASE spectrum of the Er-Yb doped fibre shows the amplification of both Yb^{3+} and Er^{3+} ions simultaneously under 980 nm pumping.

wavelength of Er shifts towards the longer wavelength as we increase the fibre length for a fixed pump power of 200 mW (Fig. 6.8).

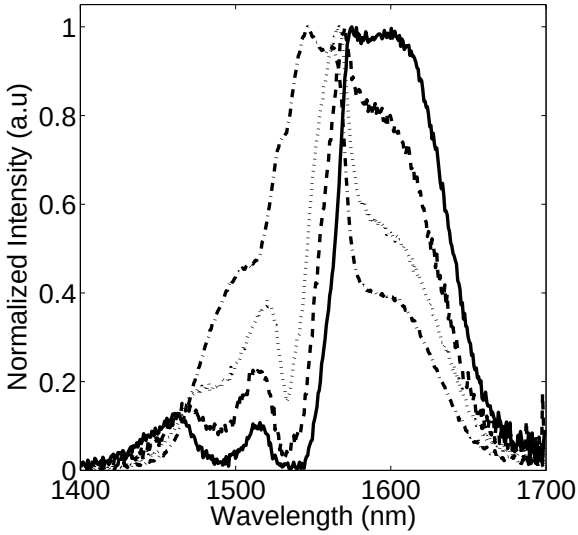

Figure 6.8: The ASE obtained for different lengths are shown.

The peak wavelengths of the normalized ASE spectrum for 25 cm, 15 cm, 10 cm and 5 cm fibres are observed at 1575 nm, 1570 nm, 1567 nm and 1546 nm respectively. The 3 dB bandwidth of 25 cm fibre is 77 nm (1563-1640 nm), while that of 5 cm fibre is only 62 nm (1515-1577 nm). In the present configuration it requires the optimization of both pump power and fibre length to obtain the maximum possible bandwidth which is around 125 nm.

ASE spectrum of fibres with longer lengths such as 10 cm, 15 cm, and 25 cm shows that superfluorescence due to Er^{3+} ions have undergone a strong reabsorption at the peak absorption wavelength 1535 nm of the Er^{3+} ions. Figure 6.8 show that in the 1420 nm-

1550 nm wavelength region of the ASE spectra look exactly like inverted Er absorption spectra. The absorption cross-section of Er in the glass is very low comparing to the emission cross-section in the wavelength region 1550 nm-1650 nm. Therefore the reabsorption of ASE is negligible in this region.

The forward Er ASE suffers reabsorption as it propagates along the fibre. Since the absorption cross-section of Yb^{3+} at 980 nm is one order of magnitude higher than Er^{3+} at 980 nm, most of the Yb ions would be excited and may be possible that number of excited Er^{3+} ions is less. Since the Yb ASE intensity in the fibre is observed to be increasing with pump it raises questions about the efficiency of the pump energy transfer to Er in the fibre. When the pump is not sufficient enough to amplify the Er-ASE signal it undergoes absorption in the shorter wavelength end of the spectrum where the difference in emission cross section and absorption cross-section is very small. The backward ASE would not suffer the reabsorption because the atoms are already in the excited state.

Er doped and Yb-Er doped ASE source has been studied in different configurations like SPF (single pass forward), SPB (single pass backward), DPF (double pass forward), DPB (double pass backward) to have more pumping efficiency, higher stable output and larger bandwidth [100, 99, 106, 154, 155, 156, 157, 158, 159, 160]. High power SFS with stable single-transverse-mode output using a heavily doped multimode fibre reported in an Er doped fibre with large core diameter and high numerical aperture [154, 101]. Long period grating (LPG) has been used for multiwavelength fibre source [102], broadening the linewidth of Er-doped SFS [103] and compensate the dependence of mean wavelength of ASE on temperature [104].

In order to use the Yb-Er doped SFS in practical devices there is need for further improvements in the fibre design as well as pumping and ASE extraction scheme.

6.4 Conclusion

We have experimentally demonstrated a Yb doped and Yb-Er codoped phosphotellurite glass fibres as a potential superfluorescence fibre source. The physical and spectroscopic characteristics of glass compositions used for fibre drawing are reported. The air clad, multimode, short length glass fibres were used for the ASE generation under 980 nm diode laser pumpimg. The doped fibres were characterized as an ASE source for different fibre lengths and pump powers. Yb doped fibres shows amplification in the wavelength range 1000-1100 nm. The highest bandwidth obtained with the Yb SFS was 64 nm for 10cm length of FY fibre pumped at 200mW. The Yb-Er codoped fibres have an advantage of producing ASE in 1000-1100 nm (due to Yb^{3+}) and 1450-1650 nm (due to Er^{3+}). There is L-band superfluorescence of bandwidth 77 nm (1563-1640 nm) in 25 cm FYE fibre optically pumped at 200 mW. We observed a red shift of the peak ASE wavelength with the increasing fibre length. This is due to the reabsorption mechanism occurring inside the fibre during the propagation of the amplified signal. By improving the pump and ASE extraction scheme the shorter length Yb and Yb-Er doped phosphotellurite glass fibres could be a potential medium for broadband and high power superfluorescent fibre sources.

Bibliography

[1] T. H. Maiman, Phys. Rev. Lett. 4 (1960) 564–566.

[2] O. Svelto, Principles of Lasers, Plenum Press. New York and London, 1989.

[3] E. Snitzer, Phys. Rev. Lett. 7 (12) (1961) 444–446.

[4] S. Taccheo, P. Laporta, S. Longhi, O. Svelto, C. Svelto, Appl. Phys. B 63 (1996) 425–436.

[5] G. N. Conti, A. Chiasera, L. Ghisa, S. Berneschi, M. Brenci, Y. Dumeige, S. Pelli, S. Sebastiani, P. Feron, M. Ferrari, G. Righini, J. Non-Cryst. Solids 352 (2006) 2360–2363.

[6] X. Penga, F. Song, S. Jiang, N. Peyghambarian, M. Kuwata-Gonokami, L. Xu, Appl. Phys. Lett. 82 (10) (2003) 1497–1499.

[7] Edited. by M. J. F. Digonnet, Rare earth doped fiber lasers and amplifiers, Marcel Dekker, Inc. New York, 1993.

[8] A. Bellemare, Prog. in Quantum Electronics 27 (2003) 211–266.

[9] G. D. Valle, S. Taccheo, G. Sorbello, V. Foglietti, E. Cianci, G. Jose, S. Jiang, G. Cerullo, R. Ossellame, M. Marangaoni, R. Ramponi, P. Laporta, Recent Research Developments in Optics 3 (2003) 667–703.

[10] http://www.bicron.com/.

[11] http://www.kigre.com/.

[12] http://www.corning.com/.

[13] M. Yamada, A. Mori, K. Kobayashi, H. Onom, T. Kanamori, K. Oikawa, Y. Nishida, Y. Ohishi, IEEE Photon. Technol. Lett. 10 (9) (1998) 1244–1246.

[14] L. Huang, A. Jha, S. Shen, X. Liu, Opt. Express 12 (11) (2004) 2429–2434.

[15] G. Jose, G. Sorbello, S. Taccheo, E. Cianci, V. Foglietti, P. Laporta, J. Non-Cryst. Solids 322 (2003) 256–261.

[16] R. Osellame, S. Taccheo, G. Cerullo, M. Marangoni, D. Polli, R. Ramponi, P. Laporta, S. D. Silvestri, Electron. Lett. 38 (17) (2002) 964–965.

[17] T. Sum, A. Bettiol, K. Liu, M. Ren, E. Pun, S. V. Rao, J. van Kan, F. Watt, Nuclear Instruments and Methods in Physics Research B 231 (2005) 394–399.

[18] S. Coffa, S. Libertino, G. Coppola, A. Cutolo, J. Lightwave Technol. 36 (2000) 1206–1213.

[19] J. Hubner, S. Guldberg-Kjaer, M. Dyngaard, Y. Shen, C. Thomsen, S. Balslev, C. Jensen, D. Zauner, T. Feuchter, Appl. Phys. B 73 (2001) 435-438.

[20] K. Shuto, K. Hattori, T. Kitagawa, Y. Ohmori, M. Horiguchi, Electron. Lett. 29 (1993) 139–141.

[21] K. ill Cho, K. H. Cho, S. H. Cho, D. W. Shin, Opt. Mat. 28 (2006) 888–892.

[22] X. Orignac, D. Barbier, X. Du, R. Almeida, O. McCarthy, E. Yeatman, Opt. Mat. 12 (1999) 1–18.

[23] R. Ghosh, J. Shmulovich, C. Kane, M. de, Barros, G. Nykolak, A. Bruce, P. Becker, IEEE Photon. Technol. Lett. 8 (1996) 518–520.

[24] D. L. Veasey, D. S. Funk, P. M. Peters, N. A. Sanford, G. E. Obarski, N. Fontaine, M. Young, A. P. Peskin, W.-C. Liu, S. N. Houde-Walter, J. S. Hayden, J. Non-Cryst. Solids 263-264 (2000) 369–381.

[25] G. Sorbello, S. Taccheo, G. D. Valle, P. Laporta, E. Cianci, V. Foglietti, S. Jiang, N. Peyghambarian, Optical and Quantum Electronics 35 (7) (2003) 669–674.

[26] S. Nolte, M. Will, J. Burghoff, A. Tuennermann, Appl. Phys. A 77 (2003) 109–111.

[27] R. Osellame, N. Chiodo, G. D. Valle, G. Cerullo, R. Ramponi, P. Laporta, A. Killi, O. Svelto, IEEE J. Sel. Top. Quantum Electron. 12 (2) (2006) 227–285.

[28] D. P. Y. Jeong, J. Sahu, J. Nilsson, Opt. Express 12 (25) (2004) 6088–6092.

[29] A. S. Kurkov, A. Y. Laptev, E. M. Dianov, A. N. Guryanov, V. I. Karpov, V. M. Paramonov, O. I. Medvedkov, A. A. Umnikov, V. N. Protopopov, N. N. Vechkanov, S. A. Vasiliev, E. V. Pershina, Proceedings of SPIE 4083 (2000) 118–126.

[30] Y. W. Lee, S. Sinha, M. J. F. Digonnet, R. L. Byer, Opt. Lett. 31 (22) (2006) 3255–3257.

[31] D.Y.Shen, J.K.Sahu, W.A.Clarkson, Opt. Express 13 (13) (2005) 4916–4921.

[32] G. Fuxi, Optical and Spectroscopic properties of glass, Springer-Verlag, Shanghai, 1992.

[33] A. K. Varshneya, Fundamentals of inorganic glasses, Academic Press, Inc., 1994.

[34] M. J. Weber, J. Non-Cryst. Solids 123 (1990) 208–222.

[35] M. Yamane, Y. Asahara, Glasses for Photonics, Cambridge University Press, 2000.

[36] M. J. Weber, Handbook of optical materials, CRC Press, 2003.

[37] http://www.schott.com/.

[38] J. S. Wang, E. M. Vogel, E. Snitzer, Opt. Mat. 3 (1994) 187–203.

[39] H. Lin, S. Jiang, J. Wu, F. Song, N. Peyghambarian, E. Y. B. Pun, J. Phys.D: Appl. Phys. 36 (2003) 812–817.

[40] R. Rolli, M. Montagna, S. Chaussendent, A. Monteil, V. K. Tikhomirov, M. Ferrari, Opt. Mat. 21 (2003) 743–748.

[41] M.Mattarelli, A. Chiappini, M. Montagna, A. Martucci, A. Ribaudi, M. Guglielmi, M. Ferrari, A. Chiasera, J. Non-Cryst. Solids 351 (2005) 1759–1763.

[42] G. Wang, S. Xu, S. Dai, J. Zhang, L. Hu, Z. Jiang, Mater. Lett. 59 (2005) 366–369.

[43] S. Dai, J. Zhang, C. Yu, G. Zhou, G. Wang, L. Hu, Mater. Lett. 59 (2005) 2333–2336.

[44] S. Shen, A. Jha, E. Zhang, S. Wilson, C. R. Chimie 5 (2002) 921–938.

[45] R. Koch, W. A. Clarkson, D. C. Hanna, S. Jiang, M. J. Myers, D. Rhonehouse, S. J. Hamlin, U. Griebner, H. Schonnagel, Opt. Commun. 134 (1997) 175–178.

[46] S. Shen, M. Nftaly, A. Jha, Opt. Commun. 205 (2002) 101–105.

[47] R. El-Mallawany, A. Patra, C. S. Friend, R. Kapoor, P. N. Prasad, Opt. Mat. 26 (2004) 267–270.

[48] Y. Luo, J. Zhang, J. Sun, S. Lu, X. Wang, Opt. Mat. 28 (2006) 255–258.

[49] G. N. Conti, S. Berneschi, M. Bettinelli, M. Brenci, B. Chen, S. Pelli, A. Speghini, G. Righini, J. Non-Cryst. Solids 345 & 346 (2004) 343–348.

[50] S. Hocde, S. Jiang, X. Peng, N. Peyghambarian, T. Luo, M. Morrell, Opt. Mat. 25 (2004) 149–156.

[51] S. Dai, C. Yu, G. Zhou, J. Zhang, G. Wang, L. Hu, J. Lumin. 117 (2006) 39–45.

[52] C. Jiang, F. Gan, J. Zhang, P. Deng, G. Huang, Mater. Lett. 41 (1999) 209–214.

[53] G. Wang, J. Zang, S. Xu, S. Dai, L. Hu, J. Yang, Z. Jiang, J. Lumin. 109 (2004) 1–7.

[54] S. Neov, I. Gerasimova, V. Kozhukharov, M. Marinov, J. Mater. Sci. 15 (1980) 1153–1166.

[55] K. Muruganandam, M. Seshasayee, J. Non-Cryst. Solids 222 (1997) 131–136.

[56] M. J. Weber, J. D. Myers, D. H. Blackburn, J. Appl. Phys. 52 (4) (1981) 2944–2949.

[57] T. Konishi, T. Hondo, T. Araki, K. Nishio, T. Tsuchiya, T. Matsumoto, S. Suehara, S. Todoroki and S. Inoue, J. Non-Cryst. Solids 324 (2003) 58–66.

[58] G. S. Murugan, T. Suzuki, Y. Ohishi, Appl. Phys. Lett. 86 (2005) 221109–1–221109–3.

[59] R. Reisfeld, C. K. Jorgensen, Lasers and excited states of rare earths, Springer-Verlag, 1977.

[60] C. C. Robinson, J. Non-Cryst. Solids 15 (1974) 1–10.

[61] C. C. Robinson, J. Non-Cryst. Solids 15 (1974) 11–29.

[62] E. Desurvire, Erbium-doped fiber amplifiers, John Wiley & Sons. New York, 1994.

[63] M. Digonnet, J. Lightwave Technol. LT-4 (11) (1986) 1631–1639.

[64] D. Hanna, I. Perry, R. Smart, P. Suni, J. Townsend, A. Tropper, Opt. Commun. 72 (1989) 230–234.

[65] S. Jiang, M. Mayer, N. Peyghambarian, J. Non-Cryst. Solids 239 (1998) 143–148.

[66] E. Snitzer, R. Woodcock, Appl. Phys. Lett. 6 (1965) 45–46.

[67] F. Auzel, J. Lumin. 45 (1990) 341-345.

[68] A. J. Kenyon, Prog. in Quantum Electronics 26 (2002) 225–284.

[69] R. Paschotta, J. Nilsson, A. Topper, D. Hanna, IEEE J. Quantum Electron. 33 (7) (1997) 1049–1056.

[70] X. Feng, C. Qi, F. Lin, H. Hu, J. Non-Cryst. Solids 256 & 257 (1999) 372–377.

[71] L. C. Courrol, L. R. P. Kassab, A. S. Morais, C. M. S. Mendes, L. Gomes, N. U. Wetter, N. D. Vieira, F. C. Cassanjes, Y. Messaddeq, S. J. L. Ribeiro, J. Lumin. 102-103 (2003) 106–111.

[72] A. Kaminski, Laser Crystals, Springer-Verlag, 1989.

[73] R. Paschotta, J. Nilsson, A. C. Tropper, D. C. Hanna, IEEE J. Quantum Electron. 33 (7) (1997) 1049–1056.

[74] X. Zou, H. Toratani, Phys. Rev. B 52 (22) (1995) 15889–15897.

[75] E. Nakzawa, S. Shionoya, Phys. Rev. Lett. 25 (25) (1970) 1710–1712.

[76] M. J. V. Bell, WGQuirino, S. LOliveira, D. F. de Sousa, L. A. O. Nunes, J. Phys.: Condens. Matter. 15 (2003) 4877-4887.

[77] S. Tanabe, J. Non-Cryst. Solids 259 (1999) 1–9.

[78] B. R. Judd, Phys. Rev. 127 (1962) 750–761.

[79] G. S. Ofelt, J. Chem. Phys. 37 (3) (1962) 511–520.

[80] W. T. Carnall, P. R. Fields, K. Rajnak, J. Chem. Phys. 49 (10) (1968) 4412–4423.

[81] W. T. Carnall, P. R. Fields, K. Rajnak, J. Chem. Phys. 49 (10) (1968) 4424–4442.

[82] M. J. Weber, Phys. Rev. 157 (1967) 262–172.

[83] D. E. McCumber, Phys. Rev. 134 (1964) A299 – A306.

[84] G. Cerullo, R. Osellame, S. Taccheo, U. Marangoni, D. Polli, R. Ramponi, P. Laporta, S. D. Silvestri, Opt. Lett. 27 (2002) 1938–1940.

[85] M. Ams, G. D. Marshall, D. J. Spence, M. J. Withford, Opt. Express 13 (2005) 5676–5681.

[86] K. M. Davis, K. Miura, N. Suimoto, K. Hirao, Opt. Lett. 21 (1996) 1729–1731.

[87] K. Minoshima, A. M. Kowalevicz, I. Hartl, E. P. Ippen, J. G. Fujimoto, Opt. Lett. 26 (19) (2001) 1516–1518.

[88] S. Taccheo, G. D. Valle, R. Osellame, G. Cerullo, N. Chiodo, P. Laporta, O. Svelto, A. Killi, U. M. M. Lederer, D. Kopf, Opt. Lett. 29 (2004) 2626–2628.

[89] E. N. Glezer, M. Milosavljevic, L. Huang, R. J. Finlay, T.-H. Her, J. P. Callan, E. Mazur, Opt. Lett. 21 (24) (1996) 2023–2025.

[90] K. Kawamura, T. Ogawa, N. Sarukura, M. Hirano, H. Hosono, Appl. Phys. B 71 (2000) 119-121.

[91] K. Miura, J. Qiu, H. Inouye, T. Mitsuyu, K. Hirao, Appl. Phys. Lett. 71 (23) (1997) 3329–3331.

[92] L. Sudrie, M. Franco, B. Prade, A. Mysyrowicz, Opt. Commun. 171 (1999) 279-284.

[93] Y. Shimotsuma, P. G. Kazansky, J. Qiu, K. Hirao, Phys. Rev. Lett. 91 (24) (2003) 247405–1–247405–4.

[94] E. Bricchi, B. G. Klappauf, P. G. Kazansky, Opt. Lett. 29 (1) (2004) 119–121.

[95] E. N. Glezer, E. Mazur, Appl. Phys. Lett. 71 (7) (1997) 882–884.

[96] J. Chan, T. Huser, S. Risbud, D. Krol, Appl. Phys. A 76 (2003) 367372.

[97] S. K. Sundaram, C. B. Schaffer, E. Mazur, Appl. Phys. A 76 (2003) 379–384.

[98] R. R. Gattass, E. Mazur, Photonics Spectra. 12 (2004) 56–60.

[99] K. Iwatsuki, IEEE Photon. Technol. Lett. 2 (4) (1990) 237–238.

[100] L. Wang, C. Chen, Electron. Lett. 33 (8) (1997) 703–704.

[101] O. Okhotnikov, J. Soma, Electron. Lett. 33 (20) (1997) 1727–1728.

[102] C. Su, L. Wang, Electron. Lett. 35 (11) (1999) 927–929.

[103] C. Su, L. Wang, Electron. Lett. 35 (4) (1999) 331–332.

[104] H. Patrick, A. Kersey, W. Burns, R. Moeller, Electron. Lett. 33 (24) (1997) 2061–2063.

[105] J. Zhang, S. Dai, G. Wang, H. Sun, L. Zhang, L. Hu, J. Lumin. 115 (2005) 4552.

[106] K. Iwatsuki, IEEE Photon. Technol. Lett. 3 (3) (1991) 281–283.

[107] A. Narazaki, K. Tanaka, K. Hirao, N. Soga, J. Appl. Phys. 85 (4) (1999) 2046–2051.

[108] V. Dimitrov, T. Komatsu, J. Non-Cryst. Solids 249 (1999) 160–179.

[109] Y. Ding, S. Jiang, T. Luo, Y. Hu, N. Peyghambarian, Proceedings of SPIE 4282 (2001) 23–30.

[110] P. M. Peter, D. S. Funk, A. P. Peskin, D. L. Veasey, N. A. Sanford, S. N. Houde-Walter, J. S. Hayden, Appl. Optics 38 (33) (1999) 6879–6886.

[111] G. F. Imbush, Advances in Nonradiative decay processes in solids, Edited by B. D. Bartolo, Plenum, 1991.

[112] S. A. Payne, L. L. Chase, L. K. Smith, W. L. Kway, W. F. Krupke, IEEE J. Quantum Electron. 28 (11) (1992) 2619–2630.

[113] L.D. DeLoach, S.A. Payne, L.L. Chase, L.K. Smith, W.L. Kway, W.F. Krupke, IEEE J. Quantum Electron. 29 (4) (1993) 1179–1191.

[114] W. J. Miniscalco, R. S. Quimby, Opt. Lett. 16 (1991) 258–260.

[115] B. J. Chen, G. C. Righini, M. Bettinelli, A. Speghini, J. Non-Cryst. Solids 322 (2003) 319—323.

[116] U. Hoppe, I. Gugov, H. Burger, P. Jovari, A. C. Hannon, J. Phys.: Condens. Matter. 17 (2005) 2365–2386.

[117] Q. Zhang, Z. Feng, Z. Yang, Z. Jiang, Journal of Quantitative Spectroscopy and Radiative Transfer 98 (2) (2006) 167–179.

[118] D. F. de Sousa, J. A. Sampaio, L. A. O. Nunes, M. L. Baesso, A. C. Bento, L. C. M. Miranda, Phys. Rev. B 62 (5) (2000) 3176–3180.

[119] M. P. Hehlen, N. J. Cockroft, T. R. Gosnell, A. J. Bruce, Phys. Rev. B 56 (15) (1997) 9302–9318.

[120] S. K. Lee, M. Tatsumisago, T. Minami, Phys. Chem. Glasses 35 (1994) 226.

[121] Y. Hmei, A. Akiyoshi, T. Nanda, Y. Miura, J. Non-Cryst. Solids 177 (1994) 164–169.

[122] T. Sekiya, N. Mochida, S. Ogawa, J. Non-Cryst. Solids 176 (1994) 105–115.

[123] A. Jha, S. Shen, M. Naftaly, Phys. Rev. B 62 (10) (2000) 6215–6227.

[124] R. Reisfeld, C. K. Jorgensen, Excited State Phenomena in Vitreous Materials, Hand Book on the Physics and Chemistry of Rare Earths, North-Holland, Amsterdam, 1987.

[125] G. J. Spuhler, R. Paschotta, M. P. Kullberg, M. Graf, M. Moser, E. Mix, G. Huber, C. Harder, U. Keller, Appl. Phys. B 72 (2001) 285–287.

[126] J. Limpert, A. Liem, H. Zellmer, A. Tnnermann, Electron. Lett. 39 (2003) 645–647.

[127] M. Jacquemet, F. Balembois, S. Chenais, F. Druon, P. Georges, R. Gaume, B. Ferrand, Appl. Phys. B 78 (2004) 13–18.

[128] G. Lei, J. Anderson, M. I. Buchwald, B. C. Edwards, R. I. Epstein, M. T. Murtagh, G. H. Seigel, IEEE J. Quantum Electron. 34 (10) (1998) 1839–1845.

[129] M. J. Weber, J. E. Lynch, D. H. Blackburn, D. J. Cronin, IEEE J. Quantum Electron. 19 (10) (1983) 1600–1608.

[130] C. Jiang, H. Liu, Q. Zeng, X. Tang, F. Gan, Opt. Mat. 61 (2000) 1217–1223.

[131] L. Zhang, H. Hu, J. Non-Cryst. Solids 292 (2001) 108–114.

[132] P. Nandi, G. Jose, Physica B 381 (2006) 66–72.

[133] L. D. DeLoach, S. A. Payne, L. L. Chase, L. K. Smith, W. L. Kway, W. F. Krupke, IEEE J. Quantum Electron. 29 (4) (1993) 1179–1191.

[134] A. S. Yasyukevich, V. G. Shcherbitskii, V. K. Kisel, A. V. Mandrik, N. V. Kuleshov, J. Appl. Spectrosc. 71 (2) (2004) 202–208.

[135] S. A. Payne, L. L. Chase, L. K. Smith, W. L. Kway, W. F. Krupke, IEEE J. Quantum Electron. 28 (11) (1992) 2619–2629.

[136] P.-H. Haumesser, R. Gaume, B. Viana, D. Vivien, J. Opt. Soc. Am. B 19 (22) (2002) 2365–374.

[137] F. Auzel, G. Baldacchini, L. Laversenne, G. Boulon, Opt. Mat. 24 (2003) 103–109.

[138] V. Petrov, U. Griebner, D. Ehrt, W. Seeber, Opt. Lett. 22 (1997) 408–410.

[139] V. D. D. Cacho, L. R. P. Kassab, S. L. Oliveria, P. Verdonck, J. Non-Cryst. Solids 352 (2006) 56–62.

[140] N. D. Psaila, R. R. Thomson, H. T. Bookey, A. K. Kar, N. Chiodo, R. Osellame, G. Cerullo, G. Brown, A. Jha, S. Shen, Opt. Express 14 (22) (2006) 10452–10459.

[141] Y. Tokuda, M. Saito, M. Takahashi, K. Yamada, W. Watanabe, K. Itoh, T. Yoko, J. Non-Cryst. Solids 326 (2003) 472–475.

[142] G. C. Righini, I. Banyasz, S. Barneschi, M. Brenci, M. Cremona, D. Ehrt, M. Ferrari, R. M. Montereali, G. N. Conti, S. Pelli, S. Sebastiani, C. Tosello, Proceedings of SPIE 5840 (2005) 649–657.

[143] P. Nandi, G. Jose, Opt. Commun. 265 (2006) 588–593.

[144] R. R. Alfano, The supercontinuum laser source, Springer-Verlag,New York, 1989.

[145] D. Guillaumond, J.-P. Meunier, IEEE J. Sel. Top. Quantum Electron. 7 (1) (2001) 17–21.

[146] P. Wysocki, M. Digonnet, B. Kim, H. Shaw, J. Lightwave Technol. 12 (3) (1994) 550–567.

[147] Y. Takushima, Opt. Express 13 (15) (2005) 5871–5877.

[148] S.-P. Chen, Y.-G. Li, J.-P. Zhu, H. Wang, Y. Zhang, T.-W. Xu, R. Guo, K.-C. Lu, Opt. Express 13 (5) (2005) 1531–1536.

[149] S. Shen, L. Huang, P. Joshi, A. Jha, Electron. Lett. 39 (25) (2003) 1797 – 1799.

[150] P. Nandi, G. Jose, IEEE J. Quantum Electron. 42 (2006) 1115–1121.

[151] R. Paschotta, J. Nilsson, A. Topper, D. Hanna, IEEE J. Sel. Top. Quantum Electron. 3 (4) (1997) 1097–1099.

[152] L. Kong, Q. Lou, J. Zhou, D. Xue, J. Dong, Y. Wei, Optics & Laser Technology 37 (2005) 597-600.

[153] http://www.npphotonics.com/.

[154] S. Gray, J. D. Minelly, A. B. Grudinin, J. E. Caplen, Opt. Express 33 (16) (1997) 1382–1383.

[155] C. D. Su, L. A. Wang, J. Lightwave Technol. 17 (10) (1999) 1896–1903.

[156] D. G. Falquier, M. J. F. Digonnet, H. J. Shaw, IEEE Photon. Technol. Lett. 12 (11) (2000) 1465–1467.

[157] R. P. Espindola, G. Ales, J. Park, T. A. Strasser, Electron. Lett. 36 (15) (2000) 1263–1264.

[158] W.C.Huang, P. Wai, H.Y.Tam, X.Y.Dong, H. Ming, J. Xie, Electron. Lett. 38 (17) (2002) 956–957.

[159] H. C. Su, L. A. Wang, IEEE Photon. Technol. Lett. 15 (10) (2003) 1357–1359.

[160] H. Lin, C. H. Chang, Opt. Express 12 (25) (2004) 6135–6140.